SATELLITE FORMATION CONTROL
USING ATMOSPHERIC DRAG

THESIS

Blake B. Hajovsky, Second Lieutenant, USAF

AFIT/GA/ENY/07-M11

DEPARTMENT OF THE AIR FORCE
AIR UNIVERSITY

AIR FORCE INSTITUTE OF TECHNOLOGY

Wright-Patterson Air Force Base, Ohio

AFIT/GA/ENY/07-M11

SATELLITE FORMATION CONTROL

USING ATMOSPHERIC DRAG

THESIS

Presented to the Faculty

Department of Aeronautics and Astronautics

Graduate School of Engineering and Management

Air Force Institute of Technology

Air University

Air Education and Training Command

in Partial Fulfillment of the Requirements for the

Degree of Master of Science in Astronautical Engineering
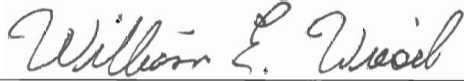
Blake B. Hajovsky, B.S.

Second Lieutenant, USAF

March 2007

AFIT/GA/ENY/07-M11

SATELLITE FORMATION CONTROL

USING ATMOSPHERIC DRAG

Blake B. Hajovsky, B.S.

Second Lieutenant, USAF

Approved:

William E. Wiesel, Ph.D.   13 Mar '07
Thesis Advisor   Date

Lt Col Nathan A. Titus, Ph.D.   13 Mar 07
Committee Member   Date

Lt Col Kerry D. Hicks, Ph.D.   13 Mar 07
Committee Member   Date

AFIT/GA/ENY/07-M11

Abstract

This study investigates the use of a linear quadratic terminal controller to reconfigure satellite formations using atmospheric drag actuated control while minimizing the loss of energy of the formation. The linearized Clohessy-Wiltshire equations of motion are used to describe the motion of the two-satellite formation about an empty reference position maintained at the formation center. Reconfigurations to final in-plane and elliptical formations are simulated at orbital radii of 6800 km and 7000 km, and the altitude loss and a Δv budget were recorded as performance measures for each reconfiguration. The final states of the spacecraft upon reconfiguration were propagated forward in time over 20 orbital periods to ensure the final conditions were achieved. Simulations proved that minimizing the loss of orbital energy effectively minimizes the loss in altitude, and drag actuated control is fully capable of controlling the radial and in-track motion of satellite formations, although the cross-track motion is uncontrollable.

Acknowledgements

First and foremost, I am deeply indebted to my advisor, Dr. Wiesel, for his wisdom and guidance throughout this process. I would also like to thank all of my fellow classmates for their continued support and encouragement over my tenure here at AFIT.

Blake B. Hajovsky

Table of Contents

List of Figures

xi

List of Tables

SATELLITE FORMATION CONTROL
USING ATMOSPHERIC DRAG

I. Introduction

1.1 Satellite Formation Overview

As technology evolves, new ideas develop to improve current processes. This evolution is found in all systems, including the space arena. Satellite formation flying is one area of improvement for satellite systems that has gained considerable interest in recent years. Although the idea has been around for over two decades, the implementation of formation flying is still in its infancy. As a result, research continues to develop in hopes of improving the level of confidence and understanding of satellite formation flying.

A satellite formation consists of two or more satellites flying in close proximity to one another in a specified geometry, cooperating as a distributed system to achieve a given mission [6]. This distributed nature of satellite formations provides several advantages over a single satellite system, leading to potential increases in capability for space systems. One area of increased capability presented by formation flying is remote sensing. Remote sensing systems, such as radar, are limited by the aperture size of the antenna on the satellite. This aperture is, in turn, hindered by physical limitations since the antenna must either be small enough to launch into orbit whole or launched in pieces and constructed on-orbit, a difficult endeavor to say the least. Moreover, the control and stability of large optical systems further restrict the current capabilities. Satellite formations, on the other hand, offer greater angular and spatial resolution through the creation of large, synthetic apertures, formed by precisely positioned satellites equipped with distributed optical systems [6]. The aperture could then be adjusted as desired by increasing or decreasing the size of the formation or by reconfiguring the formation, alleviating the physical restrictions on the aperture.

Aside from increased capabilities in remote sensing, satellite formations provide potential cost savings, increased reliability, and flexibility. The cost savings are directly tied

to the complexity of the system. Due to the importance and substantial financial investment involved with satellite systems, spacecraft are often pushed to the physical size limits prescribed by the launch vehicles as a result of redundant systems placed onboard to help reduce the risk of mission failure. By replacing large, complex, single satellite systems with a cluster of small, simply designed satellites carrying distributed payloads and cooperating to complete the mission, the system can yield substantial savings in cost and liability. For example, should one satellite in the cluster fail, the other satellites in the formation can still be used to at least partially, if not completely, accomplish the mission. The formation can be easily reconfigured to optimize its capability, and, if needed, additional satellites can be launched to restore the full capability of the system. Furthermore, as technology develops or the mission changes, satellite formations can easily be upgraded with replacement satellites as the mission sees fit. This redundancy and flexibility provides a potential advantage in the military arena as well. With the development of anti-satellite technology, a distributed system could prove more resistant to attack since an adversary would have to destroy multiple satellites to cripple the fleet, not just one [5]. The system flexibility is seen in the development of the system on the ground as well. Very often, the launch of satellites are delayed due to setbacks during procurement or development, many times due to a single component. For a distributed system, the individual satellites can be launched as they are developed, allowing partial performance of the system until all of the satellites are on-orbit, thereby mitigating any critical delays.

Although satellite formations provide extensive advantages over a single satellite system, key issues that are not as prevalent for a single satellite can quickly complicate the system. One key issue is maintaining the desired formation, or formation keeping. As discussed by Sabol et al., several factors can lead to formation degradation [18]. Semi-major axis differences result in different orbital periods, causing the formation to diverge. Eccentricity and inclination differences will cause the orbital planes to separate as an effect of J_2, a topic that will be discussed further in Section 2.1.4. Furthermore, differences in mean anomaly can lead to an in-track drift. These perturbing factors are all related to orbital element differences, but physical differences between the satellites themselves may result in formation degradation as well. Orbital perturbations from Earth's full geopo-

tential, third-body effects, atmospheric drag, solar radiation pressure, and other natural effects can cause a formation to separate if the satellites are not identical. As an example, a satellite with a larger presented area per mass will likely experience more atmospheric drag, resulting in a higher in-track deceleration, causing the formation to drift apart. Consequently, having an idea of these effects is essential to the design of the formation and to the formation scheme selected.

Two common formation designs are the leader-follower formation and the empty reference position formation. The leader-follower formation consists of a leader satellite in a reference orbit and one or more follower satellites whose position and motion are defined relative to the leader. This formation is ideal since it provides a physical reference point for the follower satellites. However, one potential drawback from the design is that the follower satellites are usually following a different orbit than the leader, causing the formation to naturally degrade. The empty reference position formation, on the other hand, consists of two or more satellites positioned with respect to some reference position at the center of the formation, unoccupied by another satellite. This design lends itself well to formation flying since all of the satellites in the formation usually have very similar orbits, reducing the degradation of the formation from orbital perturbations. These two formation designs will be further elaborated upon in Section 2.1.4.

Regardless of the formation scheme selected, each satellite formation must be capable of performing a reconfiguration, whether the maneuver is required for formation keeping purposes or to transfer into a new formation to perform some aspect of the mission. The most common and practical means of formation control is through the use of conventional thrusters. The technology involving chemical thrusters is well understood, and their high impulse nature allow researchers to treat orbital maneuvers as velocity change impulses, simplifying the dynamics of the transfer. However, one drawback to conventional thrusters is the requirement of onboard fuel. Onboard expendables increase the size and weight of the satellite and necessitates strict fuel conservation to prolong the life of the formation.

Another technique for formation control is a passive control approach using electrodynamic tethers. This technique involves a formation of satellites that are attached to one another via electrodynamic tethers. A current is then passed through the tether

to control the formation. Since the current generated through the tether is produced by electricity from fuel cells or solar power, the expendables required onboard the spacecraft are minimal, reducing the overall cost of development and launch, and possibly increasing the lifetime of the formation since the effective life is no longer dictated by the amount of fuel onboard. But tethers also present obvious difficulties that must be addressed. Since the satellites are connected, tangling the tethers during reconfiguration must be avoided. Also, should a tether sever due to high stress, fatigue, or errant space debris, the means for control is lost.

A third technique that has been considered for formation control is atmospheric drag. Using atmospheric drag for control is desirable because, like the electrodynamic tethers, drag does not require fuel onboard the spacecraft, and it is in infinite supply for all near-Earth satellites. By simply rotating either the solar panels or drag panels attached to the satellite, the amount of drag acting on the satellite can be varied, providing a source of control. However, exposing a satellite to increased drag also causes the orbit to degrade more rapidly. Without adequate fuel onboard the satellite to boost the orbit, this accelerated rate of decay will shorten the vehicle's lifetime, requiring altitude conservation methods to extend the life of the formation.

1.2 Literature Review

The control of satellite formations using conventional thrusters has been extensively studied. Ulybyshev used a discrete-time linear quadratic regulator (LQR) feedback control law to perform station keeping of a low-Earth orbit satellite constellation perturbed by atmospheric drag [21]. The control law minimized both the along-track relative displacements and the orbital period differences between the satellites to maintain the relative position of the satellites, proving a linear-quadratic control law can effectively handle the control of multiple satellites for formation keeping. Irvin compared linear and nonlinear control techniques for the reconfiguration of a satellite formation [5]. LQR, LQR with linearizing feedback, and the state dependent Riccati equation (SDRE) control methods were applied to both the linear and nonlinear forms of the Clohessy-Wiltshire equations, and the performance of each control method was compared to a near-optimal, open-loop, discrete-

time, impulsive maneuver. The study found that the linear controllers performed better than the nonlinear control law, but the continuous feedback controller was less optimal than the discrete-time, impulsive maneuver control. Sparks compared the formation keeping control costs for a LQR feedback control law formulated from the linear, unperturbed equations of motion to the control costs to directly overcome the gravitational perturbations acting on a formation [19]. The LQR control law was simulated using a high-fidelity model incorporating gravitational perturbations, atmospheric drag, and other perturbing effects. The study found that as the time interval between burns is increased, the error between the actual and desired formations increase, but the control costs approach the theoretical minimum to overcome the gravitational perturbations. Sabol et al. looked at formation keeping costs of four basic formations of two satellites: in-plane, in-track, circular, and projected circular [18]. The in-plane formation consists of the two satellites flying in the same orbital plane, but separated by mean anomaly. The in-track formation is designed such that the satellites share the same ground track, placing the satellites in different orbital planes separated by right ascension of the ascending node to account for the Earth's rotation. The circular formation is designed such that the satellites maintain a set distance from one another, making the follower appear to orbit the reference satellite. And the projected circular formation is designed such that the satellite cluster maintains a fixed distance in the in-track/cross-track plane. The study used a high fidelity perturbation model to propagate the orbital elements of the satellites forward in time to determine the stability of the formation and the formation keeping control costs. All results yielded rather high control costs to achieve the desired conditions.

While extensive research has been performed in the area of formation keeping using conventional thrusters, very little work has been done using atmospheric drag for formation control. Leonard looked at using differential drag between two spacecraft for formation keeping using a two-part control law [10]. The main control law drove the average position of the satellite to a target position relative to the reference satellite. A separate, second control law was then used to minimize the eccentricity of the orbit while maintaining that average position. Both satellites were equipped with drag panels that could be oriented at either 0 or 90 degrees to provide a set positive, negative, or zero relative acceleration.

This technique yielded favorable results as the satellite was driven to the desired position in less than 24 hours for all cases tested, and the eccentricity-minimizing control law was able to maintain the position within 4.17 feet.

More recently, Wedekind considered formation control using differential drag on a leader-follower formation [23]. In this case, a proportional-plus-integral controller was used to continuously alter the cross-sectional area of the follower satellite to counter a drag bias between the two satellites in the formation. The control of three different formations, in-plane, in-track, and circular, was considered. Wedekind achieved favorable results for these three formations when the drag biases were kept small, showing that a formation drag bias can be mitigated and the formation maintained by altering the presented area of the follower satellite.

1.3 Spacecraft Formation Missions

While extensive research into formation flying is being performed, several systems are being developed and launched to prove the viability of such techniques. NASA has embraced the idea of smaller and cheaper spacecraft, filling numerous missions to validate technology and prove formation flying concepts [6]. NASA's Earth Observing-1 (EO-1) mission, launched in 2001, "developed and validated a number of instrument and spacecraft bus breakthrough technologies designed to enable the development of future earth imaging observatories that will have a significant increase in performance while also having reduced cost and mass" [14]. EO-1 was inserted into a formation with the Landsat 7 satellite to validate autonomous operations concepts and other technologies onboard the spacecraft as part of NASA's "smaller, cheaper and more capable" spacecraft tests. NASA's Space Technology 5 mission, launched in 2006, demonstrated the enhanced capabilities formation flying provides to scientific research while testing new, miniature technology aboard its three microsatellites, each of the $25\,kg$ class [15]. The satellites were delivered into a low-Earth polar orbit with an altitude of $4500\,km$ aboard the same launch vehicle, made possible by their small size. The satellites were then configured into an in-plane formation as they made measurements of the Earth's magnetosphere, proving that the small, inexpensive spacecraft were highly capable of performing the mission.

The Air Force continues to push forward with formation flying experiments as well. In 1995, the Air Force New World Vistas Space Technology panel saw the potential presented by formation flying, advocating the exploration of "the technical challenges and benefits of replacing large single satellites with formations of microsatellites to perform the same mission" [12]. This initiative led directly to the Air Force Research Laboratory (AFRL) TechSat 21 flight experiment, designed to test and validate formation flying concepts using three microsatellites that function as one "virtual satellite." Although the mission was cancelled prior to launch, its formulation spurred considerable interest in formation flight and led to increased research in autonomous formation control. AFRL continues to push forward the concepts of satellite formations through in-house research and by sponsoring microsatellite initiatives [1].

1.4   Problem Description

Research involving satellite formation flying continues to progress. With technology advancing to facilitate the design and implementation of smaller satellites, fuel concerns begin to dominate the cost and feasibility of missions. Current control costs are not realistic to maintain a long-term formation. Additionally, the need for extensive fuel capacity dominates the design of the satellite, compromising the conception of smaller, cheaper systems. As a result, methods for reducing the fuel budget without compromising the life of the mission lie at the center of discussion. Atmospheric drag is potentially an effective actuator for formation control and carries the added benefit of being in unlimited supply to all near-Earth orbiting satellites. Without the need for expendables, the cost of developing and launching the satellite is greatly reduced. However, like most control techniques, drag has its limits. Subjecting a spacecraft to excess drag increases the rate of decay the satellite would otherwise experience. Therefore, it is important to limit the amount of drag acting on a spacecraft, especially when drag is used as an actuator.

This thesis will apply a linear-quadratic terminal feedback control law to reconfigure a two-satellite formation using atmospheric drag actuated control while minimizing the change in energy of the satellites. Since the orbital energy of a spacecraft decreases with orbital radius, minimizing the energy change and, as a direct result, the amount of control

used will maximize the lifetime of the formation. The formation will be reconfigured over a user-defined fixed time about an empty reference orbit. Each satellite is equipped with drag panels that can be rotated from 0 degrees, which is parallel to the flow and results in the minimum drag acceleration, to 90 degrees, which is normal to the flow and results in the maximum drag acceleration. The rotation of the drag panels effectively varies the presented area of the satellite, which is directly proportional to the ballistic coefficient. A maximum differential ballistic coefficient of $0.1\,m^2/kg$ is used for the study, a conservative value for the control input. Reconfigurations to both an in-plane and an elliptical formation will be performed from three initial formations: an in-plane formation, an elliptical formation, and a post-payload separation configuration. The performance of each reconfiguration will be evaluated in terms of altitude lost and total Δv required, the typical fuel budget for orbital transfers. Moreover, the final conditions of the controlled state will be propagated forward in time to verify the terminal constraints of the control law were met.

The primary goal of the study is to show that a satellite formation can be effectively controlled using atmospheric drag while minimizing the loss of altitude in the process. As such, several assumptions were made to help focus the study in this respect:

- The reference position is following a circular, equatorial orbit with the given orbital radius;

- The atmosphere is assumed to decay exponentially with increased altitude and rotates with the Earth;

- The atmospheric density at the reference altitude is constant throughout the orbit and remains constant over the duration of the reconfiguration;

- The molecular collisions transfer all energy in the in-track direction. Therefore, no lift is generated, just a retarding force against the satellite's motion;

- The satellites have identical ballistic coefficients when their drag panels are at the same orientation, and the drag panel orientation does not affect the attitude of the satellite;

- The full state of each satellite can be measured for the feedback control law;

- The relative velocities of the satellite do not contribute to the drag acceleration; only the orbital velocity of the circular reference orbit is considered since it is on the order of 10^4 larger than the relative velocities.

1.5 Thesis Outline

The dynamics of the study are discussed in Chapter II. In Section 2.1, the relative equations of motion are derived, defining the position and motion of a satellite with respect to a reference position following a circular orbit. Then, the solution to these equations of motion are developed for the unforced and forced motion to give insight into the natural dynamics of the problem. The two common formation design schemes are defined, along with the advantages and disadvantages of each design. The effects of atmospheric drag on satellite motion is outlined in Section 2.2, with a brief discussion of the exponential atmospheric density model used for the study and the derivation of the drag acceleration imparted on a satellite. The orbital energy and the change in energy due to drag is defined in Section 2.3. And finally in Section 2.4, the falling and fixed reference frames used for this study are presented.

Chapter III outlines the control law used for the reconfigurations. In Section 3.1, the controllability of a single satellite using atmospheric drag actuated control is used to define the relevant state equations of a single satellite for this study. Since the cross-track direction is uncontrollable using drag, only the radial and in-track components of each satellite are needed for the controller. Also, the control law is dependent on the states of both satellites, so the state equations of each satellite are combined in Section 3.2 to give the equations used by the controller. The optimal control law is derived in Section 3.3 from the Euler-Lagrange necessary conditions, with the performance index chosen to penalize the loss of orbital energy and to weight the difference between the desired and actual final state. Finally, the constraints needed for the control law to effectively drive the satellites into a final in-plane and elliptical formation with zero differential drift are derived in Section 3.4.

Chapter IV contains the results of the simulation. The numerically integrated equations of motion are first verified against the closed form solution for the unforced motion

and a linear approximation for the forced motion in Section 4.1. The three reconfigurations to a final in-plane formation are presented in Section 4.2, and reconfigurations to a final elliptical formation are presented in Section 4.3. The time history and radial versus in-track position plots for both the reconfiguration and post-reconfiguration analysis are presented within the two sections to give insight into the motion of the satellites and to ensure the final constraints were met within sufficient bounds. A Δv budget is also provided for each reconfiguration as a means of comparison for conventionally controlled formations.

Finally, Chapter V contains the conclusions of the study and recommendations for future work.

II. Background

2.1 Relative Satellite Motion

Within this section, the relative equations of motion applied to this study will be developed, as well as the unforced and forced solutions to these equations. Additionally, common formation types and designs will be discussed.

2.1.1 Relative Equations of Motion.

To derive the equations of motion, a cylindrical coordinate frame will be used. As shown in Figure 2.1, the radial direction, $\mathbf{e}_r$, is aligned with the position vector of the reference position and is measured radially outward. The in-track direction, $\mathbf{e}_\theta$, is perpendicular to $\mathbf{e}_r$ in the direction of the velocity vector of the reference position. For circular orbits, $\mathbf{e}_\theta$ is measured along the velocity vector of the reference position. And finally, the cross-track direction, $\mathbf{e}_z$, is normal to the orbital plane, completing the right-handed set.

Using the coordinate system defined in Figure 2.1, the position vector of the reference position, $\mathbf{r}_{ref}$, can be written as

$$\mathbf{r}_{ref} = r_0 \mathbf{e}_r \tag{2.1}$$

where r_0 is the orbital radius of the reference position, which follows a circular orbit. Define the position of a satellite relative to the reference position, $\boldsymbol{\rho}_{sat}$, such that

$$\boldsymbol{\rho}_{sat} = \delta r \mathbf{e}_r + r_0 \delta\theta \mathbf{e}_\theta + \delta z \mathbf{e}_z \tag{2.2}$$

where δr, $r_0 \delta\theta$, and δz are the radial, in-track, and cross-track displacements from the reference position, respectively. Given the definition of the relative position, the absolute position of the satellite, $\mathbf{r}_{sat}$, can be written as

$$\begin{aligned} \mathbf{r}_{sat} &= \mathbf{r}_{ref} + \boldsymbol{\rho}_{sat} \\ &= (r_0 + \delta r)\mathbf{e}_r + r_0 \delta\theta \mathbf{e}_\theta + \delta z \mathbf{e}_z \end{aligned} \tag{2.3}$$

2-1

e$_r$

(**e**$_z$ into page)

REFERENCE POSITION $\oplus$ $\longrightarrow$ **e**$_\theta$

n

EARTH
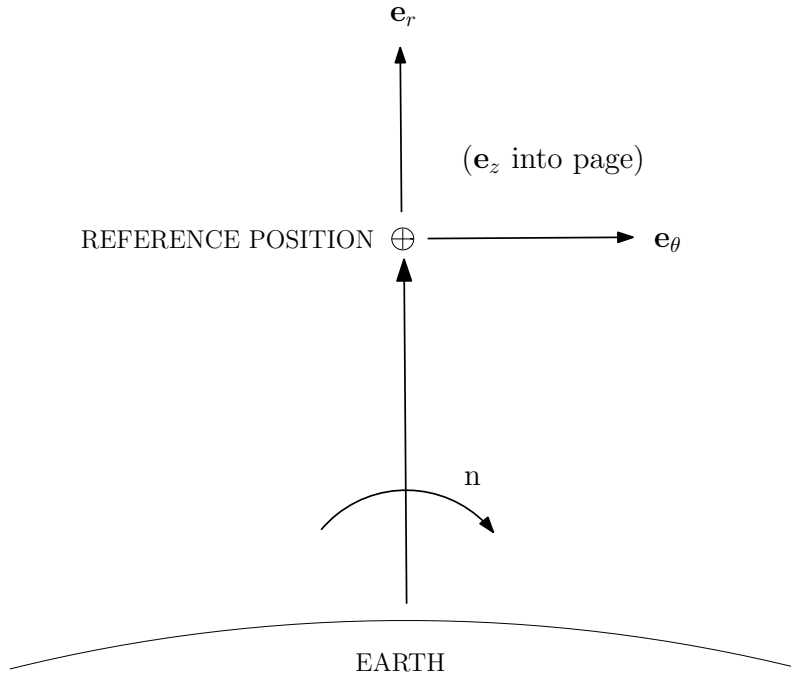
Figure 2.1   Reference Frame

This position vector is written in terms of the relative frame, which rotates with the circular reference orbit at the constant rate of n, the mean motion of the reference orbit. So the angular velocity and acceleration of the reference frame are defined as

$$\boldsymbol{\omega}^{ei} \;=\; n\mathbf{e}_z \tag{2.4}$$

$$\dot{\boldsymbol{\omega}}^{ei} \;=\; \mathbf{0} \tag{2.5}$$

$$n \;=\; \sqrt{\frac{\mu}{r_0^3}} \tag{2.6}$$

where $\dot{\boldsymbol{\omega}}^{ei}$ is zero since the angular velocity vector is constant, and μ is the gravitational parameter of Earth. The absolute acceleration of the satellite with respect to the relative frame is then defined as

$$\ddot{\mathbf{r}}_{sat} = \frac{^{\mathbf{e}}d^2}{dt^2}\mathbf{r}_{sat} + 2\boldsymbol{\omega}^{\mathbf{ei}} \times \frac{^{\mathbf{e}}d}{dt}\mathbf{r}_{sat} + \boldsymbol{\omega}^{\mathbf{ei}} \times \left(\boldsymbol{\omega}^{\mathbf{ei}} \times \mathbf{r}_{sat}\right) \qquad (2.7)$$

where $\frac{^{\mathbf{e}}d}{dt}\mathbf{r}_{sat}$ and $\frac{^{\mathbf{e}}d^2}{dt^2}\mathbf{r}_{sat}$ are the time derivatives of the satellite position vector in the relative frame only, such that

$$\frac{^{\mathbf{e}}d}{dt}\mathbf{r}_{sat} = \delta\dot{r}\mathbf{e}_r + r_0\delta\dot{\theta}\mathbf{e}_\theta + \delta\dot{z}\mathbf{e}_z \qquad (2.8)$$

$$\frac{^{\mathbf{e}}d^2}{dt^2}\mathbf{r}_{sat} = \delta\ddot{r}\mathbf{e}_r + r_0\delta\ddot{\theta}\mathbf{e}_\theta + \delta\ddot{z}\mathbf{e}_z \qquad (2.9)$$

Substituting the expressions from Equations 2.4, 2.8, and 2.9 into Equation 2.7 and equating the cross products yields the acceleration vector of the satellite in terms of the relative frame components:

$$\ddot{\mathbf{r}}_{sat} = (\delta\ddot{r} - 2nr_0\delta\dot{\theta} - n^2 r_0 - n^2\delta r)\mathbf{e}_r + (r_0\delta\ddot{\theta} + 2n\delta\dot{r} - n^2 r_0\delta\theta)\mathbf{e}_\theta + \delta\ddot{z}\mathbf{e}_z \qquad (2.10)$$

Assuming two-body motion, another expression for the acceleration vector of the satellite can be written as

$$\ddot{\mathbf{r}}_{sat} = -\frac{\mu}{r_{sat}^3}\mathbf{r}_{sat} + \mathbf{f} \qquad (2.11)$$

The first term in Equation 2.11 is the two-body gravitational acceleration acting on the satellite. The vector $\mathbf{f}$, which can be written in component form such that $\mathbf{f} = f_r\mathbf{e}_r + f_\theta\mathbf{e}_\theta + f_z\mathbf{e}_z$, contains any forces, per unit mass, other than the two-body gravitational force acting on the satellite. Substituting the position vector of the satellite from Equation 2.10 into Equation 2.11 yields

$$\ddot{\mathbf{r}}_{sat} = -\frac{\mu[(r_0 + \delta r)\mathbf{e}_r + r_0\delta\theta\mathbf{e}_\theta + \delta z\mathbf{e}_z]}{(r_0^2 + 2r_0\delta r + \delta r^2 + r_0^2\delta\theta^2 + \delta z^2)^{3/2}} + \mathbf{f} \qquad (2.12)$$

Assuming small relative displacements with respect to the orbital radius, r_0, the denominator of Equation 2.12 can be expanded using the binomial theorem, resulting in

$$\left(r_0^2 + 2r_0\delta r + \delta r^2 + r_0^2\delta\theta^2 + \delta z^2\right)^{-3/2} = r_0^{-3}\left[1 - \frac{3}{2}\left(\frac{2\delta r}{r_0} + \dots\right) + \mathcal{O}(\delta^2)\right] \qquad (2.13)$$

Substituting this result into Equation 2.12 and neglecting terms of order $\mathcal{O}(\delta^2)$ and higher yields

$$\ddot{\mathbf{r}}_{sat} = -\frac{\mu}{r_0^3}[(r_0 - 2\delta r)\mathbf{e}_r + r_0\delta\theta\mathbf{e}_\theta + \delta z\mathbf{e}_z] + \mathbf{f} \qquad (2.14)$$

Combining Equations 2.10 and 2.14 and recalling the definition of the mean motion results in the following three equations:

$$\delta\ddot{r} = 2nr_0\delta\dot{\theta} + 3n^2\delta r + f_r \qquad (2.15)$$

$$r_0\delta\ddot{\theta} = -2n\delta\dot{r} + f_\theta \qquad (2.16)$$

$$\delta\ddot{z} = -n^2\delta z + f_z \qquad (2.17)$$

These three equations are commonly known as *Hill's equations* or the *Clohessy-Wiltshire (CW) equations* and are used to describe the relative motion of two satellites when the reference satellite is following a circular orbit [25]. The double name credits both parties involved in the development of the equations. Hill first studied the equations in 1878, but Clohessy and Wiltshire redeveloped the equations in 1960 for satellite rendezvous [24, 4].

In forming these equations, several assumptions were made. One assumption is that the orbital mean motion n is constant. This assumption is valid for circular orbits, but can be extended to nearly circular orbits within bounds. Another assumption was made when
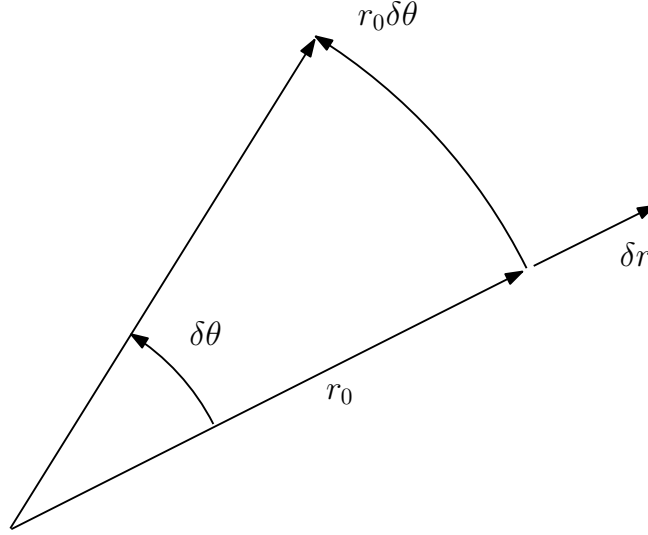
Figure 2.2   Illustration of in-track measurement

substituting the result of the binomial expansion from Equation 2.13 into the two-body gravitational acceleration in Equation 2.14. Here, terms of order $\mathcal{O}(\delta^2)$ and higher were neglected, an assumption valid for small coordinates only. However, the final equations are not limited in the $r_0\delta\theta$ direction since this quantity does not appear explicitly in the equations above and is measured circumferentially, as illustrated in Figure 2.2 [7]. This extended range of validity in the in-track direction is a benefit of using cylindrical coordinates.

2.1.2 Force Free Solution.   To further understand the relative motion of the satellite, the unforced solution to the CW equations will be developed following the same process used by Wiesel [25]. For this case, $\mathbf{f} = \mathbf{0}$, resulting in the following equations:

$$\delta\ddot{r} = 2nr_0\delta\dot{\theta} + 3n^2\delta r \tag{2.18}$$

$$r_0\delta\ddot{\theta} = -2n\delta\dot{r} \tag{2.19}$$

$$\delta\ddot{z} = -n^2\delta z \tag{2.20}$$

As can be seen from the equations above, the δz equation is decoupled from the in-plane equations of motion and represents the motion of a harmonic oscillator. So, given the initial conditions $\delta z(t=0) = \delta z_0$ and $\delta \dot{z}(t=0) = \delta \dot{z}_0$, the solution is simply

$$\delta z(t) = \delta z_0 \cos nt + \frac{\delta \dot{z}_0}{n} \sin nt \tag{2.21}$$

Integrating Equation 2.19 with initial conditions $\delta \dot{\theta}(t=0) = \delta \dot{\theta}_0$ and $\delta r(t=0) = \delta r_0$ and solving for $\delta \dot{\theta}$ yields

$$\delta \dot{\theta}(t) = \delta \dot{\theta}_0 + \frac{2n}{r_0}(\delta r_0 - \delta r) \tag{2.22}$$

Substituting this equation into the δr equation results in

$$\delta \ddot{r} + n^2 \delta r = 2nr_0 \delta \dot{\theta}_0 + 4n^2 \delta r_0 \tag{2.23}$$

This equation is a simple harmonic oscillator with a forcing function. Its solution contains both a homogeneous solution and a particular solution such that

$$\delta r(t) = \delta r_h + \delta r_p \tag{2.24}$$

where the particular solution is just

$$\delta r_p = \frac{2}{n} r_0 \delta \dot{\theta}_0 + 4 \delta r_0 \tag{2.25}$$

Solving for the homogeneous solution with initial conditions

$$\delta r_h(t=0) = \delta r_0 - \delta r_p = -\frac{2}{n} r_0 \delta \dot{\theta}_0 - 3 \delta r_0 \tag{2.26}$$

$$\delta \dot{r}_h(t=0) = \delta \dot{r}_0 \tag{2.27}$$

results in the complete solution

$$\delta r(t) = -\left(\frac{2}{n}r_0\delta\dot{\theta}_0 + 3\delta r_0\right)\cos nt + \frac{\delta\dot{r}_0}{n}\sin nt + \frac{2}{n}r_0\delta\dot{\theta}_0 + 4\delta r_0 \tag{2.28}$$

Substituting this solution into Equation 2.22 gives

$$\delta\dot{\theta}(t) = -3\delta\dot{\theta}_0 - \frac{6n}{r_0}\delta r_0 + \left(4\delta\dot{\theta}_0 + \frac{6n}{r_0}\delta r_0\right)\cos nt - \frac{2\delta\dot{r}_0}{r_0}\sin nt \tag{2.29}$$

Integrating both sides of Equation 2.29, applying initial conditions, and solving for $\delta\theta(t)$ yields

$$\delta\theta(t) = \delta\theta_0 - \left(3\delta\dot{\theta}_0 + \frac{6n}{r_0}\delta r_0\right)t + \left(\frac{4}{n}\delta\dot{\theta}_0 + \frac{6}{r_0}\delta r_0\right)\sin nt + \frac{2\delta\dot{r}_0}{nr_0}\cos nt - \frac{2}{nr_0}\delta\dot{r}_0 \tag{2.30}$$

Equations 2.21, 2.28, and 2.30 form the position solution in terms of an initial state and final time. To find the velocity solution, simply differentiate the position solution, yielding

$$\delta\dot{r}(t) = (2r_0\delta\dot{\theta}_0 + 3n\delta r_0)\sin nt + \delta\dot{r}_0\cos nt \tag{2.31}$$

$$\delta\dot{z}(t) = -\delta z_0 n\sin nt + \delta\dot{z}_0\cos nt \tag{2.32}$$

and where $\delta\dot{\theta}(t)$ is given in Equation 2.29. Equations 2.29, 2.31, and 2.32 represent the velocity solution to the unforced equations of motion. Combining the position and velocity solutions, the overall solution can be put into state variable form, producing

$$
\begin{bmatrix}
\delta r \\
r_0 \delta \theta \\
\delta z \\
\delta \dot{r} \\
r_0 \delta \dot{\theta} \\
\delta \dot{z}
\end{bmatrix}
=
\begin{bmatrix}
4 - 3\cos nt & 0 & 0 & \frac{1}{n}\sin nt & \frac{2}{n}(1 - \cos nt) & 0 \\
6(\sin nt - nt) & 1 & 0 & \frac{2}{n}(\cos nt - 1) & \frac{4}{n}\sin nt - 3t & 0 \\
0 & 0 & \cos nt & 0 & 0 & \frac{1}{n}\sin nt \\
3n\sin nt & 0 & 0 & \cos nt & 2\sin nt & 0 \\
6n(\cos nt - 1) & 0 & 0 & -2\sin nt & -3 + 4\cos nt & 0 \\
0 & 0 & -n\sin nt & 0 & 0 & \cos nt
\end{bmatrix}
\begin{bmatrix}
\delta r_0 \\
r_0 \delta \theta_0 \\
\delta z_0 \\
\delta \dot{r}_0 \\
r_0 \delta \dot{\theta}_0 \\
\delta \dot{z}_0
\end{bmatrix}
$$

$$(2.33)$$

Several trends are evident from this solution. First, the cross-track components, δz and $\delta \dot{z}$, simply oscillate with the period of the reference orbit. This oscillation results in a slight inclination for the satellite, projecting it into a separate orbital plane from the reference orbit. Also notice that the cross-track components are completely decoupled from the in-plane components, making all motion in the cross-track direction independent of any in-plane motion. The radial components, δr and $\delta \dot{r}$, contain the same oscillatory terms as the cross-track components that move with the period of the reference orbit. This motion creates a slight eccentricity in the satellite's orbit as the radius increases and decreases. Finally, the in-track components, $r_0 \delta \theta$ and $r_0 \delta \dot{\theta}$, contain the same oscillations, but $r_0 \delta \theta$ also includes a term that grows with time. This secular term causes an in-track drift between the reference position and the satellite. To maintain a formation for an extended period of time, this secular motion must be suppressed.

2.1.3 Forced Solution. Unlike the force free solution presented in Section 2.1.2, a nice, closed-form solution does not exist for the forced CW equations. However, one can be constructed that uses parameters similar to the force free solution. Following the same steps used by Meirovitch to solve a nonhomogeneous linear system of equations [13], define the forced equations of motion from Equations 2.15-2.17 in state vector form such that

$$\frac{d}{dt}\mathbf{x}(t) = A\mathbf{x}(t) + \mathbf{f}(t) \qquad (2.34)$$

where $\mathbf{x}$, A, and $\mathbf{f}$ are defined as

$$\mathbf{x} = \begin{bmatrix} \delta r & r_0 \delta\theta & \delta z & \delta\dot{r} & r_0\delta\dot{\theta} & \delta\dot{z} \end{bmatrix}^T \tag{2.35}$$

$$A = \begin{bmatrix} 0 & 0 & 0 & 1 & 0 & 0 \\ 0 & 0 & 0 & 0 & 1 & 0 \\ 0 & 0 & 0 & 0 & 0 & 1 \\ 3n^2 & 0 & 0 & 0 & 2n & 0 \\ 0 & 0 & 0 & -2n & 0 & 0 \\ 0 & 0 & -n^2 & 0 & 0 & 0 \end{bmatrix} \tag{2.36}$$

$$\mathbf{f} = \begin{bmatrix} 0 & 0 & 0 & f_r & f_\theta & f_z \end{bmatrix}^T \tag{2.37}$$

Introduce the state transition matrix, $\Phi(t)$, which satisfies the equations

$$\Phi(t_0) = I \tag{2.38}$$

$$\frac{d}{dt}\Phi(t) = A\Phi(t) \tag{2.39}$$

$$\frac{d}{dt}\Phi^{-1}(t) = -\Phi^{-1}(t)A \tag{2.40}$$

where I is the identity matrix. Note the inverse of the state transition matrix is needed in Equation 2.40. This inverse exists for all time by definition of the Jacobi-Liouville formula and Equation 2.38 [13]. Premultiplying Equation 2.34 by $\Phi^{-1}(t)$ and postmultiplying Equation 2.40 by $\mathbf{x}(t)$, the two equations can be added together to yield

$$\frac{d}{dt}\left[\Phi^{-1}(t)\mathbf{x}(t)\right] = \Phi^{-1}(t)\mathbf{f}(t) \tag{2.41}$$

Integrating Equation 2.41 with respect to time and premultiplying by $\Phi(t)$ yields the solution to the forced equations of motion:

$$\mathbf{x}(t) = \Phi(t)\mathbf{x}(t_0) + \Phi(t) \int_{t_0}^{t} \Phi^{-1}(\tau)\mathbf{f}(\tau)d\tau \tag{2.42}$$

where

$$\Phi(t) = \begin{bmatrix} 4 - 3\cos nt & 0 & 0 & \frac{1}{n}\sin nt & \frac{2}{n}(1 - \cos nt) & 0 \\ 6(\sin nt - nt) & 1 & 0 & \frac{2}{n}(\cos nt - 1) & \frac{4}{n}\sin nt - 3t & 0 \\ 0 & 0 & \cos nt & 0 & 0 & \frac{1}{n}\sin nt \\ 3n\sin nt & 0 & 0 & \cos nt & 2\sin nt & 0 \\ 6n(\cos nt - 1) & 0 & 0 & -2\sin nt & -3 + 4\cos nt & 0 \\ 0 & 0 & -n\sin nt & 0 & 0 & \cos nt \end{bmatrix} \tag{2.43}$$

2.1.4 Formation Design.   The design of a satellite formation is critical to the control costs to maintain the formation. Two common formation schemes exist: a leader-follower scheme and an empty reference position formation, both of which were alluded to in Section 1.1.

The most common design is the leader-follower scheme. This two-satellite formation consists of the leader satellite, which is usually at the center of the reference frame, and a follower satellite, which is positioned relative to the leader. The leader usually takes a passive role, meaning it is non-maneuvering. Instead, it flies in a circular orbit, and the follower satellite is controlled around it, taking on the active role. This scheme is perhaps the most common due to its similarities to orbital rendezvous, an older concept in astrodynamics. For rendezvous, the station is usually in a fixed orbit and takes no action in docking with the approaching satellite. And since the CW equations were developed for rendezvous, the dynamics translate well for the leader-follower scheme, although not completely. Since rendezvous is usually performed over a short time period, perturbing effects can be ignored with confidence since they usually require an extended period of time to noticeably impact satellite motion. Also, rendezvous usually involves a considerable

fuel budget, allowing the cancellation of any disturbances through increased control. But when describing a satellite formation that must maintain its relative positioning for several months to years at a time with a limited fuel budget, neglecting these perturbations could be costly, especially with the design of the leader-follower scheme. As is evident from the design, the two satellites are flying in separate orbits, allowing any orbital element dependent perturbations to pull the formation apart. One such disturbance that affects low-Earth orbit satellites is the J_2 perturbation, the geopotential zonal harmonic associated with the oblateness of the Earth [26]. The J_2 perturbation places a torque on the orbit that causes the orbital plane to precess and the argument of perigee to rotate at rates of [25]

$$\dot{\Omega} = -\frac{3nJ_2R_e^2}{2a^2\left(1-e^2\right)^2}\cos i \qquad (2.44)$$

$$\dot{\omega} = -\frac{3nJ_2R_e^2}{2a^2\left(1-e^2\right)^2}\left(\frac{5}{2}\sin^2 i - 2\right) \qquad (2.45)$$

where Ω is the right ascension of the ascending node, ω is the argument of perigee, J_2 is a dimensionless number with the value of 0.001082 that characterizes the Earth's oblateness, R_e is the radius of the Earth, a is the semimajor axis, e is the eccentricity, and i is the orbital inclination. The J_2 perturbation tends to pull satellite formations apart if the two satellites have different inclinations or eccentricities, which is the case for most leader-follower schemes. As an example, consider an elliptical formation with the leader-follower arrangement such that the leader is following a circular orbit and the follower is in a slightly eccentric orbit, allowing it to orbit the leader in the relative frame. Because of their eccentricity difference, the two orbital planes of the satellites will precess at slightly different rates, causing the satellites to drift apart. This drift rate is increased if a cross-track motion is also applied to the follower since the inclinations will differ. Therefore, the leader-follower formation is intrinsically unstable, requiring formation keeping maneuvers to maintain the formation.

The empty reference position design is another formation type that is sometimes employed. For this design, the reference position is left empty, meaning there is not a satellite at the center of the formation. Instead, the satellites are positioned around a defined reference point centered on the formation. This formation design is more stable than the leader-follower scheme since the satellites usually have the same semimajor axis, inclination, and eccentricity. For example, consider the same elliptical formation described for the leader-follower scheme, but using the empty reference position instead. To place the two satellites in the correct formation, their semimajor axes, eccentricities, and inclinations must be equal, with their arguments of perigee determining their placement in the formation. As a result, their orbital planes and arguments of perigee would rotate at the same rate, keeping the formation intact. The reference position would merely rotate at this rate as well to maintain the average position of the formation. As long as the overall drift of the formation is accounted for in the mission design, the empty reference position formation scheme provides a stable formation that does not require considerable formation keeping costs.

2.2   Atmospheric Drag

The effects of the J_2 zonal harmonic on satellite motion was discussed in the previous section, but the gravitational forces are not the only forces affecting satellite motion. The atmosphere, although extremely thin at orbital altitudes, can have a substantial impact on low-Earth orbit (LEO) satellites. In fact, besides gravitational forces, atmospheric drag is the most influential force acting on LEO satellites, retarding their motion and leading to eventual decay into the denser layers of the atmosphere [9]. Within this section, the atmospheric model used for this study will be introduced, and the effect of drag on satellite motion will be derived. Finally, the impact of differential drag on satellites in formation will be discussed.

2.2.1   Atmospheric Model.   Perhaps the most difficult aspect of the near-Earth space environment to model is the atmosphere. The atmosphere is a highly dynamic medium that can vary significantly at a given altitude over time. Certain variations are

predictable, such as the equatorial bulge and the diurnal bulge [26]. However, atmospheric variations due to solar radiation and the Earth's magnetic field can be highly unpredictable, making atmospheric conditions difficult to predict into the future [17, 26]. Therefore, most models are simply approximations of the atmosphere under normal conditions.

Since the purpose of this study is to prove the feasibility of controlling a satellite formation through the use of drag, a comprehensive atmospheric model complete with time dependent variations is not needed. Instead, a simple model for estimating the atmospheric density at a given altitude is sufficient. Therefore, an exponential atmospheric model is used for this study. This model assumes a static atmosphere with a spherically symmetrical distribution of particles [22]. The atmospheric density, ρ, decreases exponentially with increasing altitude, varying according to the following relationship:

$$\rho = \rho_0 exp \left[-\frac{h_{ellp} - h_0}{H} \right] \tag{2.46}$$

Here, ρ_0 is the reference density at the reference altitude h_0, h_{ellp} is the altitude measured from the Earth's surface, and H is the scale height at the reference altitude [22]. Values for these definitions are given in Table 2.1.

2.2.2 Acceleration Due to Drag. The atmosphere at orbital altitudes consists of diffuse molecules that have very little, if any, interaction with one another. This region, known as the free molecular flow regime, consists of molecules that no longer behave like a fluid, but instead behave as individual particles [17]. At orbital speeds, the individual molecular impacts on the spacecraft, when taken over an extended period of time, can greatly affect the motion of the satellite. When the molecules impact and bounce off the spacecraft, linear momentum is transferred through the inelastic collisions proportional to the velocity difference between the molecules and the spacecraft [26]. Since force is the rate of change of linear momentum, these individual impacts transfer a drag force to the spacecraft that imparts an acceleration in the direction opposite the spacecraft's motion proportional to $A\rho v^2/2$. Here, A is the presented area of the satellite, ρ is the atmospheric density at the given orbital altitude, and v is the satellite velocity with respect

Table 2.1   Exponential Atmospheric Model [22]

Altitude h_{ellp} (km)	Base Altitude h_0	Nominal Density $\rho_0(kg/m^3)$	Scale Height $H(km)$
0-25	0	1.225	7.249
25-30	25	3.899×10^{-2}	6.349
30-40	30	1.774×10^{-2}	6.682
40-50	40	3.972×10^{-3}	7.554
50-60	50	1.057×10^{-3}	8.382
60-70	60	3.206×10^{-4}	7.714
70-80	70	8.770×10^{-5}	6.549
80-90	80	1.905×10^{-5}	5.799
90-100	90	3.396×10^{-6}	5.382
100-110	100	5.297×10^{-7}	5.877
110-120	110	9.661×10^{-8}	7.263
120-130	120	2.438×10^{-8}	9.473
130-140	130	8.484×10^{-9}	12.636
140-150	140	3.845×10^{-9}	16.149
150-180	150	2.070×10^{-9}	22.523
180-200	180	5.464×10^{-10}	29.740
200-250	200	2.789×10^{-10}	37.105
250-300	250	7.248×10^{-11}	45.546
300-350	300	2.418×10^{-11}	53.628
350-400	350	9.518×10^{-12}	53.298
400-450	400	3.725×10^{-12}	58.515
450-500	450	1.585×10^{-12}	60.828
500-600	500	6.967×10^{-13}	63.822
600-700	600	1.454×10^{-13}	71.835
700-800	700	3.614×10^{-14}	88.667
800-900	800	1.170×10^{-14}	124.64
900-1000	900	5.245×10^{-15}	181.05
1000-	1000	3.019×10^{-15}	268.00

to the atmosphere. The shape of the satellite also affects the transfer of momentum to the spacecraft. As a result, the resultant drag force is also directly proportional to the coefficient of drag, C_D. This aerodynamic coefficient is a function of body shape and the Mach number, along with other various parameters, and also accounts for oblique molecular reflections [17, 26]. Thus, the acceleration due to drag, $\mathbf{a}_d$, is written as

$$\mathbf{a}_d = -\frac{1}{2}\frac{C_D A}{m}\rho v \mathbf{v} \tag{2.47}$$

where m is the satellite mass. Assuming a circular, equatorial orbit with an atmosphere that rotates with the Earth, the satellite velocity vector with respect to the atmosphere, $\mathbf{v}$, is defined as [26]

$$\mathbf{v} = \mathbf{v}_{in} - \boldsymbol{\omega}_E \times \mathbf{r} \tag{2.48}$$

where $\mathbf{v}_{in}$ is the inertial velocity of the satellite, $\boldsymbol{\omega}_E$ is the rotational velocity of the Earth, and $\mathbf{r}$ is the inertial satellite position vector.

The drag coefficient, presented area, and mass may not be separately determinable, so these three quantities are usually grouped into a single quantity called the ballistic coefficient, B^*, which is defined as [26]

$$B^* = \frac{C_D A}{m} \tag{2.49}$$

From this definition, it can be seen that increasing the ballistic coefficient increases the amount of drag acting on the satellite. Since the drag coefficient is relatively fixed, the ballistic coefficient can change only if the presented area of the satellite or the satellite mass is changed. Changing the satellite mass is an irreversible process since it usually involves the bleeding of fuel, so a change in mass is not an ideal method for altering the ballistic coefficient for control purposes. However, the presented area of the satellite can easily change by a simple rotation of the satellite itself or through the rotation of either drag panels or solar panels attached to the satellite, making it an ideal technique for control.

Note that several conventions exist for defining the ballistic coefficient, one being the inverse of the definition above such that units of pressure result [22]. However, the definition in Equation 2.49 is an interpretation developed in Wiesel's texts and is the accepted definition for this study [25, 26].

2.2.3 Differential Drag. When controlling a satellite formation with drag, one satellite is purposely subjected to increased drag to change its position with respect to the other. The drag force difference between the two satellites is called differential drag, and the force difference results in a differential acceleration that can be either negative or positive in the relative frame, although the drag acting on the satellite is always directed against the satellite's velocity vector.

To help understand the concept of differential drag, consider two identical satellites, both equipped with drag panels, flying in the same orbit but separated by true anomaly such that satellite 1 is slightly ahead of satellite 2 in an in-plane formation. Assume satellite 1 is at the center of the relative frame. If both satellites have their drag panels oriented at zero degrees such that the drag force acting on each satellite due to the panels is zero, the satellites experience zero differential drag. They will neither move toward nor away from one another. If the panels on satellite 1 were then rotated to 90 degrees such that they were normal to the velocity vector, satellite 1 would experience a negative acceleration in the absolute frame, causing satellite 2 to move toward it. As a result, satellite 2 experiences a positive acceleration in the relative frame. If the panels on satellite 2 were then rotated such that both satellites had their panels oriented at 90 degrees, the differential drag would then be zero since both satellites are experiencing the same, albeit larger, drag force. If the panels on satellite 1 were then rotated back to zero degrees while the panels on satellite 2 stayed at 90 degrees, satellite 2 would then experience a negative differential acceleration since it would then move away from satellite 1.

Now consider satellite 1 with its panels rotated at 90 degrees and satellite 2 with its panels oriented at 45 degrees. The differential acceleration experienced with this configuration is the same differential acceleration experienced when the panels on satellite 1 are oriented at 45 degrees and the panels on satellite 2 are at zero degrees, although the

first configuration is experiencing double the drag. This increased drag does nothing but increase the rate of decay of the formation altitude, decreasing the overall energy of the formation. As a result, to minimize the loss of altitude and the loss of orbital energy, only one satellite should have its panels deployed at any given time. Any control law using differential drag as an actuator should account for this fact.

2.3 Energy Function

When controlling a spacecraft with atmospheric drag, the satellite is purposely sub-jected to increased drag to achieve the desired result. Since drag acts against the motion of the vehicle, it *instantaneously* decreases the velocity of the satellite, which causes the orbital radius to decrease. Although the instantaneous velocity of the satellite decreases, the *average* velocity of the satellite increases as a result of the reduction in orbital size. The continuous decrease in orbital size will shorten the lifetime of the satellite since, without any means to raise the orbit, the satellite will continue to decay until reentering the denser layers of the atmosphere, falling out of orbit. Therefore, it is desirable to minimize this rate of degradation while achieving the desired result of the control. One way to minimize the degradation is to minimize the loss of orbital energy of the satellite. The orbital energy, $\mathcal{E}$, is defined as

$$\mathcal{E} = \frac{v^2}{2} - \frac{\mu}{r} = -\frac{\mu}{2a} \qquad (2.50)$$

Here, v and r are the orbital velocity and radius, respectively, and a is the semi-major axis. As is evident from Equation 2.50, reducing the orbital size of the satellite reduces the overall energy. And since drag acts to shrink the orbital size, minimizing the *change* in orbital energy for this case is the same as minimizing the *loss* of orbital energy. The rate of change of orbital energy due to atmospheric drag can be found by differentiating Equation 2.50:

$$\frac{d\mathcal{E}}{dt} = v\dot{v} + \frac{\mu}{r^2}\dot{r} \qquad (2.51)$$

Since drag acts against the velocity vector, the *instantaneous* change in energy due to atmospheric drag becomes

$$\frac{d\mathcal{E}}{dt} = -va_d \tag{2.52}$$

where v is the satellite velocity with respect to the atmosphere, and a_d is the acceleration due to drag.

2.4   The Relative Frame

The relative frame used for this study will be slightly different from the reference frame discussed in Section 2.1.1 and shown in Figure 2.1. The reference frame discussed earlier assumes the reference position is in a fixed, circular orbit such that its orbital radius and velocity are constant. However, for this study, atmospheric drag is used as the only means for control. As a result, the orbital radius of the reference position will decrease with increased control input, resulting in a falling reference frame. The reference position is defined as the average position of the two satellites in the formation, so it will fall at the instantaneous average rate of descent of the satellites. For example, suppose one satellite has its panels oriented such that the drag force from its panels is zero while the other satellite has its panels deployed to result in a drag acceleration, causing it to fall at a rate of $\dot{r}$. The rate of change of the reference position is defined as $\dot{r}/2$ such that the reference position remains centered on the formation.

As a result of this falling frame and as discussed in Section 2.2.3, some control inputs appear to result in a positive acceleration when plotted in the frame. This perception is from the frame's motion. A reconfiguration with an initial $20\,m$ displacement in the radial direction to a final in-plane formation with a separation distance of $100\,m$ is shown in two different relative frames: a frame fixed upon the original reference position in Figure 2.3 and the falling frame in Figure 2.4. The fixed frame clearly shows that the final reference position fell $62\,m$ in the radial direction and advanced $3400\,m$ in the in-track direction as a result of the reconfiguration. But the position of the satellites with respect to the reference position is difficult to determine. The falling frame shows the more common relative frame
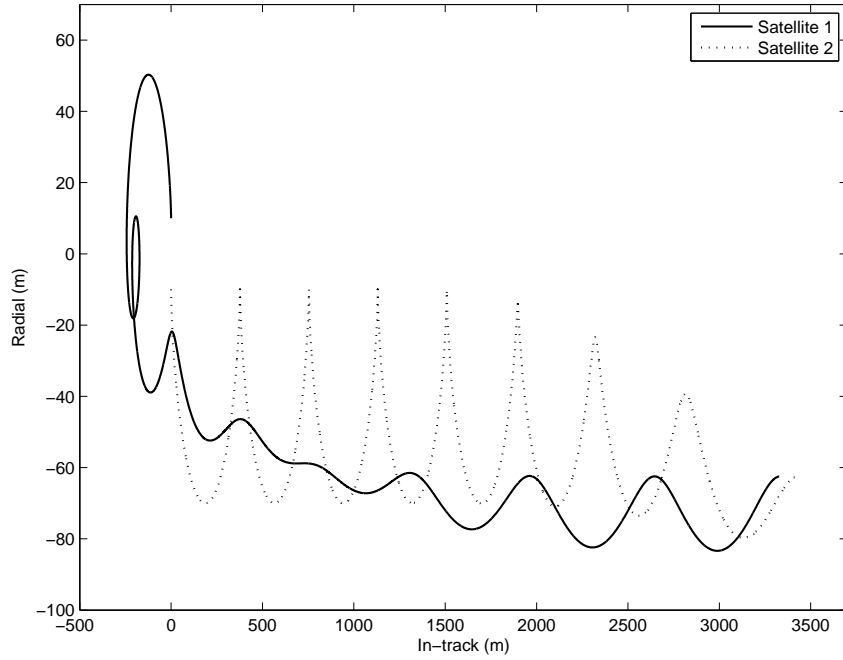
Figure 2.3   Plot of Reconfiguration in the Fixed Frame

plot with a reference position centered on the formation and fixed in the frame. This plot illustrates the appearance of a positive acceleration. When the leading satellite has a larger drag acceleration than the trailing satellite, the trailing satellite in turn experiences a positive acceleration in the relative frame. In reality, the acceleration is still negative, but the drag on the trailing satellite is less than the drag on the leading satellite.

Also, by design of the relative frame, the forces acting on the two satellites in the frame are *differential* forces only. Equal forces acting on the two satellites will result in the same motion for each such that no motion results when viewed in the relative frame. As an example, consider two satellites flying in an in-plane formation such that they occupy the same circular orbit in the absolute frame but are separated by true anomaly. The two satellites will continue in this formation as long as all forces acting on the two satellites are equivalent. If one satellite has a larger drag acceleration than the other, the two will separate indefinitely unless a control input is applied.

To show that equivalent forces cancel in the relative frame, consider two identical satellites that each have the same nominal ballistic coefficient B_0^* when their solar panels
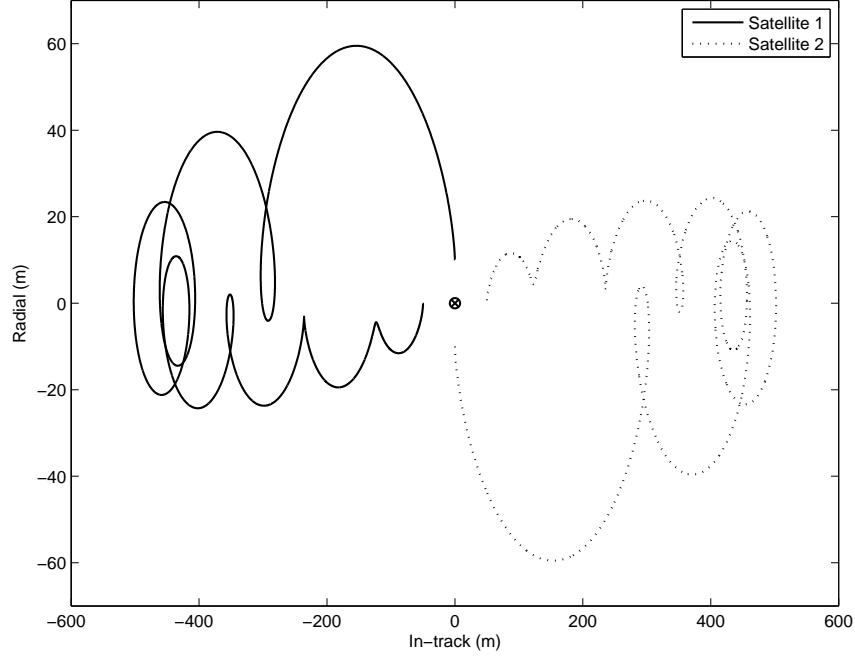
Figure 2.4   Plot of Reconfiguration in the Falling Frame

are at a zero degree orientation such that the drag force due to the panels is negligible. The equations of motion of the two satellites in the absolute frame then become

$$\ddot{\mathbf{r}}_1 \quad = \quad -\frac{\mu}{r_1^3}\mathbf{r}_1 - \frac{1}{2}\left(B_0^* + \Delta B_1^*\right)\rho v \mathbf{v} \tag{2.53}$$

$$\ddot{\mathbf{r}}_2 \quad = \quad -\frac{\mu}{r_2^3}\mathbf{r}_2 - \frac{1}{2}\left(B_0^* + \Delta B_2^*\right)\rho v \mathbf{v} \tag{2.54}$$

where ΔB_1^* and ΔB_2^* are the ballistic coefficients due to non-zero solar panel orientations for satellite 1 and satellite 2, respectively. Substituting Equation 2.3 for the position vectors of each satellite and expanding the denominator using the binomial theorem, the resulting in-track accelerations can be subtracted in the relative frame, yielding

$$r_0\delta\ddot{\theta}_1 - r_0\delta\ddot{\theta}_2 = -2n\left(\delta\dot{r}_1 - \delta\dot{r}_2\right) - \frac{1}{2}\left(\Delta B_1^* - \Delta B_2^*\right)\rho v^2 \tag{2.55}$$

2-20

As can be seen from Equation 2.55, the nominal ballistic coefficients of the two satellites cancel one another in the relative frame when they are equal, and only the *differential* ballistic coefficient due to the orientation of the panels affects the motion of the formation such that the only external acceleration seen in the relative frame is the drag acceleration

$$a_d = \frac{1}{2} \left(\Delta B_1^* - \Delta B_2^* \right) \rho v^2 \tag{2.56}$$

This same argument can be extended to the gravitational perturbations acting on the formation. As long as the two satellites are identical and are in a tight formation, the differential forces acting upon the formation will be negligible, allowing the two satellites to remain in formation with little disturbance.

III. Control Law

When considering the optimal control of a linear system using quadratic performance criteria, two linear quadratic control laws come to mind: a regulator and a terminal controller. A regulator is designed to maintain a system within an acceptable deviation of some reference condition using acceptable amounts of control, while a terminal controller is designed to drive a system from some initial state to the desired final state over a finite time period, exhibiting acceptable behavior along the way [3]. The purpose of this study is to optimally reconfigure a two-satellite formation, driving the satellites from some initial state to a final state dependent upon the desired formation while minimizing the loss of orbital energy of the formation. Since the goal is to reconfigure the formation, not to perform station keeping of a current formation, a terminal controller was selected. This is not to say that a linear quadratic regulator (LQR) control law cannot be used to reconfigure satellite formations. In fact, as mentioned in Chapter I, several instances exist where a LQR control law was used for reconfigurations. These control laws usually weight both the state error and the control usage within the performance index at every point in time, increasing the weight on the state error matrix to decrease the time required to perform the reconfiguration, or increasing the weight of the control usage penalty matrix to reduce the amount of control used to drive the state error to zero. This study is not concerned with a time optimal reconfiguration. Instead, the goal is to perform the reconfiguration over a user-specified time and meet the final conditions while minimizing the loss in energy as a result of the maneuver. Therefore, for this study, a linear quadratic terminal control law is ideal.

Within this chapter, the issue of controllability will be discussed for a single satellite in Section 3.1. Then, the state equations for the controller will be developed in Section 3.2 and applied to the terminal controller in Section 3.3. Finally, the constraint equations will be defined in Section 3.4.

3.1 State Equations and Controllability

The CW equations derived in Section 2.1.1 will be used to describe the relative motion of the satellites for this study. The current definition relates the motion of one satellite with respect to a reference position, so only one satellite will be considered for the moment. The only external force acting on the satellite that affects its relative motion with respect to the formation is atmospheric drag, which acts against the velocity vector of the satellite. Since this study assumes the reference orbit is circular, drag acts in the negative $\mathbf{e}_\theta$ direction, as defined in Figure 2.1. It is assumed that the relative velocity components of the satellite do not affect the drag acceleration. Instead, only the orbital velocity of the circular reference orbit will be considered since it is on the order of 10^4 larger than the relative velocities. As a result, the drag acceleration acts only on the in-track component of the motion, and all other differential forces will be considered zero. Therefore, the force per unit mass components from Equations 2.15-2.17 become

$$f_r = 0 \tag{3.1}$$

$$f_\theta = -\frac{1}{2}B^*\rho v^2 \tag{3.2}$$

$$f_z = 0 \tag{3.3}$$

The satellite is controlled by changing the angle of attack of the drag panels to alter the presented area of the satellite. This change in the presented area is directly proportional to the change in the ballistic coefficient, as shown in Equation 2.49. So changing the magnitude of the ballistic coefficient directly alters the amount of drag acting on the satellite. Therefore, the ballistic coefficient magnitude is the control input for this study.

The equations of motion for the satellite can now be written in state equation form such that

$$\frac{d}{dt}\mathbf{x}(t) = F\mathbf{x}(t) + Gu(t) \tag{3.4}$$

3-2

where

$$\mathbf{x} = \begin{bmatrix} \delta r & r_0 \delta\theta & \delta z & \delta\dot{r} & r_0\delta\dot{\theta} & \delta\dot{z} \end{bmatrix}^T \qquad (3.5)$$

$$F = \begin{bmatrix} 0 & 0 & 0 & 1 & 0 & 0 \\ 0 & 0 & 0 & 0 & 1 & 0 \\ 0 & 0 & 0 & 0 & 0 & 1 \\ 3n^2 & 0 & 0 & 0 & 2n & 0 \\ 0 & 0 & 0 & -2n & 0 & 0 \\ 0 & 0 & -n^2 & 0 & 0 & 0 \end{bmatrix} \qquad (3.6)$$

$$G = \begin{bmatrix} 0 & 0 & 0 & 0 & -\frac{1}{2}\rho v^2 & 0 \end{bmatrix}^T \qquad (3.7)$$

$$u = B^* \qquad (3.8)$$

Before moving forward with these equations, the controllability should be checked. For complete state controllability, an unconstrained control input that will transfer the system from some initial state, $\mathbf{x}_0$, to some final state, $\mathbf{x}_f$, in a finite time interval must exist [16]. From the state equation definition shown in Equation 3.4, it can be seen that the cross-track component, δz, is decoupled from the in-plane motion components, δr and $\delta\theta$. As a result, any motion or force that results in the cross-track direction has no effect on the in-plane motion. Likewise, any motion or force in the in-plane motion has no effect on the cross-track motion. Because of this cross-track decoupling, the δz component cannot be controlled through drag, which acts on the in-plane motion only. This lack of control can be confirmed through the controllability matrix. For a system to be completely state controllable, the rank of the the $n \times n$ controllability matrix must be n, or, written mathematically [3]:

$$Rank\left(\begin{bmatrix} G & \vdots & FG & \vdots & F^2G & \vdots & \cdots & \vdots & F^{n-1}G \end{bmatrix}_{n \times n} \right) = n \qquad (3.9)$$

This condition verifies that each column of the controllability matrix is linearly independent [16]. If the system is not complete state controllable, one or more of the states is uncontrollable. The controllability matrix for the six-state system defined in Equation 3.4 only has a rank of four, meaning two states are uncontrollable. From the decoupled cross-track discussion above, we can conclude that the δz and $\delta \dot{z}$ components are indeed uncontrollable. Therefore, redefining the state such that only the in-plane motion is accounted for yields

$$\mathbf{x} = \begin{bmatrix} \delta r & r_0 \delta \theta & \delta \dot{r} & r_0 \delta \dot{\theta} \end{bmatrix}^T \tag{3.10}$$

Then, the new system of equations becomes

$$\begin{bmatrix} \delta \dot{r} \\ r_0 \delta \dot{\theta} \\ \delta \ddot{r} \\ r_0 \delta \ddot{\theta} \end{bmatrix} = \begin{bmatrix} 0 & 0 & 1 & 0 \\ 0 & 0 & 0 & 1 \\ 3n^2 & 0 & 0 & 2n \\ 0 & 0 & -2n & 0 \end{bmatrix} \begin{bmatrix} \delta r \\ r_0 \delta \theta \\ \delta \dot{r} \\ r_0 \delta \dot{\theta} \end{bmatrix} + \begin{bmatrix} 0 \\ 0 \\ 0 \\ -\frac{1}{2}\rho v^2 \end{bmatrix} [B^*] \tag{3.11}$$

This new four-vector state yields a controllability matrix with a rank of four. As a result, the system is completely controllable.

3.2   Controller State Equations

Since the control law is dependent on the motion of both satellites in the formation, the state of the system should be defined to include the state of each satellite. So, define the controller state vector, $\mathbf{x}$, as

$$\mathbf{x}(t) = \begin{bmatrix} \mathbf{x}_1(t) \\ \mathbf{x}_2(t) \end{bmatrix}_{8 \times 1} \tag{3.12}$$

such that

$$\mathbf{x}(t) = \begin{bmatrix} \delta r_1 & r_0 \delta \theta_1 & \delta \dot{r}_1 & r_0 \delta \dot{\theta}_1 & \vdots & \delta r_2 & r_0 \delta \theta_2 & \delta \dot{r}_2 & r_0 \delta \dot{\theta}_2 \end{bmatrix}^T \tag{3.13}$$

3-4

Since each satellite is controlled separately, the control input, $\mathbf{u}$, is defined by

$$\mathbf{u}(t) = \begin{bmatrix} B_1^*(t) \\ B_2^*(t) \end{bmatrix}_{2 \times 1} \tag{3.14}$$

where B_1^* and B_2^* are the ballistic coefficients for each satellite caused by the drag panel orientation. The state equations then become

$$\dot{\mathbf{x}}(t) = F\mathbf{x}(t) + G\mathbf{u}(t) \tag{3.15}$$

where

$$F = \begin{bmatrix} F_1 & 0_{4 \times 4} \\ 0_{4 \times 4} & F_2 \end{bmatrix}_{8 \times 8} \tag{3.16}$$

$$G = \begin{bmatrix} G_1 & 0_{4 \times 1} \\ 0_{4 \times 1} & G_2 \end{bmatrix}_{8 \times 2} \tag{3.17}$$

Here, $0_{4 \times 4}$ and $0_{4 \times 1}$ are (4×4) and (4×1) zero matrices, respectively. And since the two satellites are associated with the same reference orbit,

$$F_1 = F_2 = \begin{bmatrix} 0 & 0 & 1 & 0 \\ 0 & 0 & 0 & 1 \\ 3n^2 & 0 & 0 & 2n \\ 0 & 0 & -2n & 0 \end{bmatrix} \tag{3.18}$$

$$G_1 = G_2 = \begin{bmatrix} 0 & 0 & 0 & -\frac{1}{2}\rho v^2 \end{bmatrix}^T \tag{3.19}$$

The matrices F and G are assumed time-invariant since they are functions of the orbital mean motion, n, and the satellite velocity with respect to the atmosphere, v, of the reference orbit, both of which will be considered constant over the controlled orbit.

Because the altitude of the reference orbit is decreasing with the controlled input, these variables are actually changing. However, even for large reconfigurations that result in a considerable change in altitude, the change in mean motion and satellite velocity are minimal. As an example, a large reconfiguration with an initial reference orbital radius of $6800 \ km$ that causes an altitude loss of $275 \ m$ results in a 0.0061% change in mean motion and a 0.0025% change in velocity. Therefore, the assumptions that F and G are constant are valid within the bounds of this study.

The ballistic coefficients considered for this study are the ballistic coefficients caused by the deployment of the drag panels only, not the overall ballistic coefficients of the satellites themselves. As discussed in Section 2.4, the ballistic coefficients of the satellite bodies will cancel in the relative frame, assuming the two satellites are identical. If the ballistic coefficients of the satellites are not equal and one satellite has a slightly larger nominal ballistic coefficient, the second satellite's panels can be oriented such that the two ballistic coefficients of the satellites are equal, thereby defining a new nominal state for the second satellite. As a result, the second satellite will fly with a higher drag acceleration than it would normally sustain. This increased drag will shorten the life of the formation, but this tradeoff is necessary to maintain the formation for any extended period of time. And since only the differential drag affects the motion of the satellites, the least amount of total drag should be used to achieve the desired differential state. Therefore, to minimize the drag and, as a direct result, the overall energy loss of the formation, only one satellite should have its drag panels deployed at any time during a reconfiguration. The other satellite should keep its panels in the drag minimizing state, which is zero for the relative frame. For example, when satellite 1 has its drag panels deployed, the ballistic coefficient of satellite 2 due to its drag panels is zero such that $B_2^* = 0$, and vice versa when satellite 2 has its drag panels deployed.

3.3   Linear-Quadratic Terminal Controller

The goal of the controller is to meet the terminal conditions while minimizing the change in energy of each satellite in the formation. As explained in Section 2.3, since drag acts against the motion of the satellite, any change in energy that results from the control

input in this case decreases the overall energy of the satellite. Therefore, minimizing the change in energy is equivalent to minimizing the loss in energy. This characteristic plays well into a quadratic performance index since squaring the change in energy is equivalent to squaring the loss of energy. By selecting a quadratic performance index and keeping the constraints linear, a linear-quadratic terminal controller can be implemented to reconfigure a formation with optimal control inputs that are linear feedbacks on the state variables [2]. A performance index that penalizes the change in orbital energy of each satellite is chosen, such that

$$ J = \frac{1}{2} \int_{t_0}^{t_f} \left(\left| \frac{d\mathcal{E}_1}{dt} \right|^2 + \left| \frac{d\mathcal{E}_2}{dt} \right|^2 \right) dt \tag{3.20} $$

where $\mathcal{E}_1$ and $\mathcal{E}_2$ are the orbital energies of satellite one and satellite two, respectively. To reconfigure the formation to the desired final formation, terminal conditions must be applied to the control law. By keeping the terminal constraints *soft* such that the terminal error is driven close to zero but not necessarily exactly to zero, the penalty function can be made quadratic as well and appended to the performance index. Define the quadratic penalty function on the terminal error as

$$ \phi[\mathbf{x}(t_f)] = \frac{1}{2} \mathbf{e}_f^T Q_f \mathbf{e}_f \tag{3.21} $$

where Q_f is an (8×8) diagonal error weighting matrix, and $\mathbf{e}_f$ is the terminal error vector given by

$$ \mathbf{e}_f = M_f \mathbf{x}(t_f) - \boldsymbol{\psi} \tag{3.22} $$

M_f and $\boldsymbol{\psi}$ are the terminal state matrix and the terminal state vector, respectively, and are defined to satisfy the terminal conditions. These two variables are dependent on the final formation and will be defined in Section 3.4.

Appending the penalty function from Equation 3.21 to the performance index from Equation 3.20 yields the overall performance index [2]

$$J = \frac{1}{2}\mathbf{e}_f^T Q_f \mathbf{e}_f + \frac{1}{2}\int_{t_0}^{t_f}\left(\mathbf{u}^T R\mathbf{u}\right) dt \tag{3.23}$$

subject to the conditions

$$\dot{\mathbf{x}}(t) = F\mathbf{x}(t) + G\mathbf{u}(t) \tag{3.24}$$

$$\mathbf{x}(t_0) = \mathbf{x}_0 \tag{3.25}$$

Here, F and G are the matrices defined in Equations 3.16 and 3.17 in the previous section, and R is the control penalty matrix that is defined to satisfy the performance penalty in Equation 3.20. From Equations 2.47 and 2.52, the energy rate of change for one satellite can be written as

$$\frac{d\mathcal{E}}{dt} = -\frac{1}{2}B^* \rho v^3 \tag{3.26}$$

The performance index defined in Equation 3.20 is quadratic in terms of the energy rate of change. Therefore, by this definition, the control penalty matrix R must be chosen to yield

$$\left|\frac{d\mathcal{E}_1}{dt}\right|^2 + \left|\frac{d\mathcal{E}_2}{dt}\right|^2 = \frac{1}{4}(B_1^*)^2\rho^2 v^6 + \frac{1}{4}(B_2^*)^2\rho^2 v^6 \tag{3.27}$$

Since the control input for the two-satellite system is $\mathbf{u} = [B_1^*, B_2^*]^T$, R becomes the positive definite matrix defined as

$$R = \begin{bmatrix} \frac{1}{4}\rho^2 v^6 & 0 \\ 0 & \frac{1}{4}\rho^2 v^6 \end{bmatrix} \tag{3.28}$$

From the performance index and the equations of motion, the Hamiltonian, $\mathcal{H}$, can be formed, yielding

$$\mathcal{H} = \frac{1}{2}\mathbf{u}^T R \mathbf{u} + \boldsymbol{\lambda}^T (F\mathbf{x} + G\mathbf{u}) \tag{3.29}$$

where $\boldsymbol{\lambda}$ is the costate vector. Then, from the Hamiltonian, the Euler-Lagrange necessary conditions are formed:

$$\dot{\mathbf{x}} = \frac{\partial \mathcal{H}}{\partial \boldsymbol{\lambda}} = F\mathbf{x} + G\mathbf{u} \tag{3.30}$$

$$\dot{\boldsymbol{\lambda}} = -\frac{\partial \mathcal{H}}{\partial \mathbf{x}} = -F^T \boldsymbol{\lambda} \tag{3.31}$$

$$0 = \frac{\partial \mathcal{H}}{\partial \mathbf{u}} = R\mathbf{u} + G^T \boldsymbol{\lambda} \tag{3.32}$$

Solving Equation 3.32, which is also known as the stationarity condition, for $\mathbf{u}(t)$ yields the optimal control law in terms of the costates:

$$\mathbf{u}(t) = -R^{-1} G^T \boldsymbol{\lambda}(t) \tag{3.33}$$

The final costates can be found from the final state penalty function defined in Equation 3.21:

$$\boldsymbol{\lambda}(t_f) = \left(\frac{\partial \phi}{\partial \mathbf{x}} \right)^T = M_f^T Q_f \left[M_f \mathbf{x}(t_f) - \boldsymbol{\psi} \right] \tag{3.34}$$

Then, combining Equations 3.30, 3.31, and 3.33 yields the two-point boundary value problem:

$$\begin{bmatrix} \dot{\mathbf{x}} \\ \dot{\boldsymbol{\lambda}} \end{bmatrix} = \begin{bmatrix} F & -GR^{-1}G^T \\ 0_{8\times8} & -F^T \end{bmatrix} \begin{bmatrix} \mathbf{x} \\ \boldsymbol{\lambda} \end{bmatrix} \tag{3.35}$$

subject to the boundary conditions

$$\mathbf{x}(t_0) \;=\; \mathbf{x}_0 \tag{3.36}$$

$$\boldsymbol{\lambda}(t_f) \;=\; M_f^T Q_f \left[M_f \mathbf{x}(t_f) - \boldsymbol{\psi} \right] \tag{3.37}$$

The block diagram for this linear-quadratic terminal control law is shown in Figure 3.1.
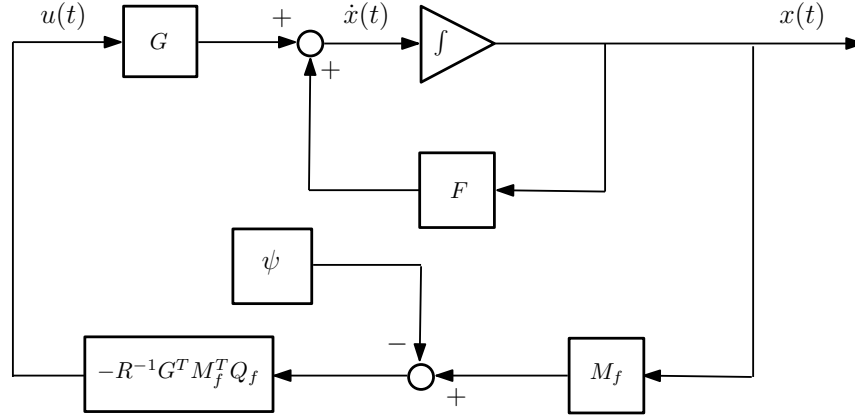
Figure 3.1   Block Diagram of the Linear-Quadratic Terminal Control Law

Since the equations are linear, a state transition matrix can be used to propagate the final costates $\boldsymbol{\lambda}_f$ from Equation 3.34 *backward* in time to obtain the initial costates $\boldsymbol{\lambda}_0$ at time t_0 [2]. Since the system is also time-invariant, the *forward* state transition matrix, $\Phi(t_f, t_0)$, can be determined from the matrix exponential, such that [8]

$$\Phi(t, t_0) = \epsilon^{H(t-t_0)} = I + H(t-t_0) + \frac{1}{2!}H^2(t-t_0)^2 + \frac{1}{3!}H^3(t-t_0)^3 + \cdots + \frac{1}{k!}H^k(t-t_0)^k + \cdots \tag{3.38}$$

where H is the (16×16) matrix defined in the two-point boundary value problem in Equation 3.35, rewritten here for convenience:

$$H = \begin{bmatrix} F & -GR^{-1}G^T \\ 0_{8\times 8} & -F^T \end{bmatrix}_{16\times 16} \tag{3.39}$$

The state transition matrix can then be partitioned such that

3-10

$$
\begin{bmatrix} \mathbf{x}(t) \\ \boldsymbol{\lambda}(t) \end{bmatrix} = \begin{bmatrix} \Phi_{11}(t,t_0) & \Phi_{12}(t,t_0) \\ \Phi_{21}(t,t_0) & \Phi_{22}(t,t_0) \end{bmatrix} \begin{bmatrix} \mathbf{x}(t_0) \\ \boldsymbol{\lambda}(t_0) \end{bmatrix} \tag{3.40}
$$

A method of obtaining the initial costates, $\boldsymbol{\lambda}(t_0)$, now exists. From the final costate equation shown in Equation 3.37 and from the system of equations defined in Equation 3.40, $\boldsymbol{\lambda}(t_0)$ becomes

$$
\boldsymbol{\lambda}(t_0) = \left\{ \Phi_{22}(t_f) - M_f^T Q_f M_f \Phi_{12}(t_f) \right\}^{-1} \left\{ \left[M_f^T Q_f M_f \Phi_{11}(t_f) - \Phi_{21}(t_f) \right] \mathbf{x}(t_0) - M_f^T Q_f \boldsymbol{\psi} \right\} \tag{3.41}
$$

where $\Phi(t_f) \equiv \Phi(t_f, t_0)$ for brevity. Now with the initial conditions $\mathbf{x}(t_0)$ and $\boldsymbol{\lambda}(t_0)$, the system of equations in Equation 3.35 can be integrated forward in time, yielding $\mathbf{x}(t)$ and $\boldsymbol{\lambda}(t)$. Then, from Equation 3.33, the optimal control input $\mathbf{u}(t)$ can be found.

The Euler-Lagrange equations, shown in Equations 3.30-3.32, are the necessary conditions that must be satisfied for an optimal solution. Meeting these conditions ensures a stationary solution has been found, but it does not necessarily guarantee a minimum solution. A second-order sufficient condition for a minimum solution is given by the Legendre-Clebsch condition, defined as [20]

$$
\frac{\partial^2 \mathcal{H}}{\partial \mathbf{u}^2} > 0 \tag{3.42}
$$

Satisfying both the Euler-Lagrange necessary conditions and the Legendre-Clebsch sufficient condition guarantees the control solution found for $\mathbf{u}(t)$ provides at least a local minimum for the Hamiltonian. For this study, the Legendre-Clebsch condition yields

$$
\frac{\partial^2 \mathcal{H}}{\partial \mathbf{u}^2} = R \tag{3.43}
$$

where R is the control penalty matrix defined in Equation 3.28. This matrix is positive definite, satisfying the Legendre-Clebsch condition and proving that the solution found is indeed the optimal solution.

The equations derived in this section are dependent on the terminal state matrix M_f and the terminal state vector ψ, which dictate the final formation type. These conditions will be developed next in Section 3.4.

3.4 Terminal Constraints

Since drag allows only in-plane control, the formation types a drag-actuated controller can achieve are limited. Therefore, only two formation designs will be considered for this study: in-plane and elliptical. These formation-types are the bases for more sophisticated formations that require cross-track, or out-of-plane, control, such as repeat groundtrack, circular, and projected circular formations [18]. The reconfigurations of the formation began with some initial state for the satellites based on the initial formation, and the terminal state for the controller was defined for a zero radial displacement between the two such that, when the control ended, the satellites had an in-track displacement only with some specified radial and in-track velocity to achieve the desired formation. Also, to eliminate any confusion, the leading satellite in the formation at the beginning of the control input has been designated satellite 1, while the trailing satellite is satellite 2. For reconfigurations where the satellites have a zero in-track displacement, the satellite at the lower altitude is designated satellite 1.

Upon reconfiguration of the formation, certain final conditions must be satisfied to place the satellites in the desired final formation. These conditions vary depending on the formation type. However, one condition that must be met regardless of the formation type is a zero, or at least a highly suppressed, in-track drift between the satellites. Minimizing or zeroing the in-track drift between the two satellites keeps the uncontrolled formation from drifting apart, reducing the need for additional control to maintain the formation. This reduction in control results in long-term cost savings, whether the cost relates to conventional expendables or, in this case, altitude.

To suppress the in-track drift, the secular terms of the uncontrolled solution developed in Section 2.1.2 must be minimized or zeroed. The in-track solution contains the only secular terms in the force free solution. From Equation 2.33, the resulting secular drift for one satellite with respect to the reference position is

$$\delta\theta_{secular} = r_0\delta\dot{\theta} + 2n\delta r \tag{3.44}$$

For formation keeping about an empty reference position, the only concern is that the two satellites in the formation are not drifting apart, not necessarily drifting apart with respect to the reference point. So as long as the two satellites are drifting away from the reference position with the same rate and direction, the formation will remain intact. Then, the reference position can be redefined to match the resulting drift from the original reference position, thereby zeroing any drift in the newly selected frame. Therefore, the *relative* drift of the satellites should be zeroed, such that

$$r_0(\delta\dot{\theta}_1 - \delta\dot{\theta}_2) + 2n(\delta r_1 - \delta r_2) = 0 \tag{3.45}$$

Achieving this constraint ensures the formation will not degrade due to the nominal motion of the satellites.

Depending upon the desired formation, additional constraints must be imposed along with the in-track constraint described above. The constraints required to achieve the in-plane and elliptical formations will be discussed.

3.4.1 In-Plane Formation. The in-plane formation is perhaps the simplest of all formations. The two satellites share the same orbital plane but are separated in the in-track direction by their true anomaly [18]. So one satellite is flying ahead of the other in the same orbit, as shown in Figure 3.2. Again, since drag does not allow cross-track control, the initial cross-track displacement and velocity must be zero. For the in-plane formation, a constraint must be imposed on the radial component to dampen out the radial oscillation. As the satellite radius increases with respect to the reference position, the satellite's orbital period increases, causing it to fall behind in the in-track direction. Likewise, when the radius decreases, the satellite moves ahead of the reference position. As a result of this radial oscillation, an in-track oscillation also results. Therefore, to maintain the two satellites in the same orbital plane and at a fixed distance apart, the radial oscillation must be suppressed. The radial component from Equation 2.28 is
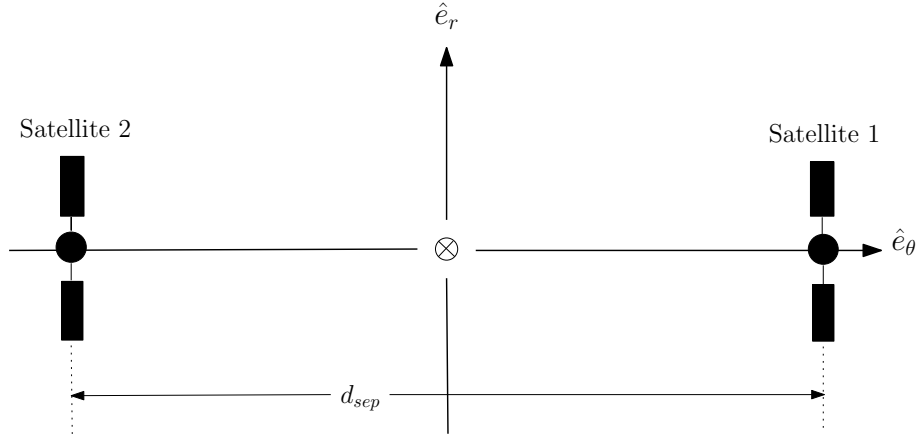
Figure 3.2   Illustration of the In-Plane Formation in the Relative Frame

$$\delta r(t) = -\left(\frac{2}{n}r_0\delta\dot{\theta}_0 + 3\delta r_0\right)\cos nt + \frac{\delta\dot{r}_0}{n}\sin nt + \frac{2}{n}r_0\delta\dot{\theta}_0 + 4\delta r_0 \qquad (3.46)$$

The δr_0 and $r_0\delta\dot{\theta}$ terms are already being constrained to zero the in-track drift, as shown in Equation 3.45. So the only term left to work with is the radial velocity from the sine coefficient. Again, the interest is to have the two satellites move together. As a result, the sine coefficients from each satellite should be subtracted, such that

$$\delta\dot{r}_1 - \delta\dot{r}_2 = 0 \qquad (3.47)$$

Suppressing this term ensures the satellites will not oscillate, or will at least oscillate together, in the radial direction over time.

Satisfying the constraint in Equation 3.47 ensures the satellites are in the same orbital plane, but the distance between the two satellites is not specified. Therefore, to place the satellites a set distance apart, a constraint must be placed on the in-track distance component of the system equations. To achieve a set separation distance of d_{sep}, the following constraint must be met:

$$r_0\delta\theta_1 - r_0\delta\theta_2 = d_{sep} \qquad (3.48)$$

This in-track separation distance constraint, coupled with the radial oscillation constraint in Equation 3.47 and the suppressed in-track drift constraint from Equation 3.45, results in the desired in-plane formation.

These constraints can then be used to form the terminal constraint matrix, M_f, and the terminal state vector, ψ, both of which were defined in Equation 3.22. Therefore, from the constraints defined in Equations 3.45, 3.47, and 3.48, define the very sparse diagonal matrix M_f and the terminal state vector ψ:

$$M_{f(in-plane)} = \begin{bmatrix} 2n & 0 & \dots & & & & & \\ 0 & 1 & 0 & \dots & & & & \\ \dots & 0 & 1 & 0 & \dots & & & \\ & \dots & 0 & 1 & 0 & \dots & & \\ & & \dots & 0 & -2n & 0 & \dots & \\ & & & \dots & 0 & -1 & 0 & \dots \\ & & & & \dots & 0 & -1 & 0 \\ & & & & & \dots & 0 & -1 \end{bmatrix} \tag{3.49}$$

$$\psi_{in-plane} = \begin{bmatrix} 0 & \frac{d_{sep}}{2} & 0 & 0 & \vdots & 0 & \frac{d_{sep}}{2} & 0 & 0 \end{bmatrix}^T \tag{3.50}$$

Applying Equations 3.49 and 3.50 in the optimal control law defined in Section 3.3 results in the desired in-plane formation.

3.4.2 Elliptical Formation.   In an elliptical formation, the two satellites appear to orbit the reference position on the order of one orbital period of the system. A 2-by-1 ellipse is the natural formation, with the maximum in-track separation being twice the maximum radial separation as illustrated in Figure 3.3. These dimensions are evident in the solution to the CW equations shown in Equation 2.33. The coefficients of both the cosine and the sine terms of the $r_0 \delta\theta$ solution are double the coefficients of the δr solution, resulting in a natural 2-by-1 ellipse given any radial or in-track velocity or a radial displacement.
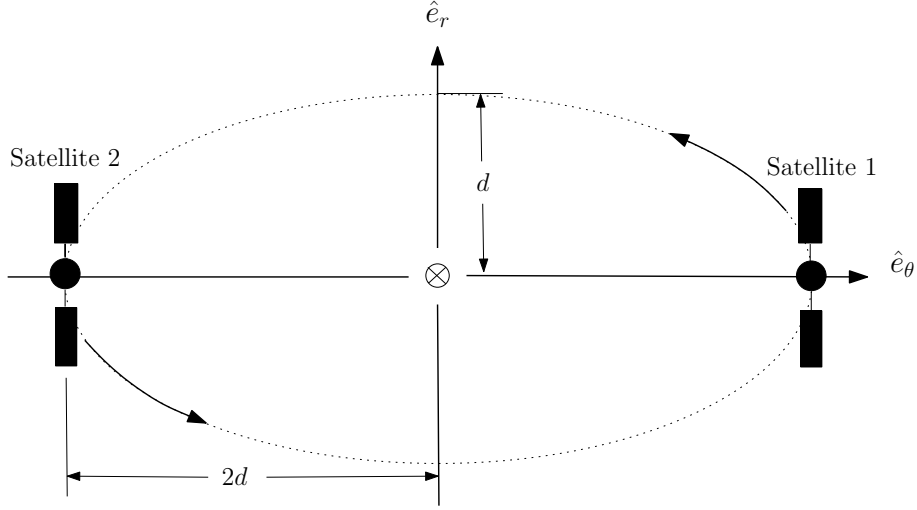
Figure 3.3   Illustration of the Elliptical Formation in the Relative Frame

For an elliptical formation, a prescribed radial oscillation is required to enable the satellite to orbit the reference position in a 2-by-1 ellipse. This prescribed oscillation can be achieved by just focusing on the sine term. By choosing the proper radial velocity difference, the desired ellipse can be formed. Subtracting the two sine terms results in

$$\frac{\delta \dot{r}_1}{n} - \frac{\delta \dot{r}_2}{n} = \delta r_{max} \tag{3.51}$$

where δr_{max} is the radial separation required to place the satellites in the prescribed elliptical formation. Since the maximum radial distance is half the maximum in-track distance, δr_{max} can be solved for in terms of $\delta \dot{r}_{rel}$, the velocity magnitude of each satellite required to place the satellites in the elliptical formation, such that

$$\delta r_{max} = \frac{d_{sep}}{2} = \frac{\delta \dot{r}_{rel}}{n} \tag{3.52}$$

$$\delta \dot{r}_{rel} = \frac{n d_{sep}}{2} \tag{3.53}$$

Then, the radial velocity constraint can be defined as

3-16

$$\delta \dot{r}_1 - \delta \dot{r}_2 = \delta \dot{r}_{rel} \tag{3.54}$$

By meeting this radial velocity constraint defined in Equation 3.54 along with the in-track drift constraint from Equation 3.45 and the in-track separation distance constraint from Equation 3.48, each satellite will trace the same 2-by-1 ellipse in the radial/in-track plane.

These constraints can then be used to form the terminal state vector, $\boldsymbol{\psi}$, which was defined in Equation 3.22. Since the same states from the in-plane formation are being constrained, the terminal constraint matrix M_f is the same as the one defined in Equation 3.49. Based on the constraints defined in Equations 3.45, 3.48, and 3.54, the terminal constraint matrix M_f and the terminal state vector $\boldsymbol{\psi}$ become

$$M_{f(elliptical)} = M_{f(in-plane)} \tag{3.55}$$

$$\boldsymbol{\psi}_{elliptical} = \begin{bmatrix} 0 & \frac{d_{sep}}{2} & \frac{\delta \dot{r}_{rel}}{2} & 0 & \vdots & 0 & \frac{d_{sep}}{2} & \frac{\delta \dot{r}_{rel}}{2} & 0 \end{bmatrix}^T \tag{3.56}$$

Applying this vector along with the matrix defined in Equation 3.49 in the optimal control law defined in Section 3.3 results in the desired elliptical formation.

IV. Results

Reconfigurations to both the in-plane and elliptical formations were performed from initial formations of in-plane, elliptical, and a post-payload separation position. The post-payload separation is intended to represent an initial formation placement after the satellites have been released from their launch vehicle, assuming they were launched together. The optimal control law presented in Chapter III is a fixed-time routine, meaning the user specifies the amount of time over which the optimization will take place. The fixed-time input allows the user to extend the time of the reconfiguration to reduce the control input magnitude throughout the reconfiguration. The ability to increase or decrease the time allows the user to specify a transfer that will most effectively make use of the allotted control input without exceeding that amount. Also, extending the time allowed for the transfer tightens the constraints for most cases, resulting in terminal conditions that match the terminal constraints more closely. A conservative value of $0.1 \, m^2/kg$ was chosen for the maximum differential ballistic coefficient magnitude for this study. As for the time allowed for the reconfiguration, a natural time-scale for orbital motion is an orbital period. And for the elliptical formation, each satellite completes one full orbit of the reference position in the relative frame over one orbital period. As such, the reconfiguration durations have been specified in terms of orbital periods for the reference orbit.

A concern when applying optimization routines with soft terminal constraints is the final weight of both the final constraints and the control cost within the performance index. The goal is to minimize the performance index while meeting the terminal constraints and minimizing the control cost. But if too much effort is applied to reducing the final constraint error, the control input is not necessarily optimal. As such, a small terminal constraint cost is desired, so the final control and terminal constraint costs are provided for each maneuver as a performance measure. Note that the units are ignored for these costs since only the weight of each measure is needed. Also, when dealing with spacecraft transfers and formation reconfigurations, maneuver costs are generally quantified by a Δv budget since the actual fuel budget is dependent upon the spacecraft mass. While the method of transfer for this study is different from conventional techniques, a Δv budget will be determined for each reconfiguration based on the total amount of control applied

to each satellite. Due to the continuous, low-thrust nature of the control input, these maneuvers will result in a higher fuel cost than optimal impulsive burn maneuvers using conventional thrusters, but the costs are within the same order of magnitude. Also, these costs are associated with different fuel measures; a conventional thruster fuel cost is related directly to expendables onboard the spacecraft, while the fuel cost in this study is related to altitude. Despite the difference, a Δv budget is provided for each reconfiguration.

The post reconfiguration plots presented in Sections 4.2 and 4.3 contain a radial position deviation from the expected final position and an in-track separation between the two satellites over the duration of the 20 orbital period propagation. The radial position deviation is on the sub-millimeter level for most cases, a level of precision that is most likely undetectable with current positioning techniques. But the author feels it is important to present this deviation to provide insight into the cause of the in-track drift, which is on the centimeter level over the duration of the propagation. This centimeter-level drift would be detectable for phased array applications, so for a thorough investigation, the drift is presented.

This chapter presents the results of the simulation based on the equations of motion presented in Chapter II and the control law presented in Chapter III. Section 4.1 verifies the equations of motion used for this study were properly coded by checking against a separate set of equations. Sections 4.2 and 4.3 present the results of reconfigurations into in-plane and elliptical formations. All of the results presented within this chapter had a reference orbital radius of $6800\,km$. For the reverse of the reconfigurations presented within this chapter, see Appendix A, and for reconfigurations performed at a reference orbital radius of $7000\,km$, see Appendix B.

4.1 Code Verification

The equations of motion were numerically integrated using MATLAB's *ode45* integrator. To verify the integrated equations of motion were correct, both the unforced and the forced equations were tested using different methods. The unforced equations were verified versus the force free solution presented in Section 2.1.2. Integrating over the same final time as that entered for the final time of the closed form solution given a zero control

input and equal initial conditions, the solutions should be equal within integration error. For the forced solution, a state transition matrix solution was formed to verify the results from the numerical integration. Both of these validation tests will be further discussed.

4.1.1 Unforced Solution. To verify the numerically integrated solution to the unforced equations of motion, the closed form solution developed in Section 2.1.2 was used. The equations of motion of a satellite was integrated over three orbital periods. With a reference orbital radius of $6800\,km$, the state vector of the satellite for this example was

$$\mathbf{x}_0 = \left[\begin{array}{cccc} 10m & 0 & 0 & 0 \end{array}\right]^T \tag{4.1}$$

The total time was divided into 500 equal intervals, and the differences between the radial and in-track results for both the numerically integrated solution and the closed form solution were plotted. Figure 4.1 shows the plot of the solution in the radial/in-track plane to give an idea of the general motion of the satellite, and Figure 4.2 shows the radial and in-track differences over the length of the integration. As shown in Figure 4.1, the satellite falls behind the reference position as expected due to its larger orbital radius, which results in a larger orbital period. The radius also oscillates as a direct result of its slight orbital eccentricity, returning to its original position with each orbital period. Figure 4.2 shows the two solutions agree to the sub-micrometer level over the three orbital periods, proving the equations of motion are properly coded. The solutions begin to deviate more toward the end of the integration period due to the integration error, not errors in the equations. Because the integrator uses only the previous solution for each subsequent time-step, discarding all other points, the integration error tends to build with time. However, the error is acceptable for this study since the maximum time of integration in most cases is limited to 20 orbital periods, although this time is increased for several simulations with an orbital radius of $7000\,km$.

4.1.2 Forced Solution. While the force free solution to the CW equations has a nice closed form solution, such an analytical solution does not exist for the forced equations. Even the forced solution presented in Section 2.1.3 must be integrated. Also, the
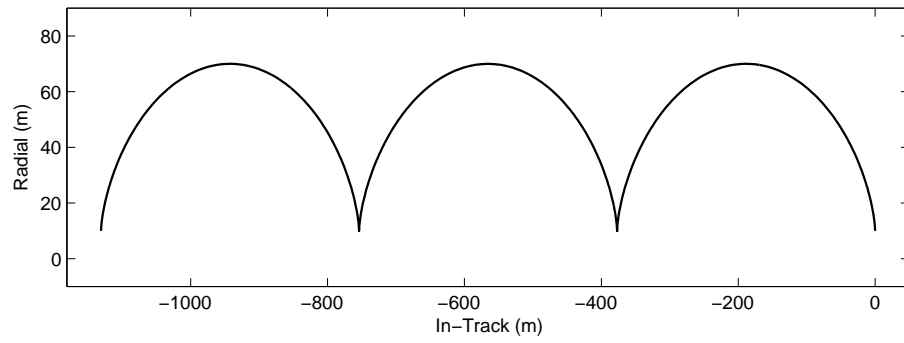
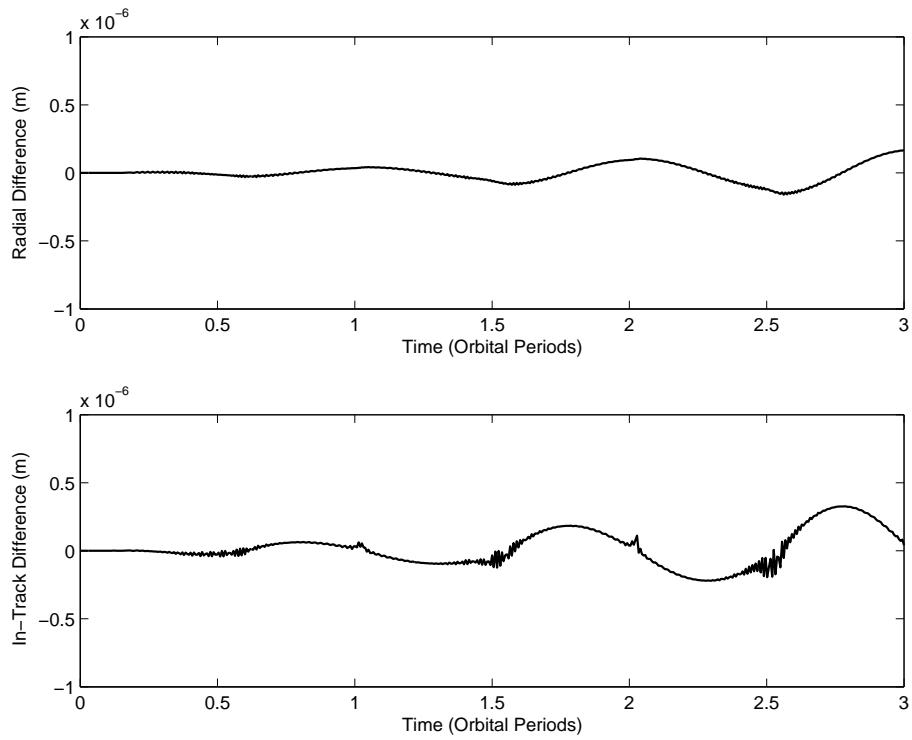Figure 4.1   In-Plane Plot of the Unforced Solution

Figure 4.2   Radial and In-Track Differences: Unforced Solution

way in which the forced solution is presented for this study is slightly different from the solution shown in Section 2.1.3. The initial control input in terms of the costates, $\boldsymbol{\lambda}(t_0)$, is prescribed, and the following control inputs are then determined from the overall system of equations. To correctly verify the numerically integrated system of equations, a system that performs in the same way should be implemented. Therefore, a separate linear model was developed to meet this requirement.

Using the same state transition matrix derived in Section 3.3, an approximate linear solution is developed, such that

$$
\begin{bmatrix} \mathbf{x}(t + \Delta t) \\ \boldsymbol{\lambda}(t + \Delta t) \end{bmatrix} = \begin{bmatrix} \Phi_{11}(t + \Delta t, t) & \Phi_{12}(t + \Delta t, t) \\ \Phi_{21}(t + \Delta t, t) & \Phi_{22}(t + \Delta t, t) \end{bmatrix} \begin{bmatrix} \mathbf{x}(t) \\ \boldsymbol{\lambda}(t) \end{bmatrix} \tag{4.2}
$$

As can be seen from this solution, the subsequent inputs for both the state, $\mathbf{x}(t)$, and costates, $\boldsymbol{\lambda}(t)$, are contained within the system, equivalent to the system of equations that are integrated. As such, this linear solution should provide a solution that relates closely to the numerical integration.
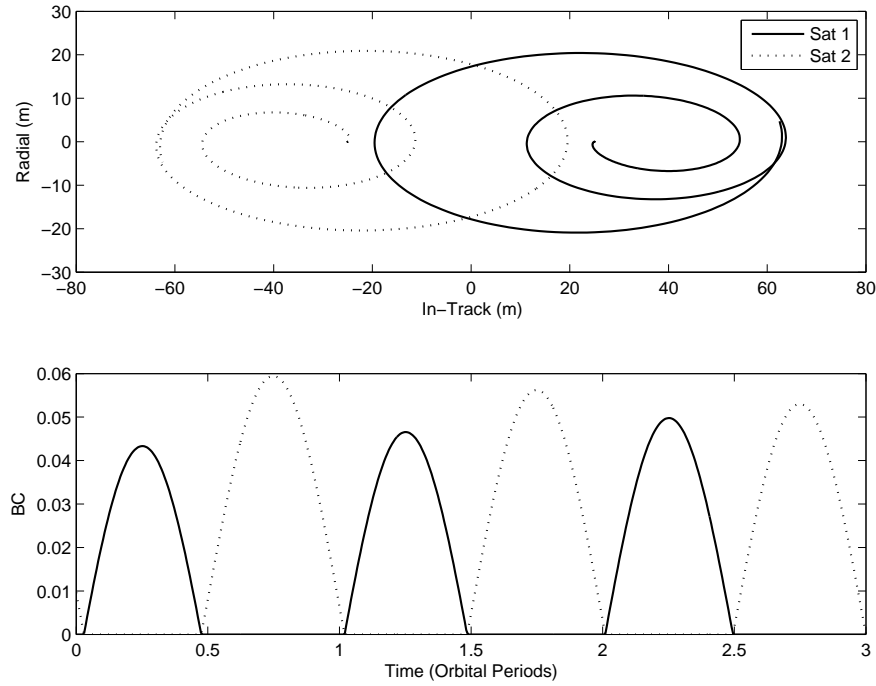

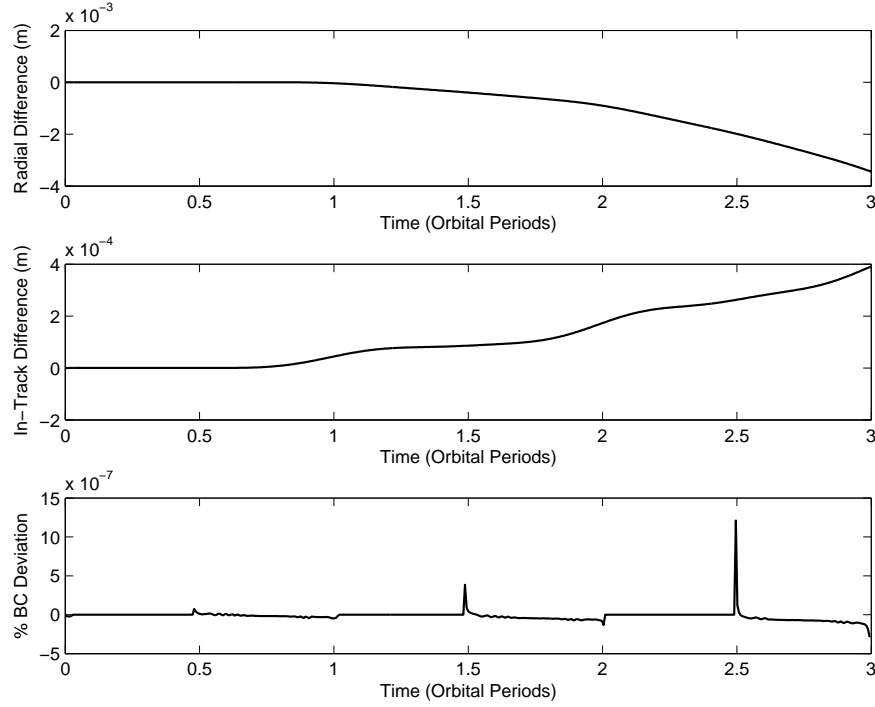Figure 4.3   In-Plane Plot of the Forced Solution

4-5

Figure 4.4   Radial, In-Track, and Control Input Differences: Forced Solution

To check the numerically integrated system of equations against this linear formulation, a reconfiguration was ordered from an initial in-track formation with a $50\,m$ separation to a final elliptical formation with an in-track width of $200\,m$. The entire transfer will not be performed; instead, only the first three orbital periods will be calculated to remain consistent with the unforced solution verification. Propagating over three orbital periods provides a sufficient number of data points to verify the equations are being implemented correctly. Figure 4.3 shows the in-plane motion of the two satellites in the falling relative frame along with their control inputs with respect to time. These plots were provided to give an idea of the overall motion and inputs of each satellite in the formation, with the motion of Satellite 1 depicted by the solid line and Satellite 2 by the dotted line. Figure 4.4 shows the differences between the numerically integrated solution and the linear solution for the radial displacement and in-track displacement, and plots the percent difference for the control input solutions. As shown by the plots, the radial solutions agree to within a few millimeters, while the in-track solutions agree to sub-millimeter accuracy. Also, the

control inputs agree on the order of 10^{-6} of a percent, verifying that the forced system of equations are properly coded.

4.2   Reconfiguration to an In-Plane Formation

This section contains the results for reconfigurations into a final in-plane formation with a separation distance of $500\,m$ from three separate initial formations: an in-plane formation with a separation distance of $50\,m$, an elliptical formation with a semimajor axis of $25\,m$ such that the satellites are $50\,m$ apart in the in-track position, and a post-payload separation with initial conditions defined to represent two satellites that have recently separated upon delivery to their parking orbit. The satellite positions and motion are with respect to a $6800\,km$ reference orbit.

4.2.1   In-Plane to In-Plane.   An initial in-plane formation with a separation distance of $50m$ was reconfigured to a final in-plane formation with a separation distance of $500\,m$. This reconfiguration is relatively easy to perform since both satellites currently have no radial oscillations. So the goal for the reconfiguration is to induce an in-track drift to increase the size of the formation, then zero the drift by bringing the satellites back in-line at the same altitude. Since this is a relatively simple reconfiguration, only four orbital periods were required for the transfer. Figure 4.5 shows the control inputs for each satellite, with satellite 1 plotted with a solid line and satellite 2 plotted with a dotted line. A maximum ballistic coefficient input of only $0.029\,m^2/kg$ was required to perform the transfer, well below the maximum value allowed. To effect the reconfiguration, satellite 1, the leading satellite, deployed its panels first, dropping in altitude to gain the needed separation before satellite 2 initiated its control input. The figure also shows that both satellites required the same control input, just in reverse order, resulting in a final Δv of $0.01048\,m/sec$ for each satellite to perform the maneuver. Figures 4.6 and 4.7 show the radial/in-track position plots of the satellite motion in both the fixed relative frame and the falling relative frame. As shown in the fixed frame, the overall altitude decreases approximately $18\,m$ due to the reconfiguration. The plots also confirm the control usage as both satellites follow equivalent trajectories to their final states. Figure 4.8 shows the

radial and in-track displacements from the reference position plotted over the duration of the reconfiguration. This figure shows that the satellites exhibit acceptable behavior throughout the transfer and that the motion of the satellites responded well to the input. Also, the maximum radial displacement occurs midway through the reconfiguration, which is expected to occur at this point since the two satellites increase their relative velocities over the first half of the reconfiguration, and then use the second half of the transfer to decrease their relative velocities to zero as they approach the $500\,m$ separation distance. Finally, the optimality performance was verified, with the performance index yielding a control cost of 0.65, while the terminal constraint cost was only $1e-5$, several orders of magnitude less.

After the transfer was completed, the post-reconfiguration analysis was performed at the new altitude and with the new mean motion. The final state from the controlled motion was propagated over 20 orbital periods, or approximately 30 hours, to ensure the transfer met the desired, final formation. Figure 4.9 shows the result of the reconfiguration in the radial/in-track plane. As shown in the figure, a final in-plane formation with an in-track separation distance of $500\,m$ resulted from the transfer. The figure contains the radial and in-track position for each satellite over the full 20 orbital periods. From the figure, no drift is evident between the two satellites, but due to the scale, a small drift would be difficult to detect. Therefore, the difference between the actual and expected radial position, as well as the difference between the actual and expected in-track separation between the two satellites, were calculated for this position data set and were plotted over the duration over the propagation, as shown in Figure 4.10. As evident from the figure, each satellite has a slight oscillation in the radial direction with an amplitude of $0.24\,mm$, and the two satellites have slightly different orbital radii, with satellite 2 flying approximately $0.5\,mm$ above satellite 1 on average. This radial difference leads to a slight drift between the two satellites, causing the formation to spread approximately $8\,cm$ over the 20 orbit propagation, as shown in the in-track deviation plot. This drift is well within the bounds of the constraints and does not have noticeable effects on the formation, proving that the optimization routine satisfied the constraints of the problem.

Table 4.1   In-Plane to In-Plane Reconfiguration Details, $6800\,km$

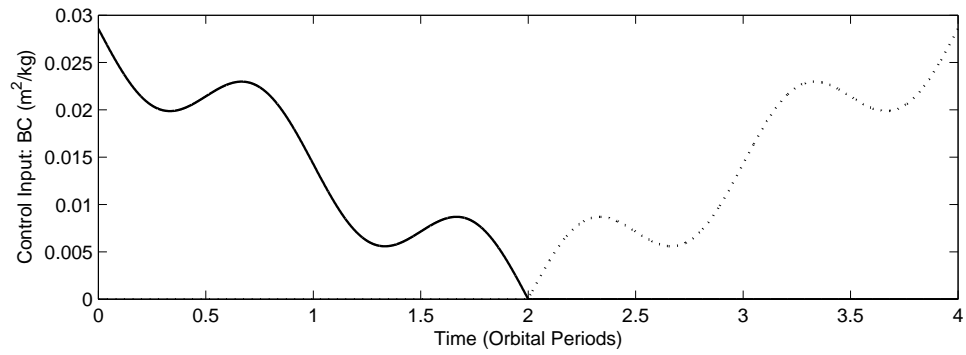| Reference Orbital Radius	$6800\,km$
Initial Formation	In-Plane: $50\,m$ separation
Final Formation	In-Plane: $500\,m$ separation
Total Time for Reconfiguration	4 Orbital Periods ($6\,hr$, $12\,min$, $2\,sec$)
Maneuver Cost	$\Delta v_1\,=\,0.01048\,m/sec$
	$\Delta v_2\,=\,0.01048\,m/sec$
Altitude Loss	$18.41\,m$
Control Cost	0.65
Constraint Cost	$1e{-}5$

Figure 4.5   Control Input: In-Plane to In-Plane, $6800\,km$
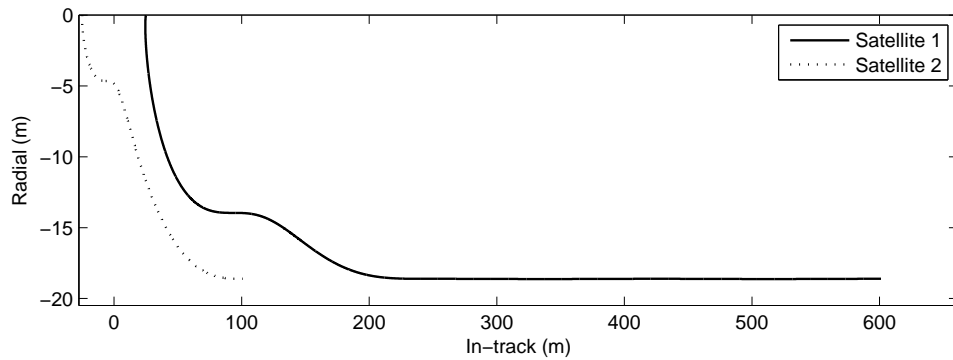

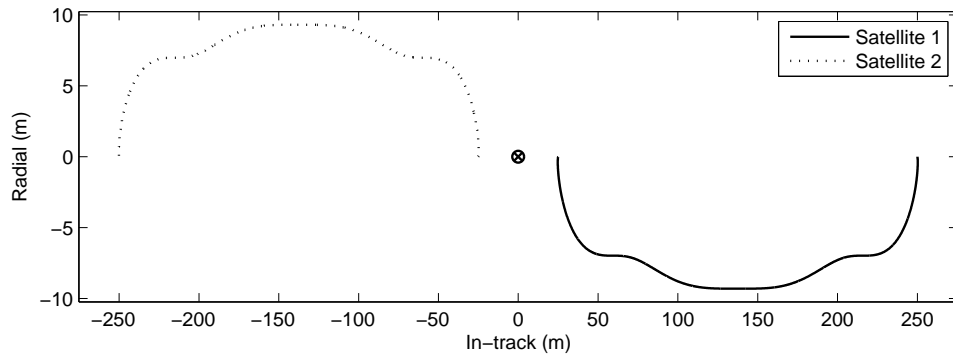Figure 4.6   Fixed Frame Plot: In-Plane to In-Plane, $6800\,km$

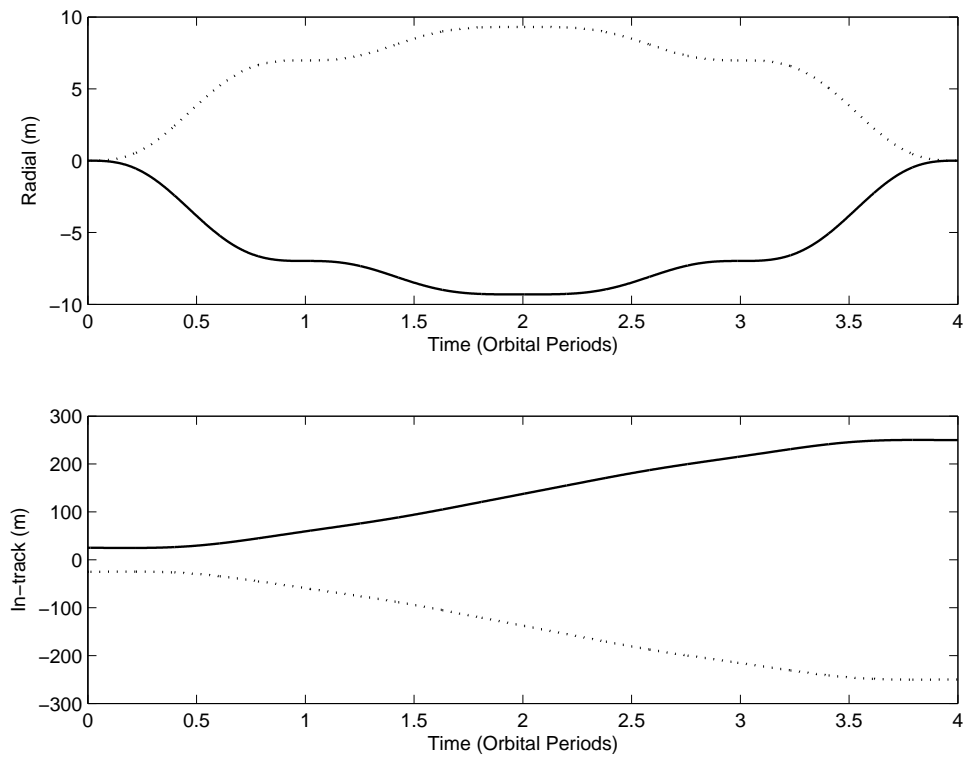Figure 4.7   Falling Frame Plot: In-Plane to In-Plane, $6800\,km$

Figure 4.8   Reconfiguration Time History Plot: In-Plane to In-Plane, $6800\,km$
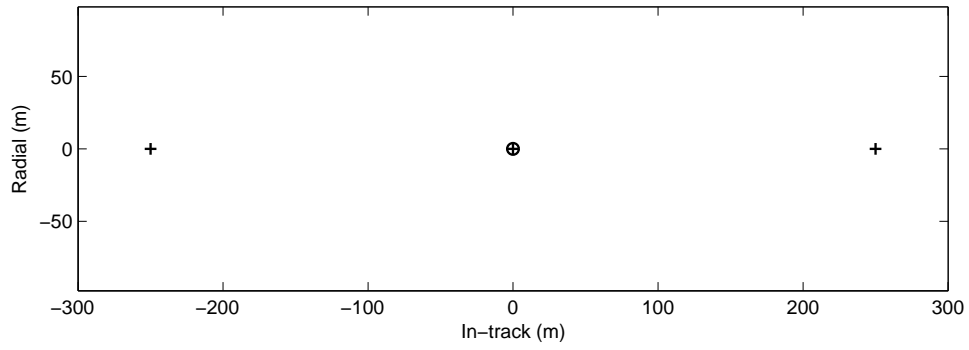
Figure 4.9   Post Transfer Plot: In-Plane to In-Plane, $6800\,km$
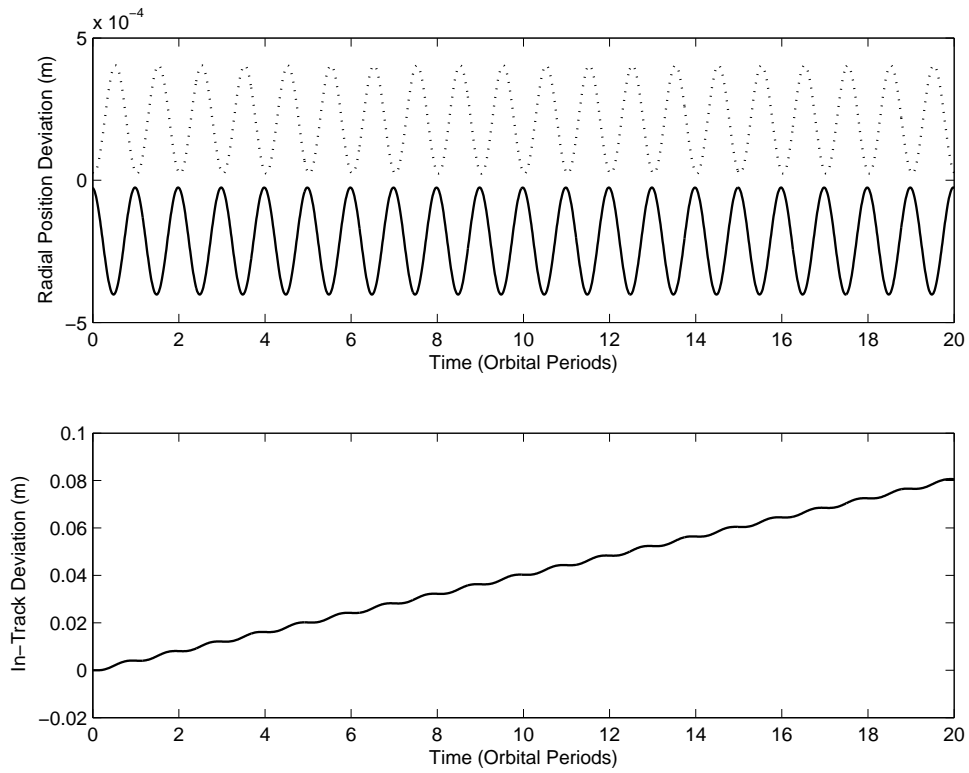

Figure 4.10   Post Transfer Time History: In-Plane to In-Plane, $6800\,km$

4.2.2   Elliptical to In-Plane.   The next reconfiguration performed started from an elliptical formation with an in-track separation distance of $50\,m$, or a relative semimajor axis of $25\,m$, and transferred to an in-plane formation with a separation distance of $500\,m$, the same final formation as in Section 4.2.1. To effect the transfer, the controller must reduce the radial oscillations of both satellites, effectively zeroing their eccentricities, while driving them into the proper in-plane formation at the correct separation distance. Due to the initial orbital eccentricities of the satellites, this transfer required a slightly larger control input than the previous reconfiguration. So the controlled time was increased to six orbital periods for this maneuver. Figure 4.11 shows the control inputs for each satellite. With the increased time for reconfiguration, a maximum ballistic coefficient input of only $0.028\,m^2/kg$ was required for the transfer. Again, notice that the control inputs for the two satellites are equal, but in reverse order. This trend is expected since the satellites have the same initial conditions at the start of the reconfiguration, but the directions are reversed. As a result, both satellites required the same total Δv of $0.01151\,m/sec$ to perform the reconfiguration. Figures 4.12 and 4.13 show the reconfiguration in both the fixed and falling reference frames. As shown in the fixed frame, the satellites drop $19\,m$ in altitude as a result of the reconfiguration. These plots also give insight into the trajectory taken by each satellite. Both satellites dampened their radial oscillation as they approached the appropriate in-track separation distance, but satellite 1 initially decreased its radial position while satellite 2 increased its radius to effect the drift, taking full advantage of their natural dynamics. Figure 4.14 confirms this approach, showing the time history plots of the reconfiguration for both the radial and the in-track distance components. Again, both satellites exhibit acceptable behavior throughout the reconfiguration. The radial oscillation is dampened to zero as the in-track separation distance is increased $500\,m$. The transfer resulted in a control cost of 0.61, while the terminal constraint cost was only $4e-6$, again several orders of magnitude less.

The post-reconfiguration results were then propagated over 20 orbital periods to show the resulting motion of the formation. Figure 4.15 shows a plot of the satellites' positions in the radial/in-track plane over the duration of the propagation. The satellites maintain the in-plane formation with a separation distance of $500\,m$ without much deviation. Plots of

the radial and in-track position deviations over time are shown in Figure 4.16. Again, the radial velocity components were not driven completely to zero, resulting in sub-millimeter oscillations with each orbital period, well within the bounds of the constraints but still enough to result in a slight drift. Since satellite 2 has a larger average radial displacement, a positive drift in the formation results, causing the satellites to drift apart $4.5\,cm$ over the 20 orbital periods.

Table 4.2   Elliptical to In-Plane Reconfiguration Details, $6800\,km$

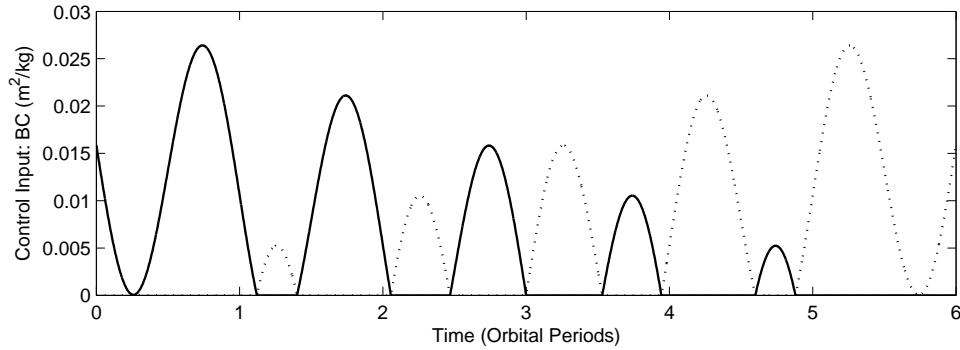| Reference Orbital Radius	$6800\,km$
Initial Formation	Elliptical: $25\,m$ semimajor axis
Final Formation	In-Plane: $500\,m$ separation
Total Time for Reconfiguration	6 Orbital Periods ($9\,hr$, $18\,min$, $3\,sec$)
Maneuver Cost	$\Delta v_1 = 0.01151\,m/sec$
	$\Delta v_2 = 0.01151\,m/sec$
Altitude Loss	$20.12\,m$
Control Cost	0.61
Constraint Cost	$4e{-}6$

Figure 4.11   Control Input: Elliptical to In-Plane, $6800\,km$
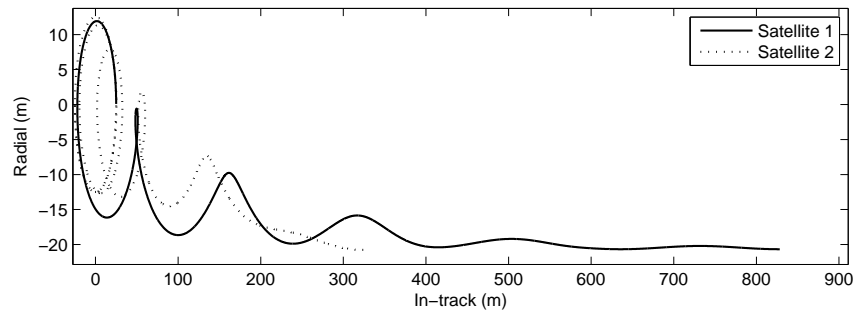
Figure 4.12   Fixed Frame Plot: Elliptical to In-Plane, $6800\,km$
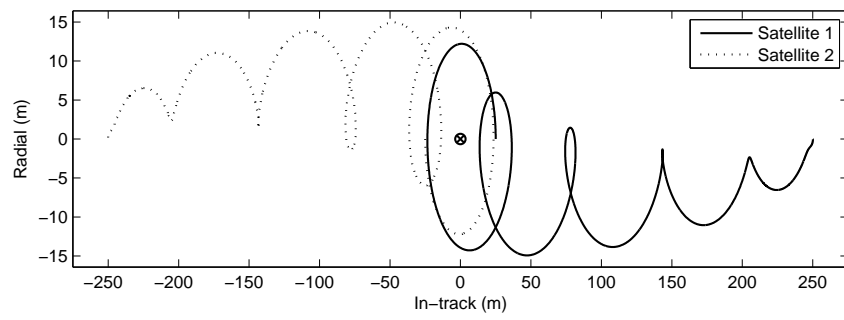

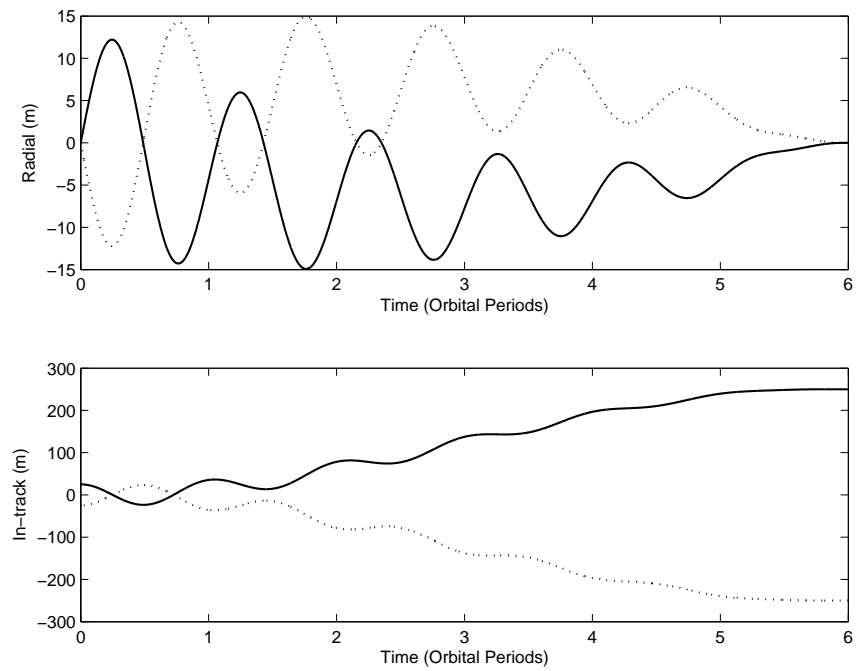Figure 4.13   Falling Frame Plot: Elliptical to In-Plane, $6800\,km$

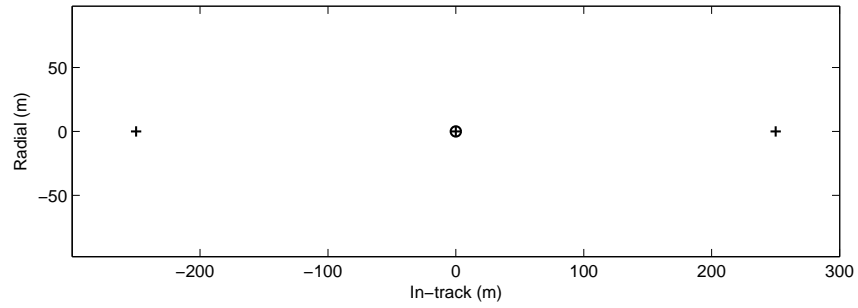Figure 4.14   Reconfiguration Time History Plot: Elliptical to In-Plane, $6800\,km$

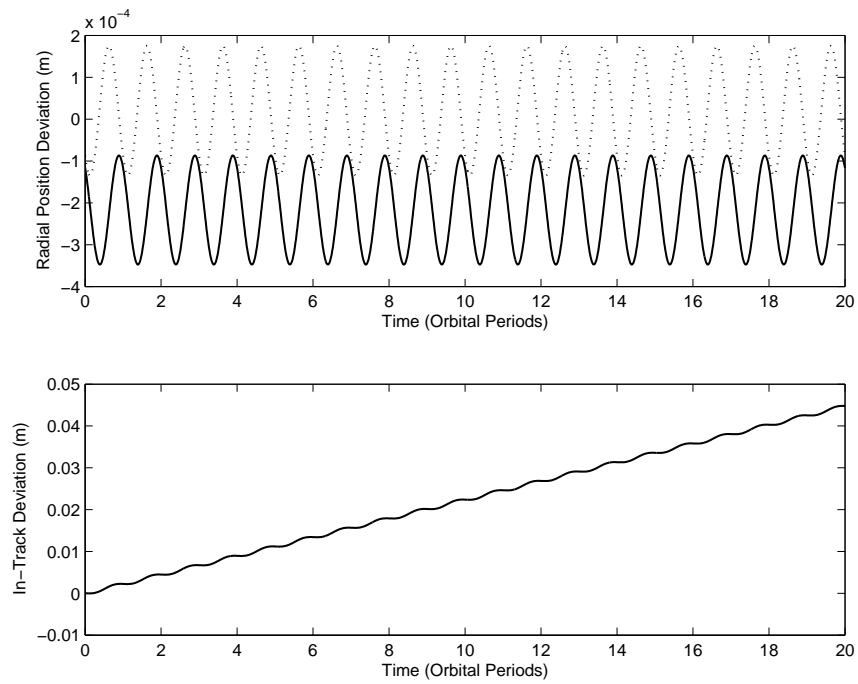Figure 4.15   Post Transfer Plot: Elliptical to In-Plane, $6800\,km$

Figure 4.16   Post Transfer Time History: Elliptical to In-Plane, $6800\,km$

4.2.3 Post-Payload Separation to In-Plane. Finally, a transfer to an in-plane formation from a post-payload separation configuration was performed. The initial states for the two satellites were defined as

$$\mathbf{x}_1 = [-10\,m,\ 20\,m,\ -0.04\,m/s,\ 0.005\,m/s] \tag{4.3}$$

$$\mathbf{x}_2 = [10\,m,\ -20\,m,\ 0.04\,m/s,\ -0.005\,m/s] \tag{4.4}$$

Again, the final in-plane formation had a separation distance of $500\,m$, equal to the previous two reconfigurations as shown in Table 4.3. The results from this transfer are quite different from the previous two reconfigurations to an in-plane formation. First, from the control input shown in Figure 4.17, satellite 2 uses more control than satellite 1, whereas the previous transfers required equal control inputs for each satellite. Some intuition into this control difference can be seen in the plot of the fixed reference frame, shown in Figure 4.18. Satellite 1 takes advantage of its natural dynamics from the initial conditions, going uncontrolled for most of three orbital periods, allowing its unforced trajectory to carry it forward approximately $1200\,m$ before slowing itself down and dampening its oscillation. The natural dynamics of satellite 2, on the other hand, were carrying it in the opposite direction, requiring the satellite to expend substantial control early into the reconfiguration to overcome this nominal motion. As a result, satellite 2 required a fuel budget of $\Delta v_2 = 0.05644\,m/sec$, while satellite 1 only required a budget of $\Delta v_1 = 0.02139\,m/sec$, less than half the amount of satellite 2. Despite the large reconfiguration, the maximum ballistic coefficient input required was only $0.06\,m^2/kg$ due to the amount of time allowed for the reconfiguration. Figure 4.20 shows the time history plots of the radial and in-track positions over the duration of the reconfiguration. Again, both satellites exhibit acceptable behavior, dampening out their radial oscillations over the course of the reconfiguration. Because of the larger reconfiguration and the need for a larger control input, the performance index cost was much higher, yielding a control cost of 4.14, while the constraint cost was lower than the previous maneuvers at only $2e - 6$.

The post-reconfiguration propagation results can be seen in Figures 4.21 and 4.22. The radial/in-track position plot shows the satellites in the in-plane formation with a separation distance of $500\,m$ without much deviation. The position deviation plots in Figure 4.22 shows a small radial oscillation with a total displacement of approximately $1.5\,mm$ that is slightly offset from zero, but both satellites are nearly oscillating together with satellite 1 following a slightly larger orbit. As a result, a negative drift results, causing the satellites to move together $2\,cm$ over the propagation. Again, these results are well within the bounds of the constraints and show that the optimization routine met the desired results.

Table 4.3   Payload Separation to In-Plane Reconfiguration Details, $6800\,km$

Reference Orbital Radius	$6800\,km$
Initial Conditions	$\mathbf{x}_1 = [-10\,m,\ 20\,m,\ -0.04\,m/s,\ 0.005\,m/s]$
	$\mathbf{x}_2 = [10\,m,\ -20\,m,\ 0.04\,m/s,\ -0.005\,m/s]$
Final Formation	In-Plane: $500\,m$ separation
Total Time for Reconfiguration	10 Orbital Periods ($15\,hr,\ 30\,min,\ 5\,sec$)
Maneuver Cost	$\Delta v_1\ =\ 0.02139\,m/sec$
	$\Delta v_2\ =\ 0.05644\,m/sec$
Altitude Loss	$64.65\,m$
Control Cost	4.14
Constraint Cost	$2e{-}6$
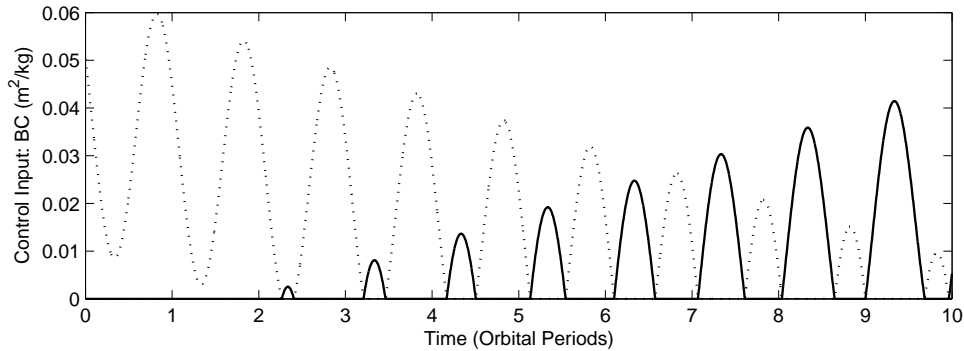
Figure 4.17   Control Input: Payload Separation to In-Plane, $6800\,km$

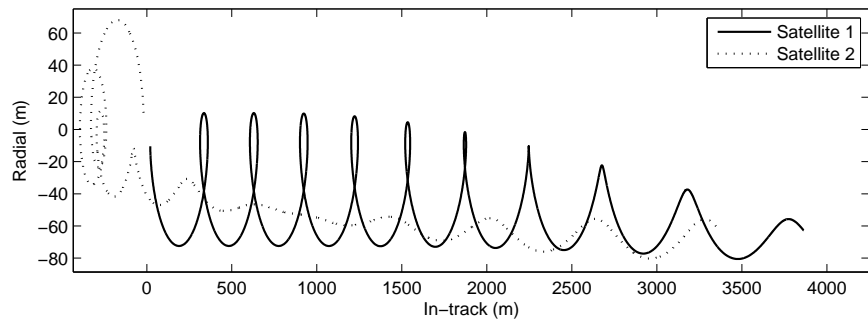Figure 4.18   Fixed Frame Plot: Payload Separation to In-Plane, $6800\,km$
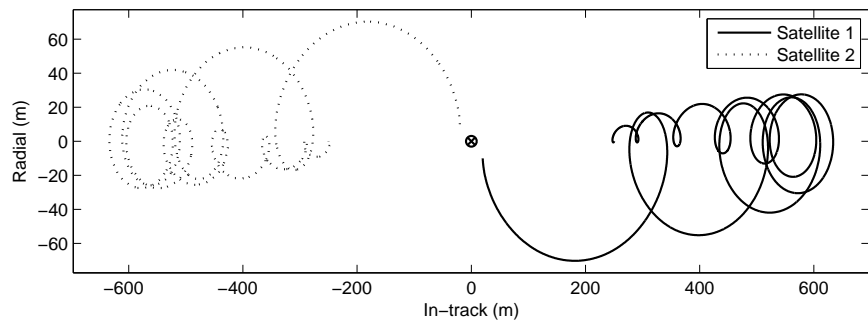

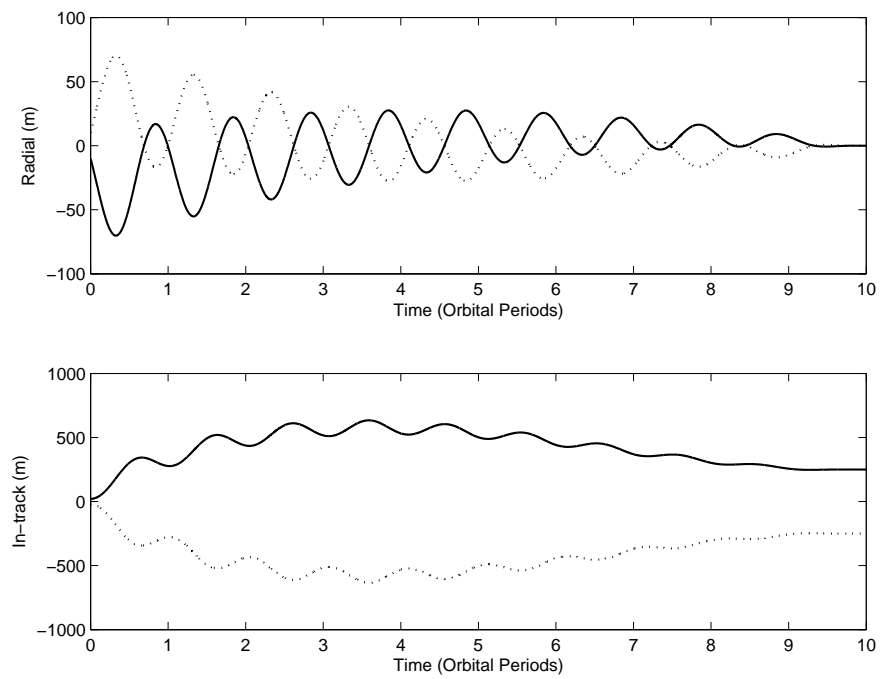Figure 4.19   Falling Frame Plot: Payload Separation to In-Plane, $6800\,km$

Figure 4.20   Reconfiguration Time History Plot: Payload Separation to In-Plane, $6800\,km$
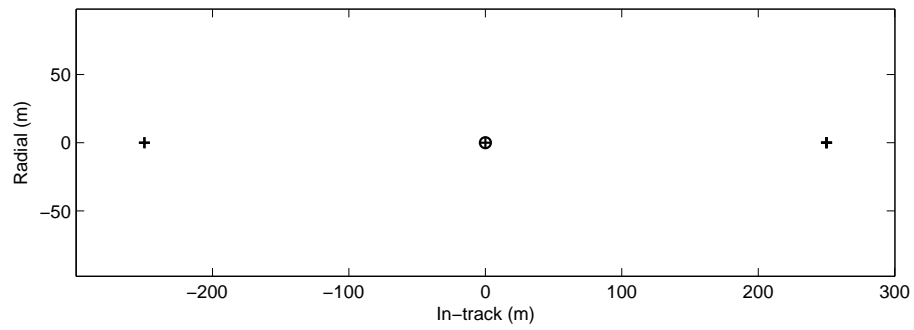
Figure 4.21   Post Transfer Plot: Payload Separation to In-Plane, $6800\,km$
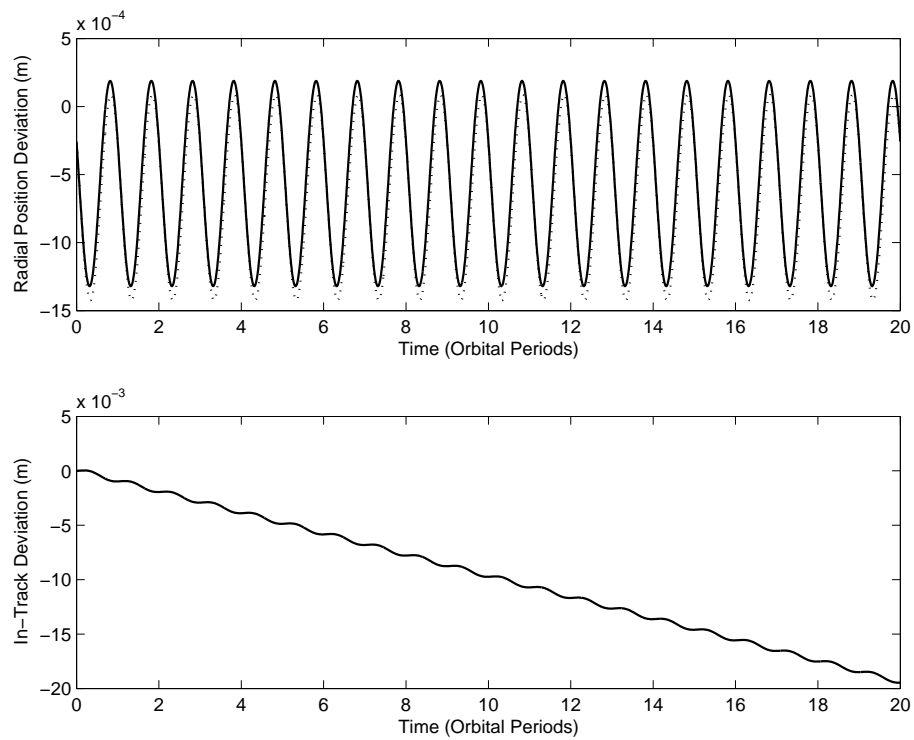

Figure 4.22   Post Transfer Time History: Payload Separation to In-Plane, $6800\,km$

4.3   Reconfiguration to an Elliptical Formation

This section contains the results for reconfigurations into a final elliptical formation with a semimajor axis of $250\,m$, such that the satellites are $500\,m$ apart when aligned in the in-track direction, from three separate initial formations: an in-plane formation with a separation distance of $50\,m$, an elliptical formation with a semimajor axis of $25\,m$, and a post-payload separation with the same initial conditions defined in Section 4.2. The satellite positions and motion are with respect to a $6800\,km$ reference orbit.

4.3.1   In-Plane to Elliptical.   The first transfer performed reconfigured a two-satellite in-plane formation with a separation distance of $50\,m$ to an elliptical formation with a semimajor axis of $250\,m$. The goal here is to create a radial oscillation that will project the satellites into the desired formation while limiting the drift and defining the proper dimensions of the relative orbit. Creating the radial oscillation to project the satellites into the correct orbital eccentricity required more control effort than the previous reconfigurations, so the transfer was performed over ten orbital periods to reduce the maximum input required. Figure 4.23 shows the control input required to effect the transfer for both satellites. A maximum ballistic coefficient input of $0.084\,m^2/kg$ was required for each satellite. Again, the inputs are equivalent, but in reverse order to most effectively take advantage of the natural motion of the system. This total control input resulted in a Δv for each satellite of $0.08964\,m/sec$. The fixed and falling reference frame plots of the radial/in-track motion of the satellites can be seen in Figures 4.24 and 4.25. As shown in the fixed frame plot, the formation altitude decreases approximately $150\,m$ as a result of the reconfiguration. The reference frame plots show that the satellites take advantage of their natural motion, gradually increasing their radial oscillation as they spiral outward to the desired position. To gain the needed separation, satellite 1 decreased its average, relative altitude as satellite 2 increased its average, relative altitude to obtain the needed in-track separation. These dynamics are also evident in the radial and in-track position time history plots shown in Figure 4.26. The radial oscillation increases over the duration of the reconfiguration, producing the needed in-track oscillation as well. The plots show

that the satellites exhibit acceptable behavior throughout the transfer, remaining within the bounds of the final motion.

The resulting state from the reconfiguration was then propagated over 20 orbital periods to ensure the desired conditions were met. The radial/in-track position plot of the satellite motion is shown in Figure 4.27. As shown in the figure, the desired elliptical formation resulted from the reconfiguration with both satellites following the same relative orbit with no noticeable drift. The position deviation plots in Figure 4.28 shows the radial oscillation is slightly larger than prescribed, but well within any reasonable constraint bounds. Also, satellite 1 is in a slightly larger orbit, effecting a $2\,cm$ negative drift between the satellites over the propagated time.

Table 4.4   In-Plane to Elliptical Reconfiguration Details, $6800\,km$

Reference Orbital Radius	$6800\,km$
Initial Formation	In-Plane: $50\,m$ separation
Final Formation	Elliptical: $250\,m$ semimajor axis
Total Time for Reconfiguration	10 Orbital Periods ($15\,hr$, $30\,min$, $5\,sec$)
Maneuver Cost	$\Delta v_1 = 0.08964\,m/sec$
	$\Delta v_2 = 0.08964\,m/sec$
Altitude Loss	$148.92\,m$
Control Cost	18.32
Constraint Cost	$1e{-}5$

Figure 4.23   Control Input: In-Plane to Elliptical, $6800\,km$
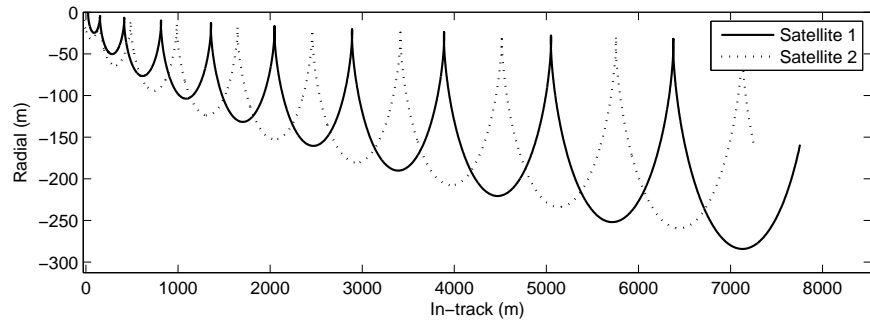
Figure 4.24 Fixed Frame Plot: In-Plane to Elliptical, $6800\,km$
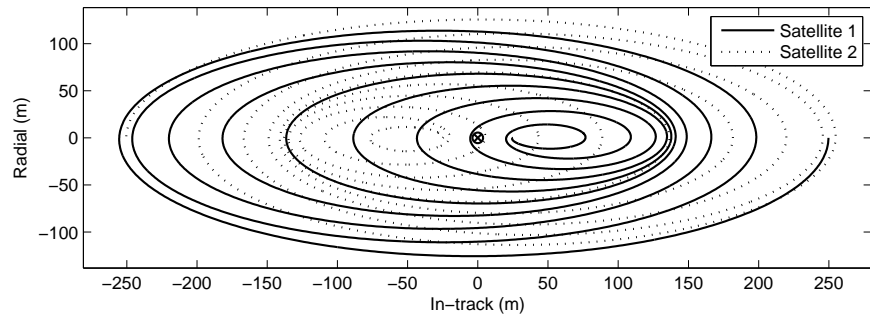

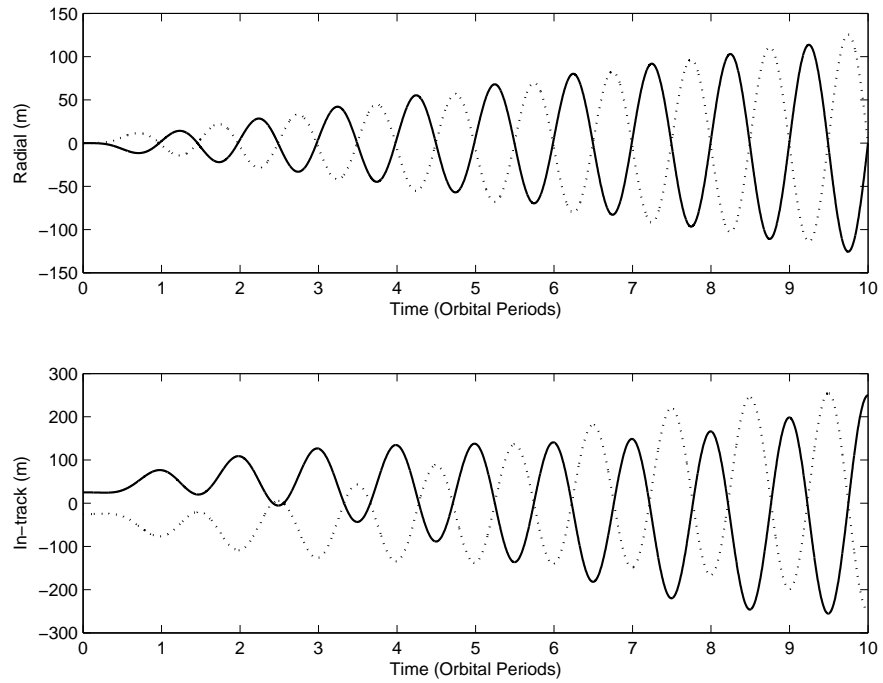Figure 4.25 Falling Frame Plot: In-Plane to Elliptical, $6800\,km$

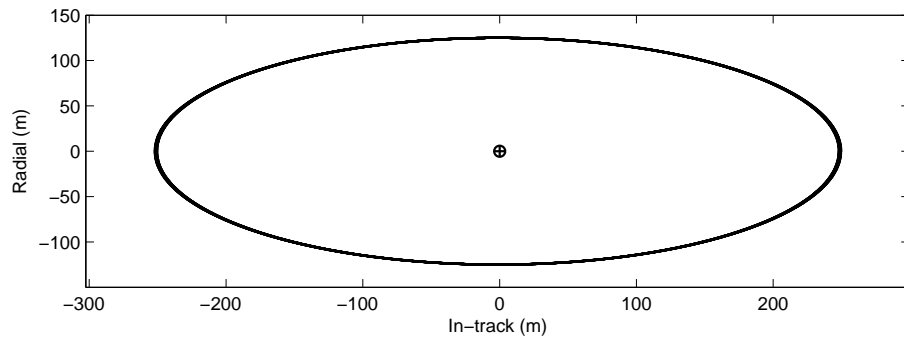Figure 4.26 Reconfiguration Time History Plot: In-Plane to Elliptical, $6800\,km$

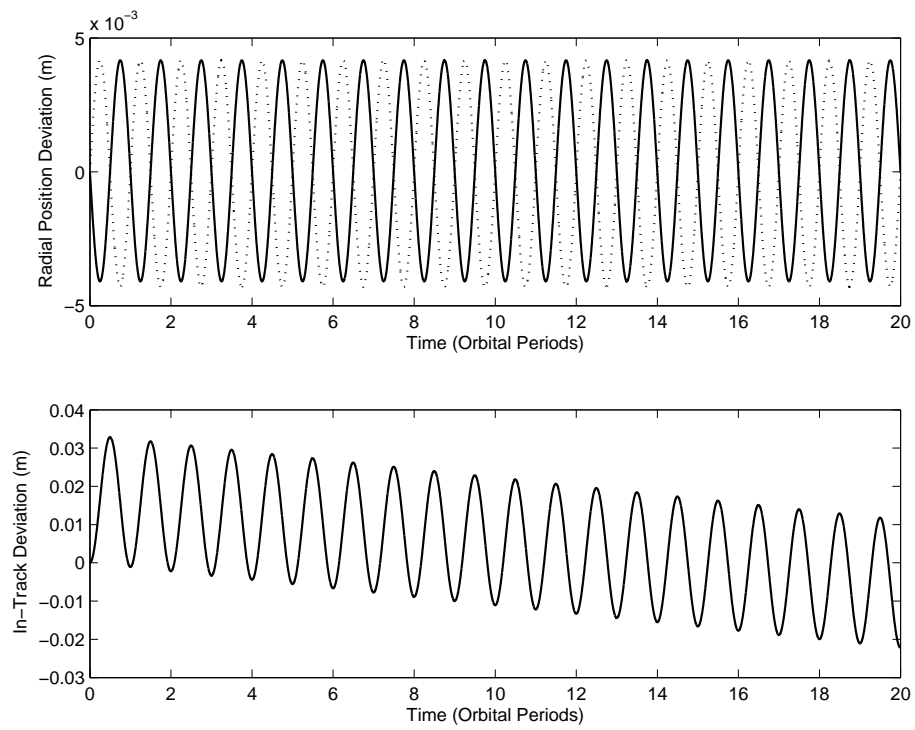Figure 4.27   Post Transfer Plot: In-Plane to Elliptical, $6800\,km$

Figure 4.28   Post Transfer Time History: In-Plane to Elliptical, $6800\,km$

4.3.2 Elliptical to Elliptical. An elliptical formation with a semimajor axis of $25\,m$ was expanded to $250\,m$ for this reconfiguration. Both satellites already have a radial oscillation, so the magnitude of the oscillation must be increased while the satellites move apart to position themselves into the new formation. This reconfiguration was performed over 8 orbital periods, as shown in Table 4.5, which provides an overview of the transfer. The control inputs for each satellite are shown in Figure 4.29. Again, both control inputs are equal, resulting in a total Δv of $0.08069 m/sec$ for each satellite with a maximum ballistic coefficient input of approximately $0.096 m^2/kg$. Figures 4.30 and 4.31 show the radial/in-track position plots of the satellite motion in both the fixed and falling frames. From the falling frame, it is evident that the controller is simply spiralling the two satellites outward, increasing both their radial oscillation and in-track separation distance over the length of the reconfiguration. Figure 4.32 confirms this motion, showing a radial and in-track oscillation whose amplitude increases with time. The radial and in-track position time histories are very similar for the two satellites, both increasing to the final displacements over the controlled time without exceeding the final bounds. Staying within these bounds confirms that no control was wasted as the controller allocated just enough to achieve the desired result. The performance index yielded a control cost of 18.6 with a terminal constraint cost of $2e-5$.

Again, the final state from the reconfiguration was propagated over 20 orbital periods to ensure the final conditions were satisfied. Figure 4.33 shows the plot of the radial/in-track motion over the propagated time. As evident from the plot, the resultant elliptical formation has a semimajor axis of $250\,m$, as desired, without any noticeable drift. Moreover, the two satellites are tracing the same relative trajectory without any deviation. The position deviation plots shown in Figure 4.34 further confirm that the two satellites are in the proper formations, although differing from the prescribed on the millimeter level. The resulting semimajor axis of satellite 1 is smaller than that of satellite 2 on the sub-millimeter level, effecting a negative drift of $3\,cm$ over the course of the propagation. These differences are again well within the bounds of the constraints, proving the reconfiguration was successful.

Table 4.5   Elliptical to Elliptical Reconfiguration Details, $6800\,km$

Reference Orbital Radius	$6800\,km$
Initial Formation	Elliptical: $25\,m$ semimajor axis
Final Formation	Elliptical: $250\,m$ semimajor axis
Total Time for Reconfiguration	8 Orbital Periods ($12\,hr$, $24\,min$, $4\,sec$)
Maneuver Cost	$\Delta v_1 \,=\, 0.08069\,m/sec$ $\Delta v_2 \,=\, 0.08069\,m/sec$
Altitude Loss	$134.05\,m$
Control Cost	18.60
Constraint Cost	$2e-5$

Figure 4.29   Control Input: Elliptical to Elliptical, $6800\,km$
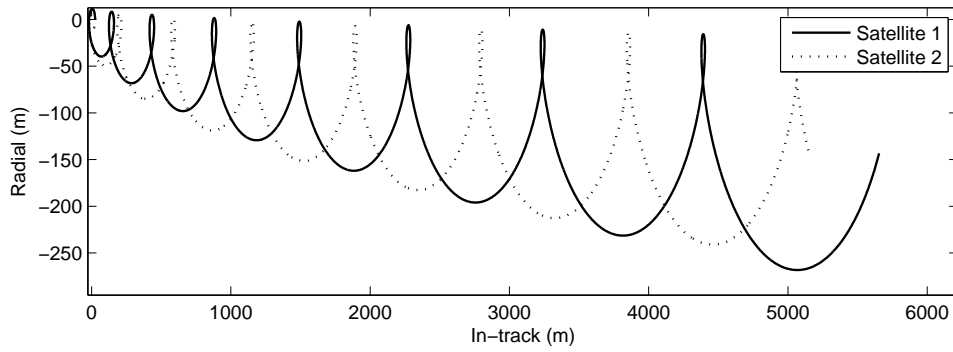

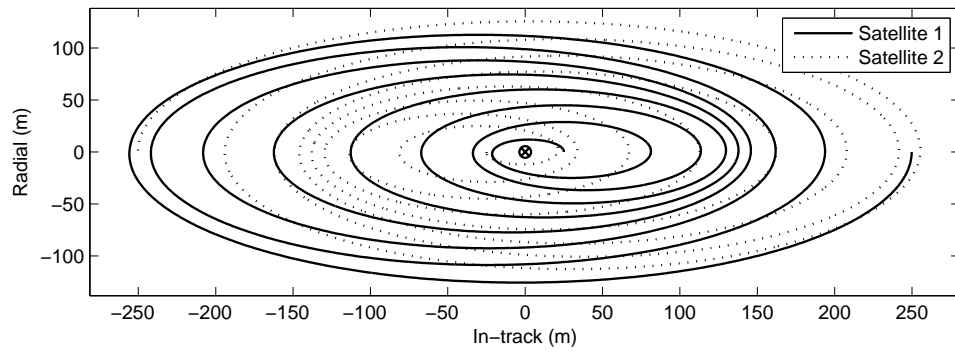Figure 4.30   Fixed Frame Plot: Elliptical to Elliptical, $6800\,km$

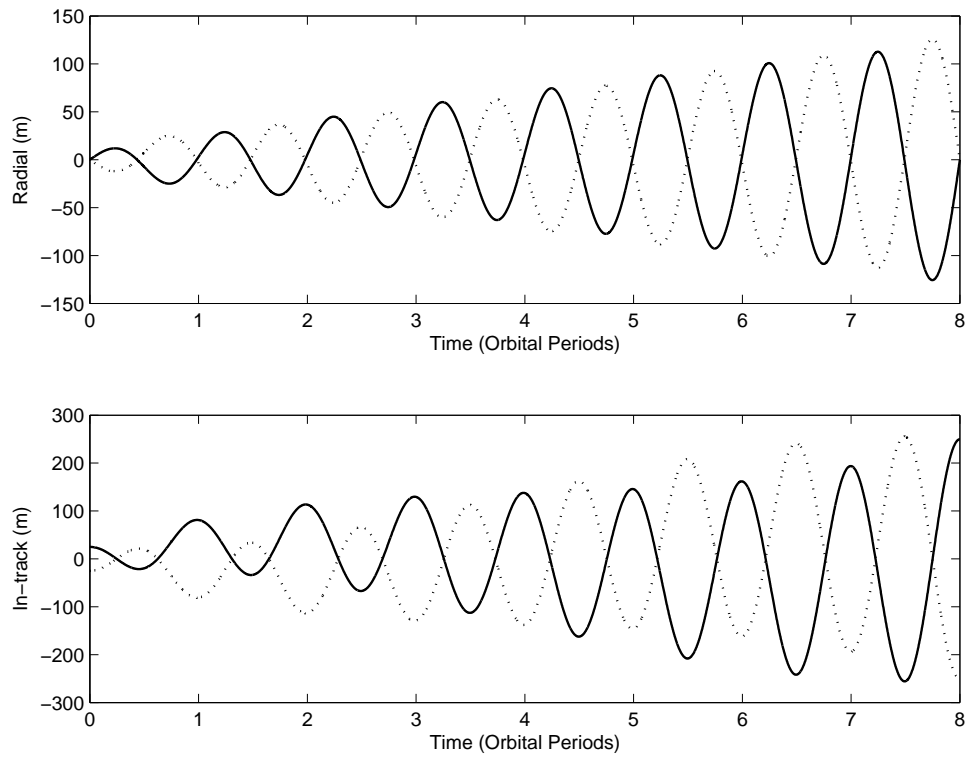Figure 4.31   Falling Frame Plot: Elliptical to Elliptical, $6800\,km$

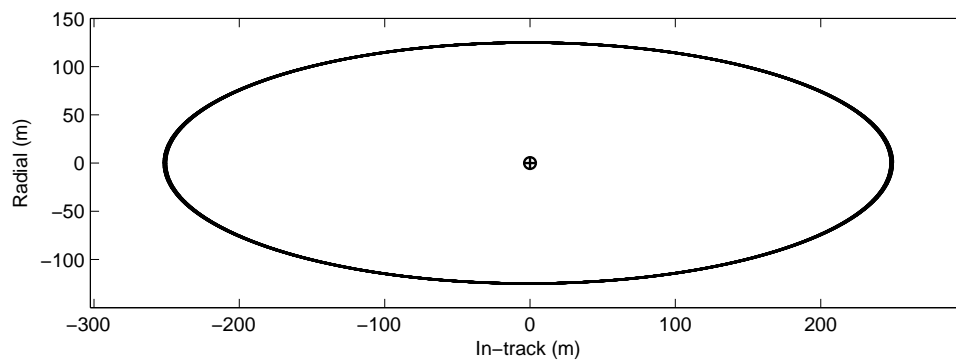Figure 4.32   Reconfiguration Time History Plot: Elliptical to Elliptical, $6800\,km$

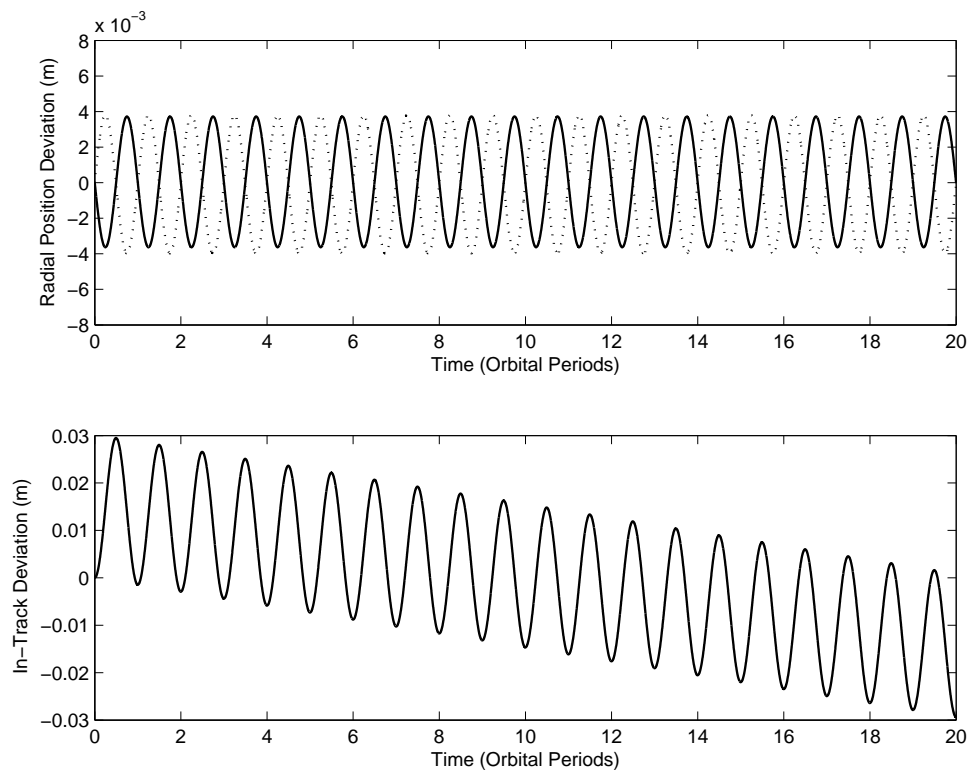Figure 4.33   Post Transfer Plot: Elliptical to Elliptical, $6800\,km$

Figure 4.34   Post Transfer Time History: Elliptical to Elliptical, $6800\,km$

4.3.3 Post-Payload Separation to Elliptical.   Finally, a transfer to an elliptical formation from a post-payload separation configuration was performed. The initial states for this reconfiguration were the same used for the reconfiguration to an in-plane formation, but are reprinted here for convenience:

$$\mathbf{x}_1 = [-10\,m,\ 20\,m,\ -0.04\,m/s,\ 0.005\,m/s] \tag{4.5}$$

$$\mathbf{x}_2 = [10\,m,\ -20\,m,\ 0.04\,m/s,\ -0.005\,m/s] \tag{4.6}$$

The final elliptical formation had a semimajor axis of $250\,m$, equivalent to the previous two final formations. This reconfiguration was the largest performed, requiring 16 orbital periods for the control time to keep from exceeding the maximum input allowed. Even with the large reconfiguration time, the control input for this reconfiguration was still relatively large, as shown in Figure 4.35, requiring a maximum ballistic coefficient input of $0.09\,m^2/kg$. The fuel budget resulted in a total Δv fuel budget of $0.10148\,m/sec$ for satellite 1 and $0.13653\,m/sec$ for satellite 2. The resulting reconfiguration, which is plotted in the radial/in-track plane for both the fixed and falling reference frames in Figures 4.36 and 4.37, had some interesting qualities. Satellite 1 took advantage of its favorable initial conditions, slowly increasing its in-track separation to allow satellite 2 time to overcome its unfavorable initial position. But both satellites also reduced their radial oscillations as satellite 1 increased its semimajor axis and satellite 2 decreased its semimajor axis, allowing the separation distance between the two satellites to decrease. Then, as the in-track distance continued to decrease toward the required separation, both satellites began increasing their radial oscillations again to meet the final formation conditions as their average radial position moved back to zero. These time history plots of the radial and in-track positions are shown in Figure 4.38.

Finally, as a check to ensure the desired formation resulted from the control, the resulting state was propagated over 20 orbital periods. A plot of the radial/in-track plane motion over the 20 periods is shown in Figure 4.39. The two satellites are tracing out the same elliptical formation with a semimajor axis of $250\,m$ as a result of the control input,

and the formation is not drifting apart. This negligible drift is confirmed in the radial and in-track position deviation plots in Figure 4.40. These plots confirm that the satellites are in the proper formation, although the resulting eccentricities slightly differ from the ones prescribed, resulting in a $5\,mm$ radial position deviation. Also, a sub-millimeter difference between the two semimajor axes results, leading to a negative drift between the satellites that brings the satellite $1\,cm$ closer over the 20 orbital periods. Again, these plots confirm the successful reconfiguration, meeting the prescribed constraints and achieving desired formations.

Table 4.6   Payload Separation to Elliptical Reconfiguration Details, $6800\,km$

Reference Orbital Radius	$6800\,km$
Initial Conditions	$\mathbf{x}_1 = [-10\,m,\ 20\,m,\ -0.04\,m/s,\ 0.005\,m/s]$
	$\mathbf{x}_2 = [10\,m,\ -20\,m,\ 0.04\,m/s,\ -0.005\,m/s]$
Final Formation	Elliptical: $250\,m$ semimajor axis
Total Time for	16 Orbital Periods
Reconfiguration	($24\,hr$, $48\,min$, $8\,sec$)
Maneuver	$\Delta v_1 = 0.10148\,m/sec$
Cost	$\Delta v_2 = 0.13653\,m/sec$
Altitude Loss	$197.70\,m$
Control Cost	21.08
Constraint Cost	$8e{-}6$
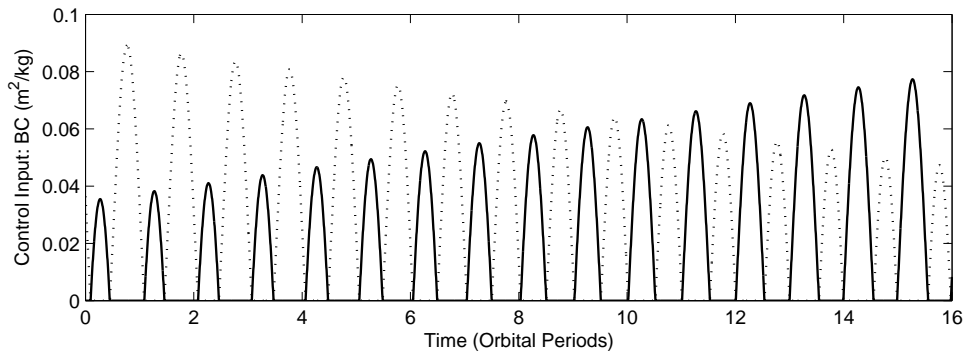
Figure 4.35   Control Input: Payload Separation to Elliptical, $6800\,km$
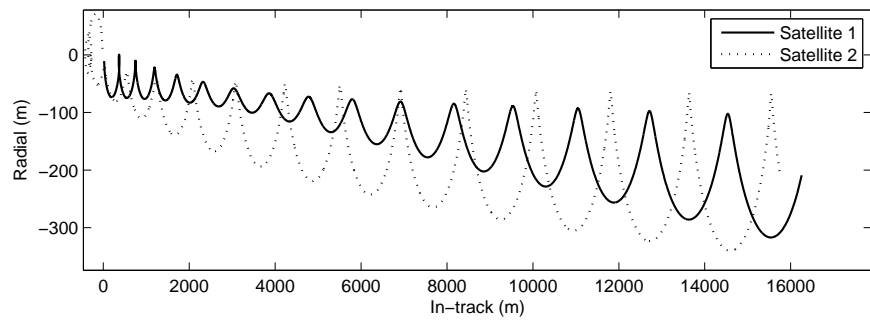
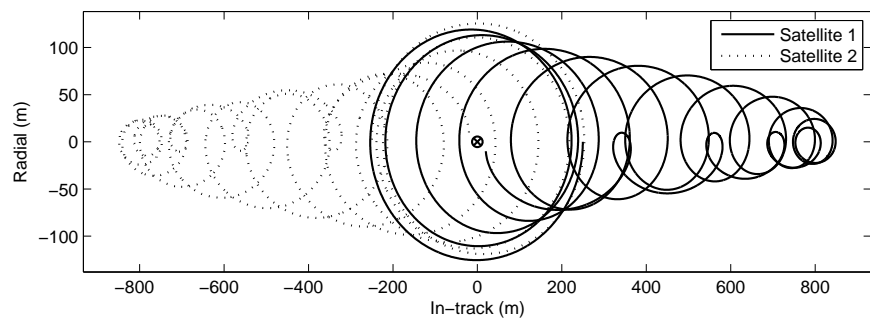Figure 4.36   Fixed Frame Plot: Payload Separation to Elliptical, $6800\,km$

Figure 4.37   Falling Frame Plot: Payload Separation to Elliptical, $6800\,km$
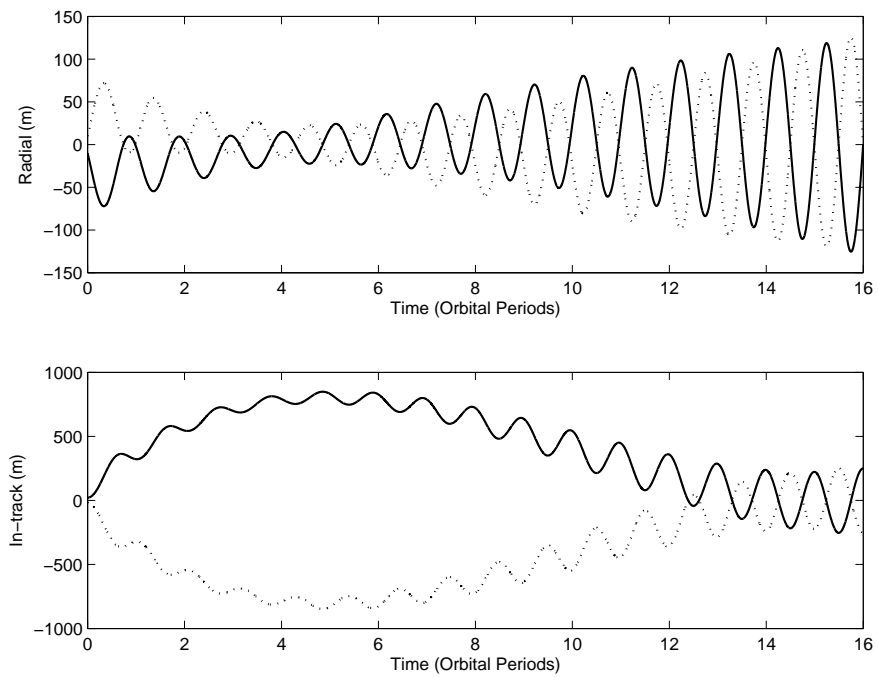

Figure 4.38   Reconfiguration Time History Plot: Payload Separation to Elliptical, $6800\,km$
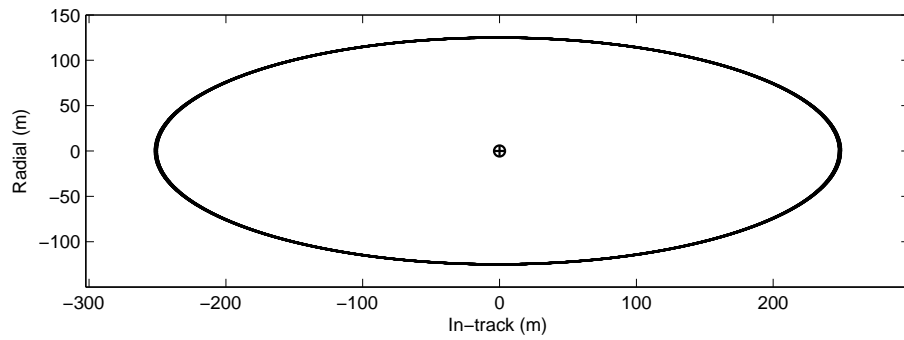
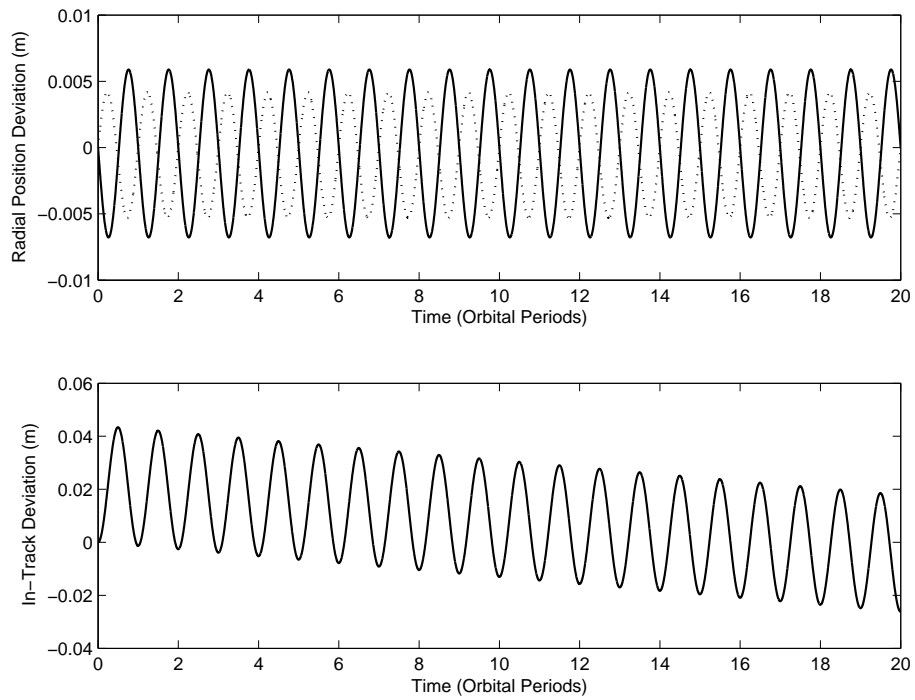Figure 4.39   Post Transfer Plot: Payload Separation to Elliptical, $6800\,km$

Figure 4.40   Post Transfer Time History: Payload Separation to Elliptical, $6800\,km$

V. Conclusions and Recommendations

A linear quadratic terminal controller was used to optimally reconfigure a satellite formation using atmospheric drag actuated control while minimizing the loss of energy of each satellite in the formation. Since the energy is directly related to orbital altitude, this control law effectively minimized the loss of altitude as a result of the reconfiguration. Reconfigurations to in-plane and elliptical formations were performed at an orbital altitude of $6800\,km$ from three separate initial formations: an in-plane formation, an elliptical formation, and a post-payload separation state whose initial conditions were selected to resemble the state of each spacecraft shortly after separating from the launch vehicle. These six reconfigurations went from small to large formations, but Appendix A presents results for the reverse reconfigurations, excluding the post-payload separation initial state. Additional results were compiled for reconfigurations from in-plane and elliptical formations at an orbital altitude of $7000\,km$. These results are presented in Appendix B. In each case, the altitude loss and the total control effort, measured in terms of the conventional Δv budget, were recorded as performance measures for the reconfiguration. Upon completion of the reconfiguration, the final formation state was propagated forward over 20 orbital periods to ensure the desired formation and constraints were satisfied.

The results of this study show that the radial and in-track motion of a satellite formation can be effectively controlled using an atmospheric drag actuated control scheme, whereas the cross-track motion is uncontrollable, as shown in Chapter III. Additionally, minimizing the loss of energy conserves the loss of altitude during the reconfiguration. The desired formations were met for each case, although the time requirement varied depending upon the initial and final conditions. The change in orbital eccentricity proved to dictate the control time for a given altitude, and the time requirement increased substantially with altitude. Further increasing the allotted time for the reconfiguration tended to tighten the final constraints for each transfer performed. The control law also proved sufficient in limiting the drift, even though the terminal constraints were kept soft in the optimization routine. The maximum post-reconfiguration drift due to the final conditions of the optimization routine was only $8\,cm$ over the 20 orbital periods.

5-1

Of all the reconfigurations performed, the in-plane to in-plane transfer proved the most efficient. For the $6800\,km$ reference orbit, the formation lost only $18.41\,m$ of altitude over the 4 orbital period time of reconfiguration. The strategy for this transfer provides intuition into its simplicity. Satellite 1, the leading satellite at transfer initiation, deployed its panels first, letting the drag acceleration decrease its altitude to the final altitude before zeroing the panel orientation. The lower altitude allowed the separation distance between the satellites to increase to the desired $500\,m$ value as satellite 2 maneuvered down to the final altitude. For the in-plane to in-plane transfer presented in Section A.1.1 from an initial separation distance of $500\,m$ to a final separation of $50\,m$, which is the reverse reconfiguration of the transfer shown in Section 4.2.1, the control strategy was exactly the same, just applied to the opposite satellite. In this case, satellite 2 deployed its panels first to close the separation distance between the two satellites before satellite 1 initiated control, resulting in the same altitude loss and Δv budget. More importantly, the control effort was simplified since an initial radial oscillation from an orbital eccentricity difference was not present, causing the controller to overcome a large eccentricity.

This large eccentricity dampening can be seen in Section A.1.2 where an initial elliptical formation for a $250\,m$ semimajor axis is reconfigured to an in-plane formation with a $50\,m$ separation distance. The initial orbit of each satellite has a nonzero eccentricity that must be zeroed as the satellites approach the desired $50\,m$ separation in the same, circular orbit. A substantial control effort is required to circularize the orbit, resulting in an altitude loss of approximately $150\,m$. However, this substantial control effort is required due to the size of the initial eccentricity. In Section 4.2.2, the initial formation is elliptical with only a $25\,m$ semimajor axis, resulting in a smaller eccentricity than the previous. The control effort to overcome this radial oscillation was not nearly as substantial, and the controller was actually able to take advantage of the oscillation to increase the separation distance of the satellites while circularizing the orbits. This transfer resulted in a total altitude loss of only $20\,m$.

The higher altitude orbits posed the most significant problem for the control effort. Due to the substantially lower atmospheric density when the altitude was increased $200\,m$, the controller required much more time to perform the reconfiguration. A reconfiguration

from an elliptical formation with a $25\,m$ semimajor axis to an in-plane formation with a separation distance of $250\,m$ required 21 orbital periods, or roughly 34 hours, to complete the transfer. This control time increased when an eccentricity had to be imposed on a circular orbit. A reconfiguration from an in-plane formation with a separation of $50\,m$ to an elliptical formation with a semimajor axis of $75\,m$ required 54 orbital periods to perform the transfer, a control time of over 87 hours. Although the control time increased substantially for these test cases, the altitude loss remained within the bounds of the previous reconfigurations since this value is dependent only on the overall control input applied. The time requirement could be reduced if the maximum differential ballistic coefficient achievable for the formation was increased. This study used a conservative maximum value of $0.1\,m^2/kg$ for the differential ballistic coefficient to provide a middle point for drag actuated control. But this value could be increased through an efficient spacecraft design, resulting in decreased reconfiguration times at all altitudes.

Future research efforts should focus on further validating drag actuated control and its potential cost savings. This study was primarily a proof of concept study. As such, a simple model was applied to prove that reasonable results are obtainable for the prescribed control approach. To further validate both the effectiveness and usefulness of this control technique, high fidelity atmospheric and gravity models should be applied with a control technique to account for these variations in the motion. A study that encompasses a full range of inclinations, and perhaps even accounts for different reference orbit eccentricities, could help expand this concept.

With a full dynamic model, formation degradation is likely to occur on some time scale. This study argued that through the proper formation design and selection of orbital elements, this degradation could be effectively minimized. A formation keeping cost comparison between drag actuated controlled formations and conventionally controlled formations using high impulse thrusters could further expand this concept. Past research shows that a low-thrust, continuous input control law will likely result in a higher Δv budget than high impulse, finite control inputs, but these costs cannot be directly compared since they relate to entirely different costs; drag actuated control costs relate to altitude

while conventional control costs are associated with onboard expendables. So a proper characterization of the costs would involve the time on-orbit with available control.

Another interesting study would compare the potential fuel savings formation flying with drag actuated control can provide over formation flying using conventional thruster. When flying with drag, the primary source of fuel is provided by altitude. So the remaining lifetime of the satellite is characterized by its current altitude. For formation flying with conventional thrusters, the fuel onboard the satellite is usually depleted before the satellite falls out of orbit, allowing a characterization of its lifetime based on the remaining fuel onboard. Since the drag actuated control satellites do not require much fuel onboard, they would be lighter in weight at launch, reducing the cost of orbital injection. Moreover, the overall satellite could be smaller in design since the bulky fuel tanks would not be needed, allowing a single launch vehicle to lift more satellites into orbit. However, to control the formation, the satellites are sacrificing altitude, which may require the launch vehicle to place the satellites into a higher orbit to optimize the formation time on orbit. So a comparison of the costs required to place a drag actuated controlled satellite formation in a higher orbit versus placing a conventionally control formation with a greater total mass would provide insight into the overall cost savings of drag controlled system. Additionally, the time on orbit for each scenario can be derived from a common mission schedule requiring an equal number of reconfigurations and offering the same formation keeping constraints as a separate cost analysis.

Overall, the results of the study confirmed that a satellite formation can be effectively controlled in the radial/in-track plane using atmospheric drag actuated control while the overall energy, which is directly tied to the altitude of the formation, is conserved. The only drawback to such a control effort is the time requirement for the reconfigurations. However, if the reconfiguration time is not an issue, atmospheric drag proves to be an ideal and effective control source for satellite formations in low-Earth orbit.

Appendix A.   Additional Reconfigurations at 6800 km

A.1   Reconfiguration to an In-Plane Formation

This section contains the results for reconfigurations into a final in-plane formation with a separation distance of $500\,m$ from two separate initial formations: an in-plane formation with a separation distance of $50\,m$ and an elliptical formation with a semimajor axis of $25\,m$ such that the satellites are $50\,m$ apart in the in-track position. The satellite positions and motion are with respect to a $6800\,km$ reference orbit.

A.1.1   In-Plane to In-Plane.   The following figures show the results of a reconfiguration from an in-plane formation with a separation distance of $500\,m$ to a smaller in-plane formation with a separation distance of $50\,m$:

Table A.1   Large In-Plane to Small In-Plane Reconfiguration Details, $6800\,km$

Reference Orbital Radius	$6800\,km$
Initial Formation	In-Plane: $500\,m$ separation
Final Formation	In-Plane: $50\,m$ separation
Total Time for Reconfiguration	4 Orbital Periods ($6\,hr$, $12\,min$, $2\,sec$)
Maneuver Cost	$\Delta v_1 = 0.01048\,m/sec$ $\Delta v_2 = 0.01048\,m/sec$
Altitude Loss	$18.41\,m$
Control Cost	0.65
Constraint Cost	$1e{-}5$

Figure A.1   Control Input: Large In-Plane to Small In-Plane, $6800\,km$

Figure A.2   Fixed Frame Plot: Large In-Plane to Small In-Plane, $6800\,km$

Figure A.3   Falling Frame Plot: Large In-Plane to Small In-Plane, $6800\,km$

Figure A.4   Reconfiguration Time History Plot: Large In-Plane to Small In-Plane, $6800\,km$

Figure A.5   Post Transfer Plot: Large In-Plane to Small In-Plane, $6800\,km$

Figure A.6   Post Transfer Time History: Large In-Plane to Small In-Plane, $6800\,km$

A.1.2 Elliptical to In-Plane.   The following figures show the results of a reconfiguration from an elliptical formation with a semimajor axis of $250\,m$ to an in-plane formation with a separation distance of $50\,m$. Note that the post-transfer plot shows the satellites drifting over time. However, as shown in the in-track drift plot, the satellites are actually drifting in the same direction such that their total separation after 20 orbital periods is only $2.2\,cm$.

Table A.2   Large Elliptical to Small In-Plane Reconfiguration Details, $6800\,km$

Reference Orbital Radius	$6800\,km$
Initial Formation	Elliptical: $250\,m$ semimajor axis
Final Formation	In-Plane: $50\,m$ separation
Total Time for Reconfiguration	10 Orbital Periods ($15\,hr$, $30\,min$, $5\,sec$)
Maneuver Cost	$\Delta v_1 = 0.08964\,m/sec$ $\Delta v_2 = 0.08964\,m/sec$
Altitude Loss	$148.92\,m$
Control Cost	18.32
Constraint Cost	$1e{-}5$

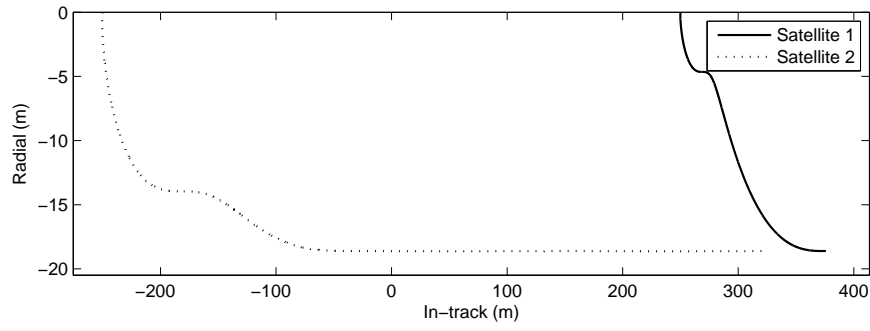Figure A.7   Control Input: Large Elliptical to Small In-Plane, $6800\,km$
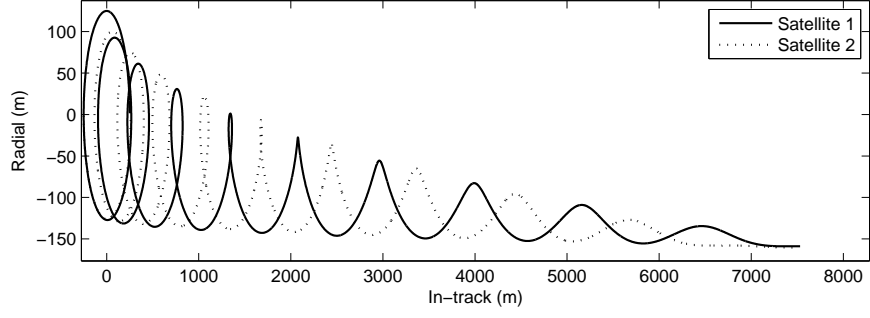
Figure A.8   Fixed Frame Plot: Large Elliptical to Small In-Plane, $6800\,km$
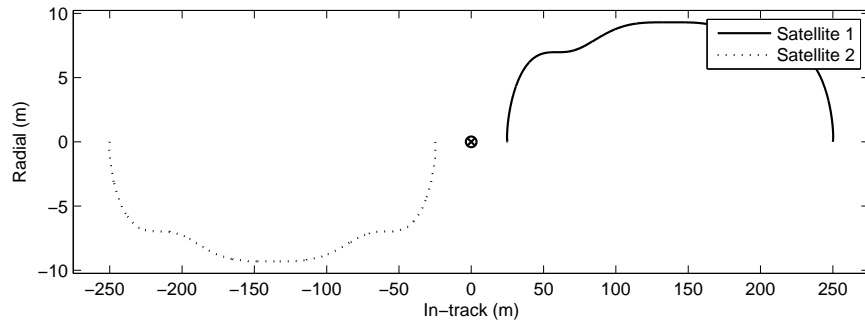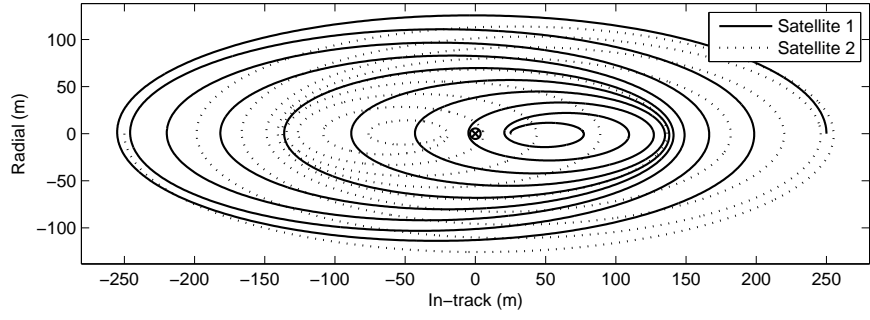

Figure A.9   Falling Frame Plot: Large Elliptical to Small In-Plane, $6800\,km$
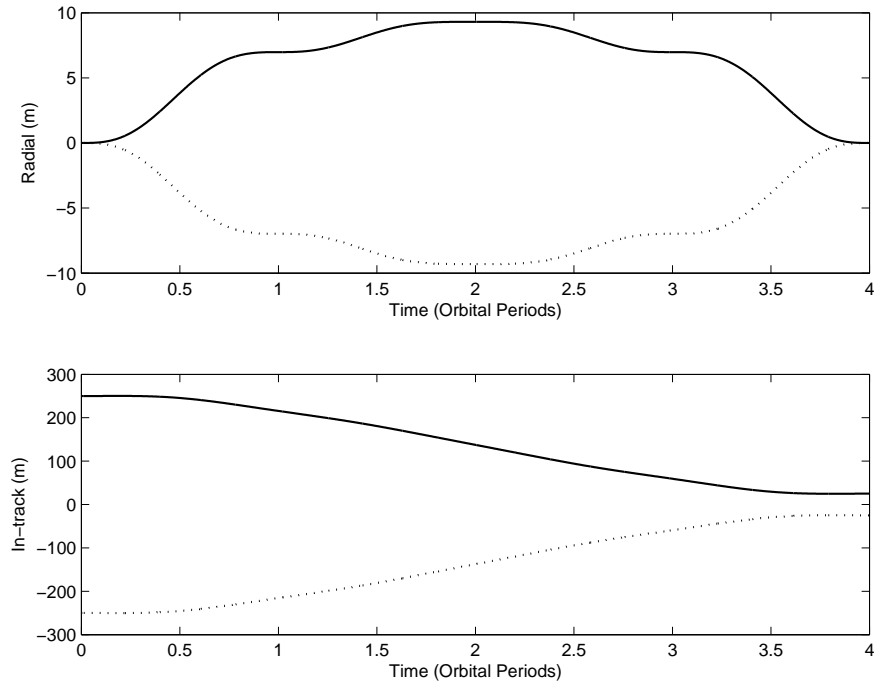

Figure A.10   Reconfiguration Time History Plot: Large Elliptical to Small In-Plane, $6800\,km$
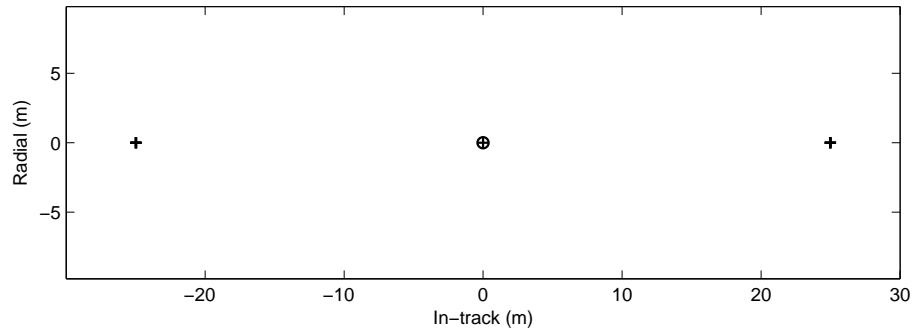
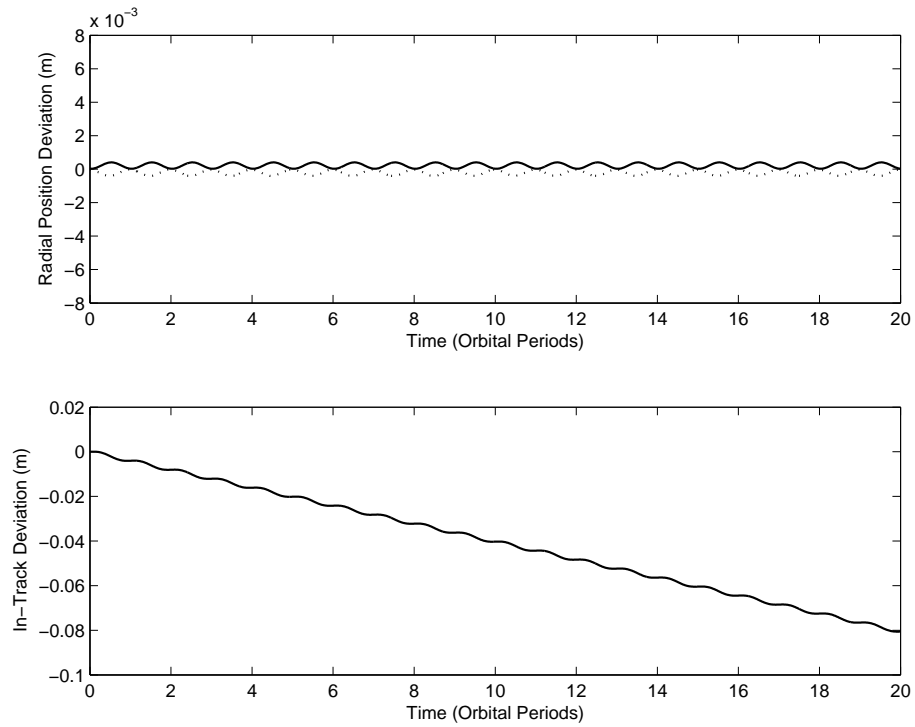Figure A.11   Post Transfer Plot: Large Elliptical to Small In-Plane, $6800\,km$

Figure A.12   Post Transfer Time History: Large Elliptical to Small In-Plane, $6800\,km$

A.2   Reconfiguration to an Elliptical Formation

This section contains the results for reconfigurations into a final elliptical formation with a semimajor axis of $25\,m$, such that the satellites are $50\,m$ apart when aligned in the in-track direction, from two separate initial formations: an in-plane formation with a separation distance of $500\,m$ and an elliptical formation with a semimajor axis of $250\,m$. The satellite positions and motion are with respect to a $6800\,km$ reference orbit.

A.2.1   In-Plane to Elliptical.   The following figures show the results of a reconfiguration from an in-plane formation with a separation distance of $500\,m$ to an elliptical formation with a semimajor axis of $25\,m$:

Table A.3   Large In-Plane to Small Elliptical Reconfiguration Details, $6800\,km$

Reference Orbital Radius	$6800\,km$
Initial Formation	In-Plane: $500\,m$ separation
Final Formation	Elliptical: $25\,m$ semimajor axis
Total Time for Reconfiguration	6 Orbital Periods ($9\,hr$, $18\,min$, $3\,sec$)
Maneuver Cost	$\Delta v_1 \ = \ 0.01151\,m/sec$
	$\Delta v_2 \ = \ 0.01151\,m/sec$
Altitude Loss	$19.12\,m$
Control Cost	0.61
Constraint Cost	$4e{-}6$
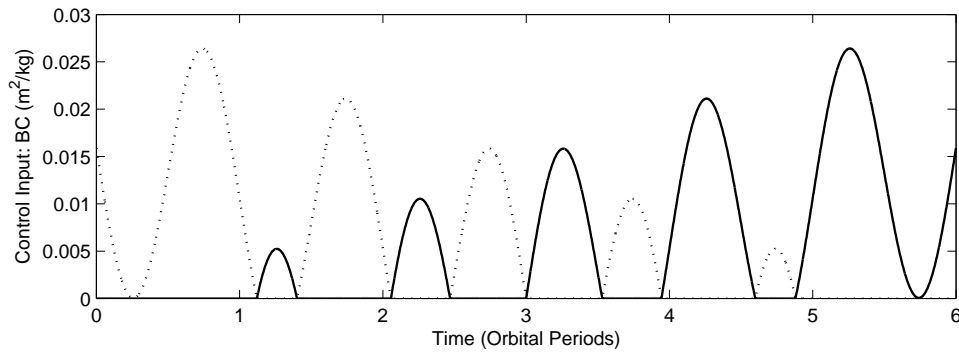
Figure A.13   Control Input: Large In-Plane to Small Elliptical, $6800\,km$

A-7
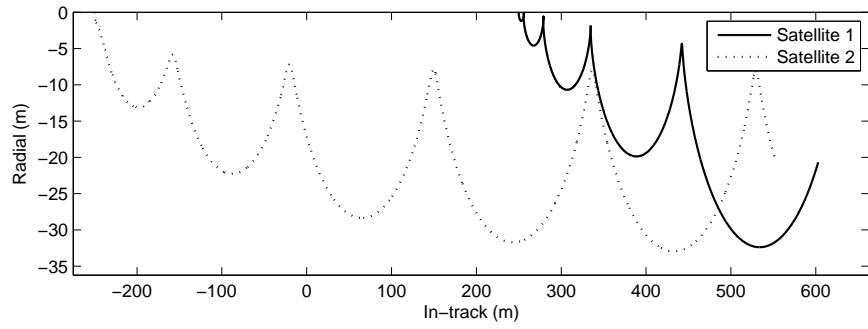
Figure A.14   Fixed Frame Plot: Large In-Plane to Small Elliptical, $6800\,km$
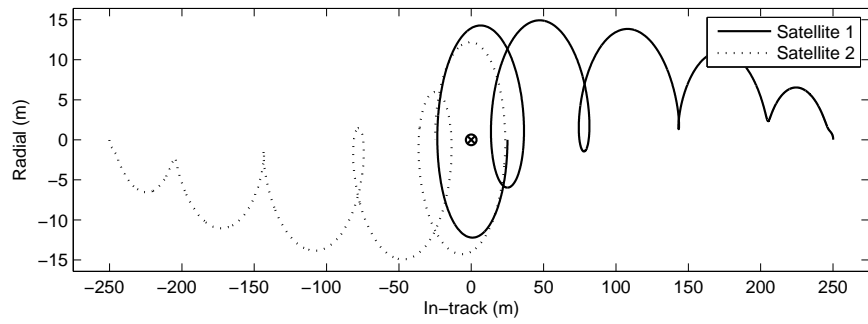
Figure A.15   Falling Frame Plot: Large In-Plane to Small Elliptical, $6800\,km$
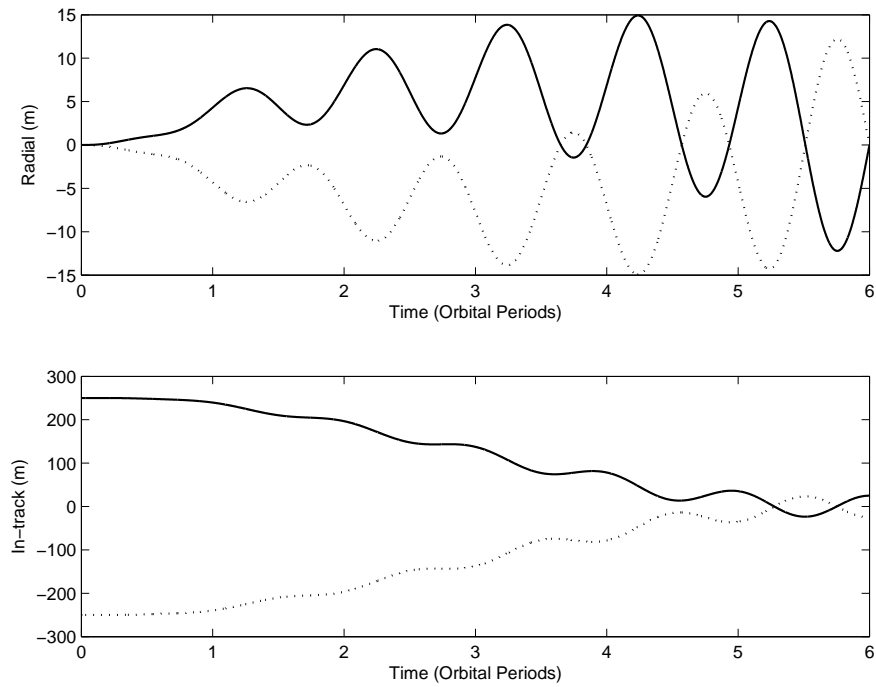
Figure A.16   Reconfiguration Time History Plot: Large In-Plane to Small Elliptical, $6800\,km$
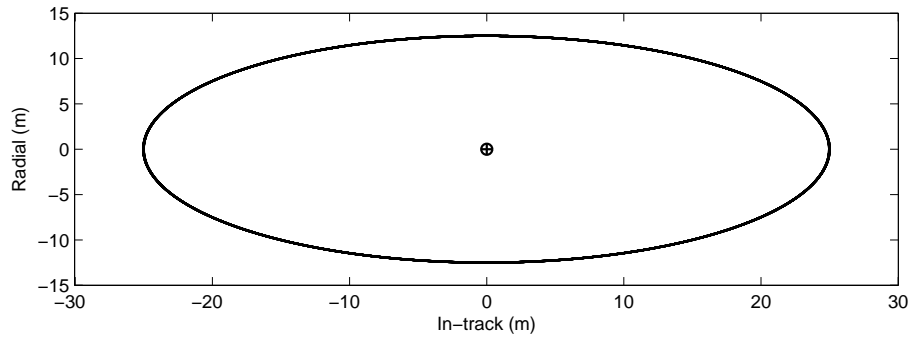
Figure A.17   Post Transfer Plot: Large In-Plane to Small Elliptical, $6800\,km$
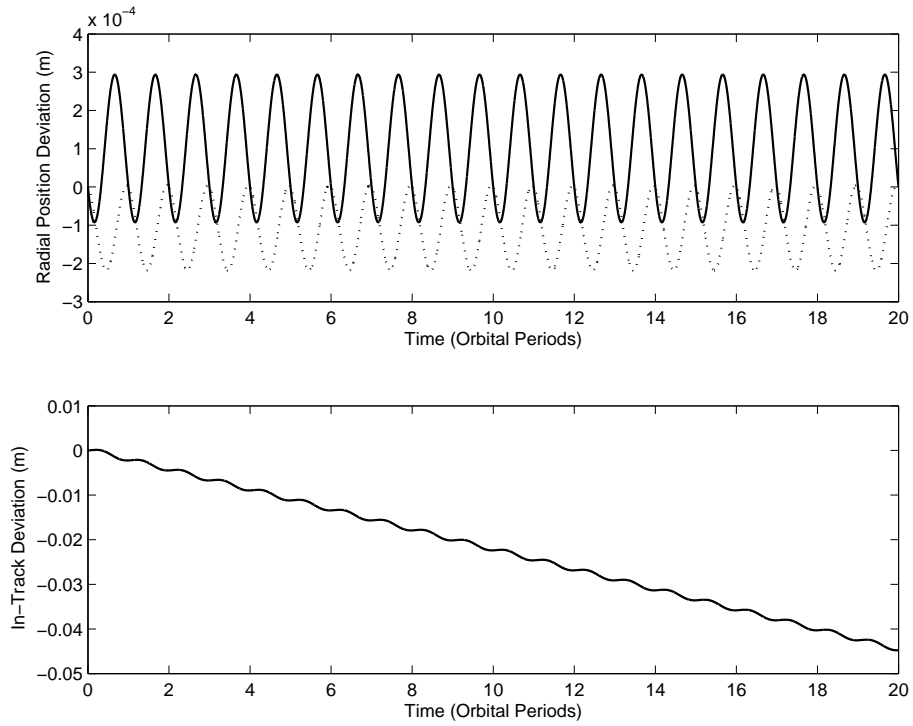
Figure A.18   Post Transfer Time History: Large In-Plane to Small Elliptical, $6800\,km$

A.2.2   Elliptical to Elliptical.   The following figures show the results of a reconfiguration from an elliptical formation with a $250\,m$ semimajor axis to a smaller elliptical formation with a $25\,m$ semimajor axis. Note that the post transfer plot shows a drift in the formation over time. However, as shown in the in-track deviation plot in Figure A.24, the two satellites are drifting together, resulting in a total positive drift of only $3\,cm$.

Table A.4   Large Elliptical to Small Elliptical Reconfiguration Details, $6800\,km$

Reference Orbital Radius	$6800\,km$
Initial Formation	Elliptical: $250\,m$ semimajor axis
Final Formation	Elliptical: $25\,m$ semimajor axis
Total Time for Reconfiguration	8 Orbital Periods ($12\,hr$, $24\,min$, $4\,sec$)
Maneuver Cost	$\Delta v_1 = 0.08069\,m/sec$ $\Delta v_2 = 0.08069\,m/sec$
Altitude Loss	$134.05\,m$
Control Cost	18.60
Constraint Cost	$2e{-}5$

Figure A.19   Control Input: Large Elliptical to Small Elliptical, $6800\,km$
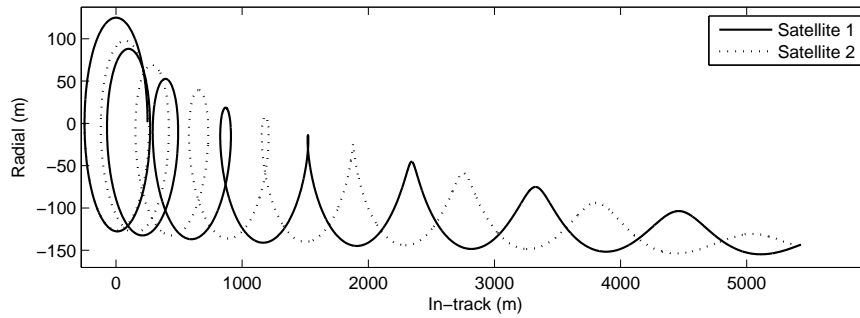
Figure A.20   Fixed Frame Plot: Large Elliptical to Small Elliptical, $6800\,km$
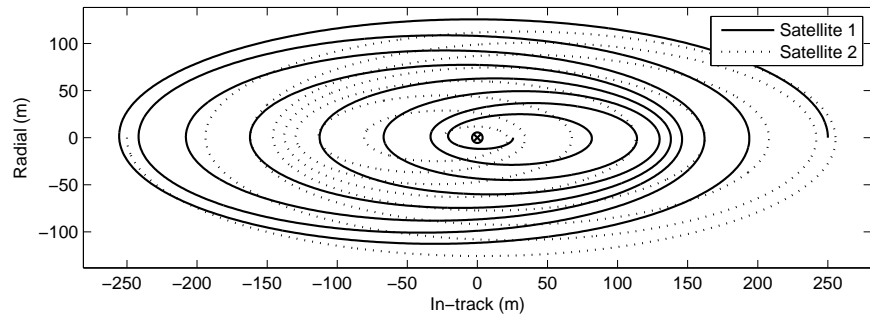
Figure A.21   Falling Frame Plot: Large Elliptical to Small Elliptical, $6800\,km$
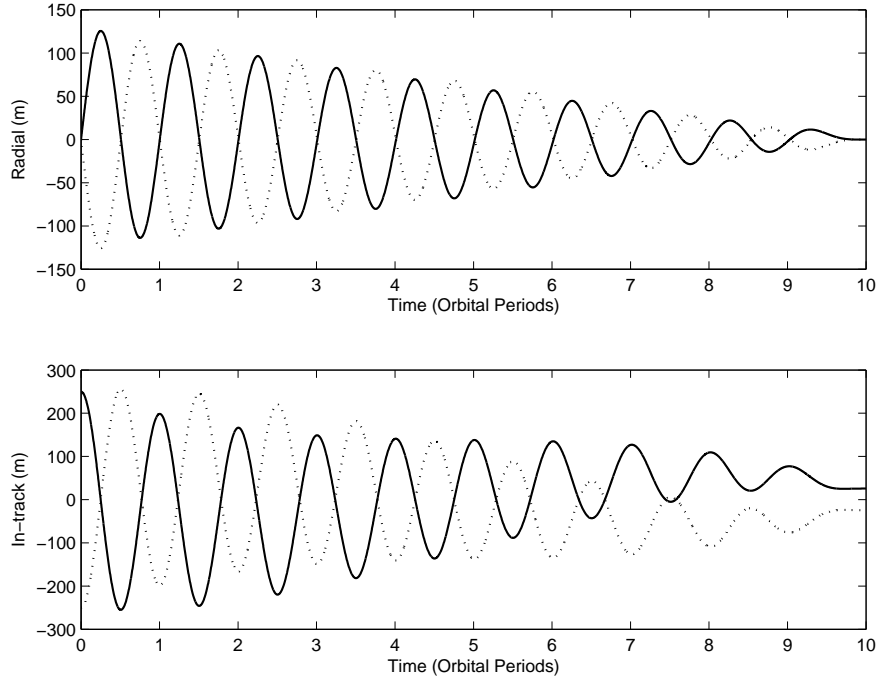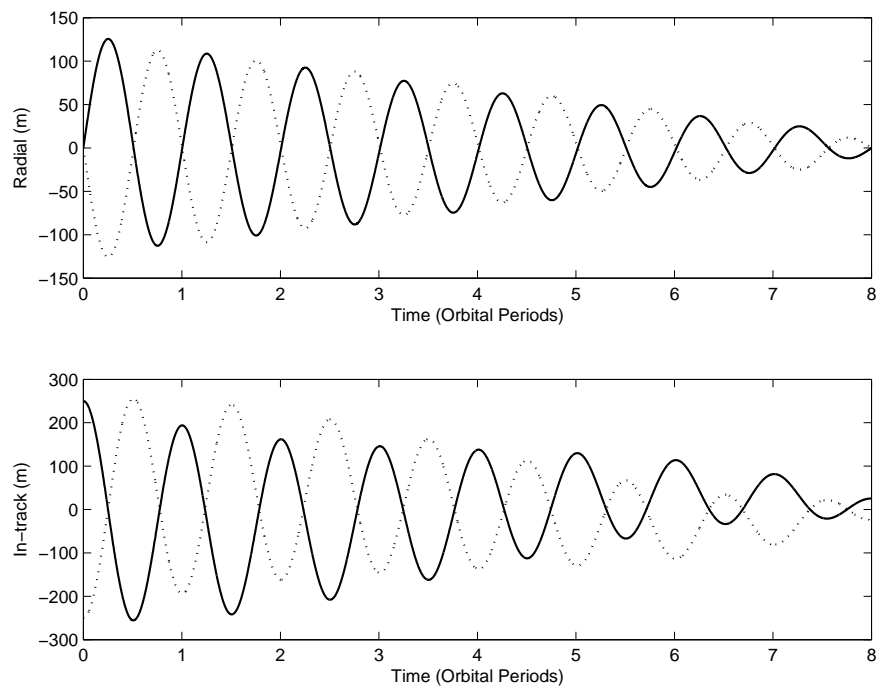

Figure A.22   Reconfiguration Time History Plot: Large Elliptical to Small Elliptical, $6800\,km$
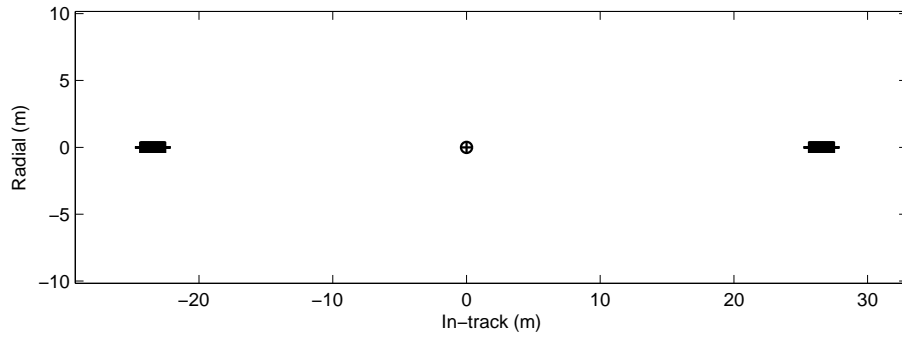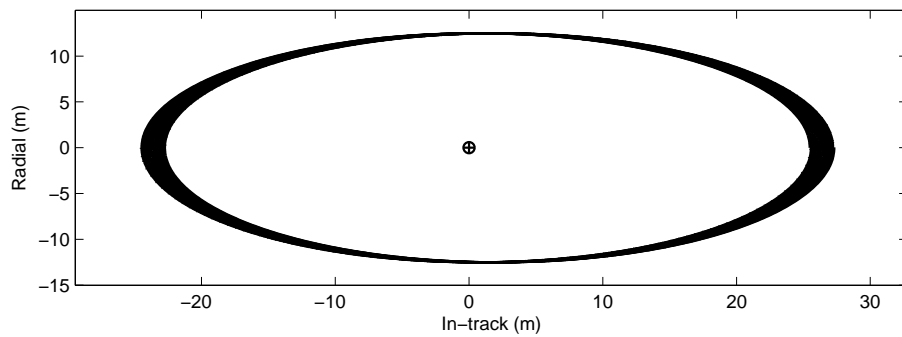

Figure A.23   Post Transfer Plot: Large Elliptical to Small Elliptical, $6800\,km$
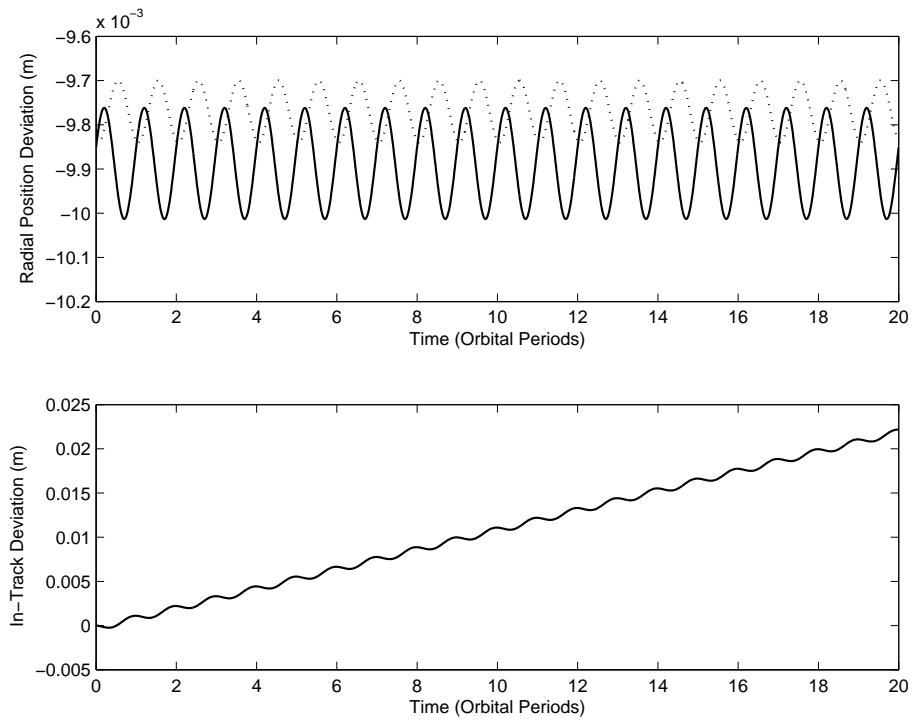
A-11
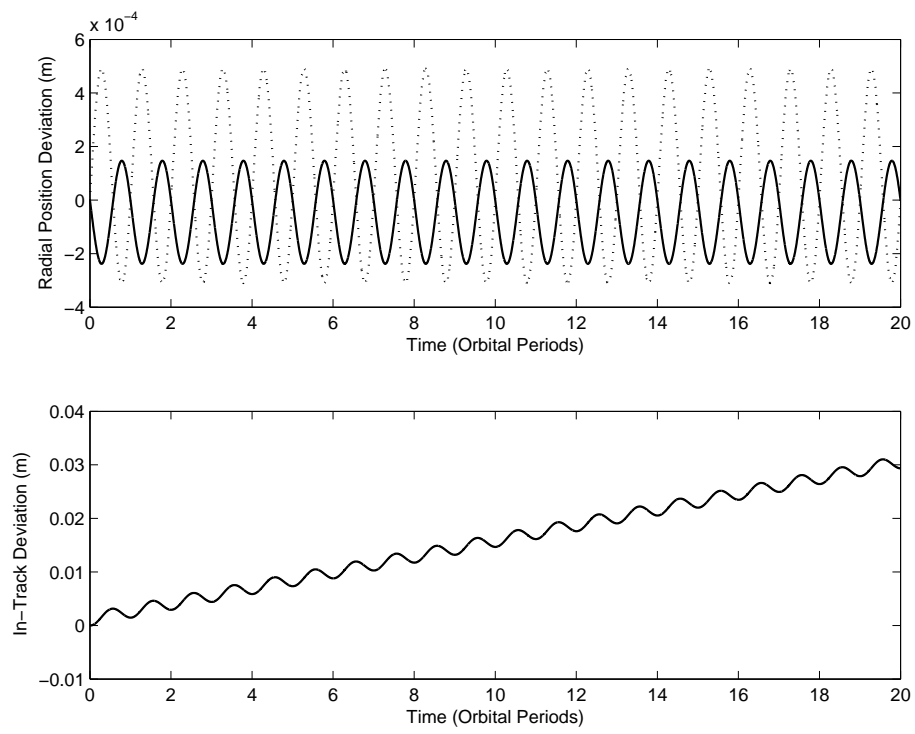
Figure A.24   Post Transfer Time History: Large Elliptical to Small Elliptical, $6800\,km$

Appendix B.   Reconfigurations at 7000 km

B.1   Reconfiguration to an In-Plane Formation

This section contains the results for reconfigurations into a final in-plane formation with a separation distance of $250\,m$ from two separate initial formations: an in-plane formation with a separation distance of $50\,m$ and an elliptical formation with a semimajor axis of $25\,m$ such that the satellites are $50\,m$ apart in the in-track position. The satellite positions and motion are with respect to a $7000\,km$ reference orbit.

B.1.1   In-Plane to In-Plane.   The following figures show the results of a reconfiguration from an in-plane formation with a separation distance of $50\,m$ to another in-plane formation with a separation distance of $250\,m$ at a reference orbital radius of $7000\,km$:

Table B.1   In-Plane to In-Plane Reconfiguration Details, $7000\,km$

Reference Orbital Radius	$7000\,km$
Initial Formation	In-Plane: $50\,m$ separation
Final Formation	In-Plane: $250\,m$ separation
Total Time for Reconfiguration	7 Orbital Periods ($11\,hr$, $19\,min$, $59\,sec$)
Maneuver Cost	$\Delta v_1 \ = \ 0.00246\,m/sec$
	$\Delta v_2 \ = \ 0.00246\,m/sec$
Altitude Loss	$4.55\,m$
Control Cost	0.02
Constraint Cost	$2e{-}7$
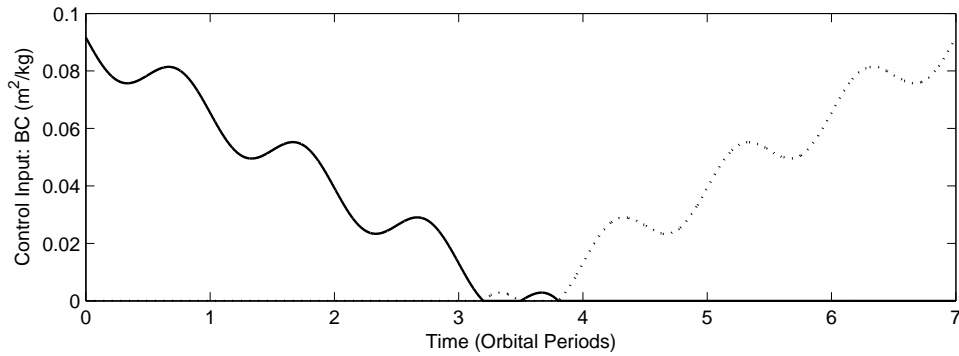
Figure B.1   Control Input: In-Plane to In-Plane, $7000\,km$
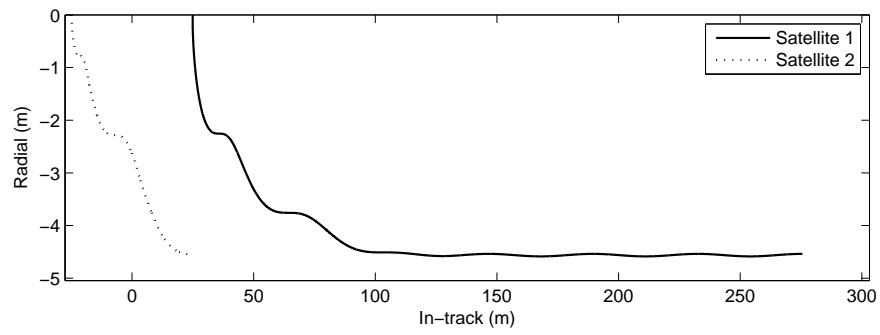
Figure B.2   Fixed Frame Plot: In-Plane to In-Plane, $7000\,km$
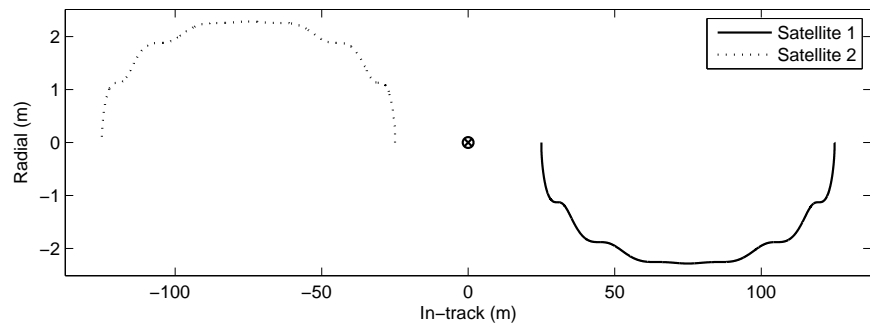
Figure B.3   Falling Frame Plot: In-Plane to In-Plane, $7000\,km$
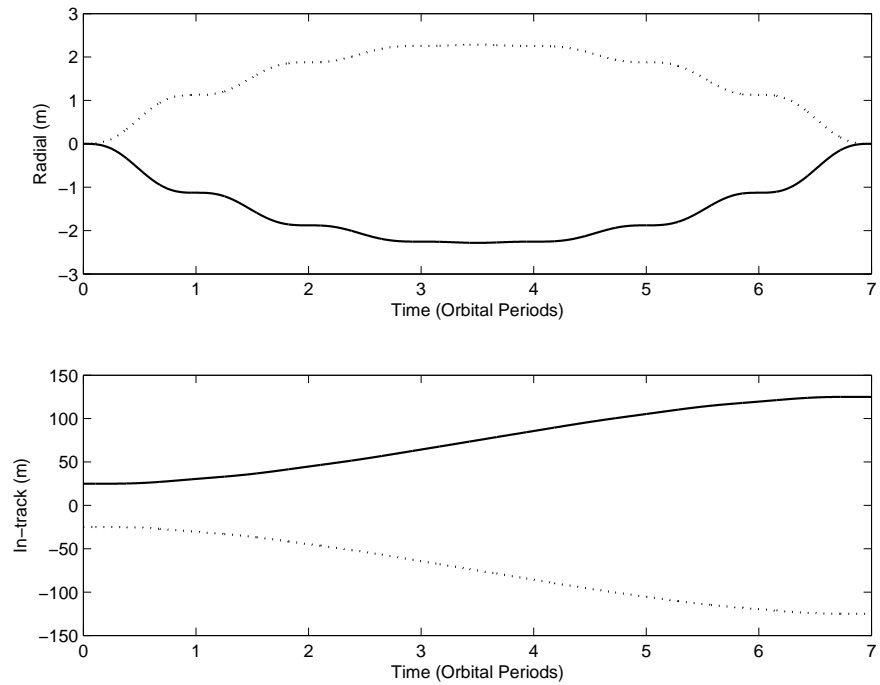
Figure B.4   Reconfiguration Time History Plot: In-Plane to In-Plane, $7000\,km$
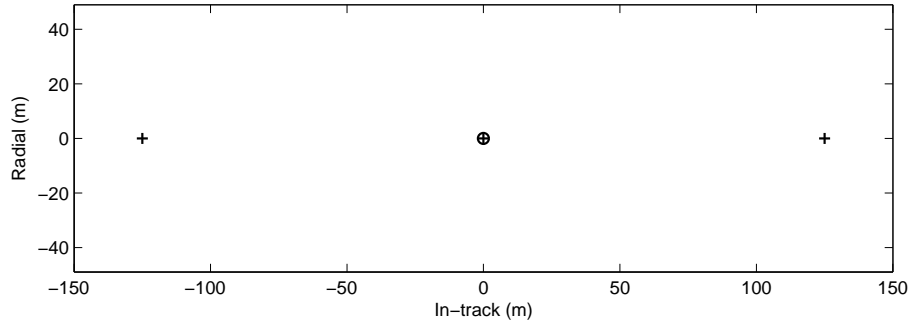
Figure B.5   Post Transfer Plot: In-Plane to In-Plane, $7000\,km$
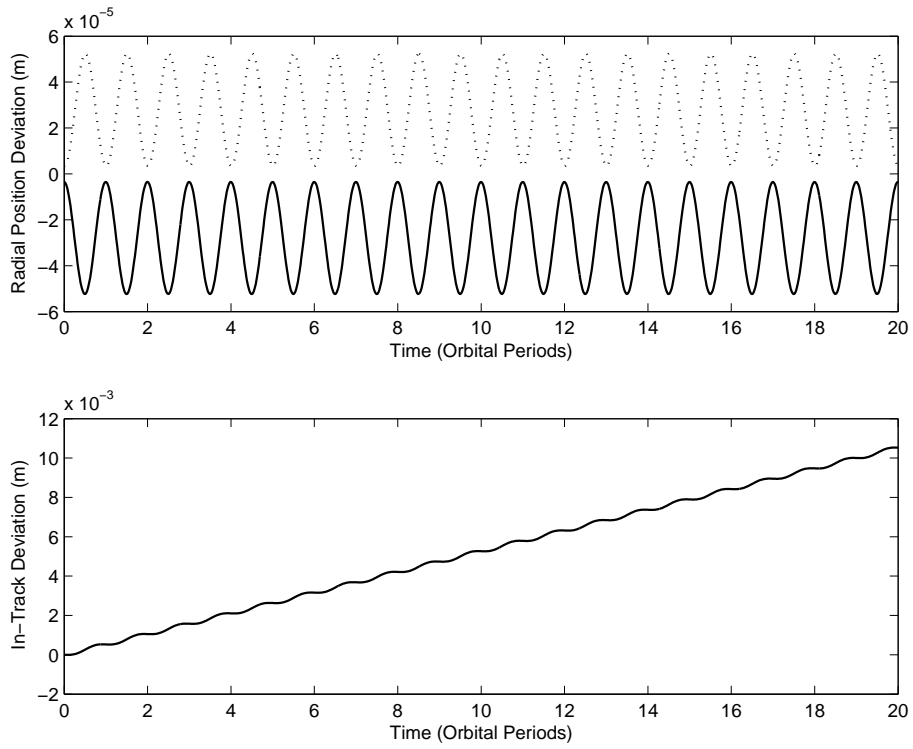
Figure B.6   Post Transfer Time History: In-Plane to In-Plane, $7000\,km$

B-3

B.1.2 Elliptical to In-Plane.   The following figures show the results of a reconfiguration from an elliptical formation with a $25\,m$ semimajor axis to an in-plane formation with a separation distance of $250\,m$ at a reference orbital radius of $7000\,km$:

Table B.2   Elliptical to In-Plane Reconfiguration Details, $7000\,km$

Reference Orbital Radius	$7000\,km$
Initial Formation	Elliptical: $25\,m$ semimajor axis
Final Formation	In-Plane: $250\,m$ separation
Total Time for Reconfiguration	21 Orbital Periods ($33\,hr$, $59\,min$, $59\,sec$)
Maneuver Cost	$\Delta v_1 = 0.00863\,m/sec$
	$\Delta v_2 = 0.00863\,m/sec$
Altitude Loss	$15.92\,m$
Control Cost	0.08
Constraint Cost	$1e\!-\!8$
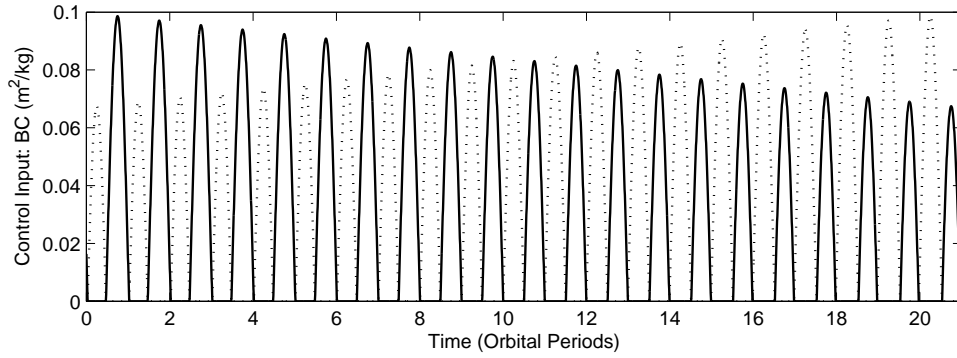
Figure B.7   Control Input: Elliptical to In-Plane, $7000\,km$
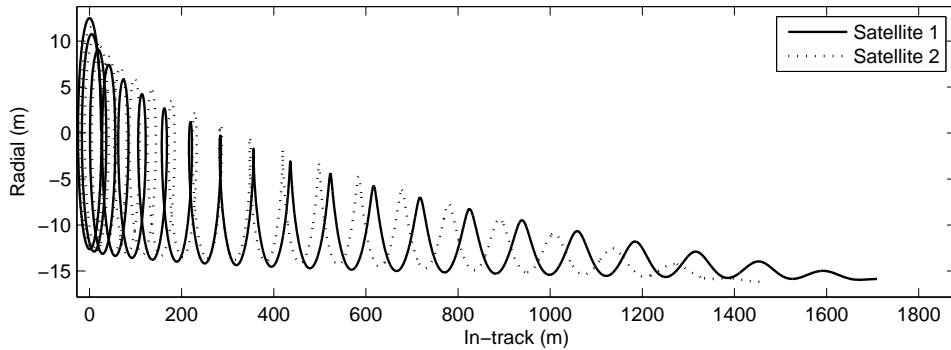
Figure B.8   Fixed Frame Plot: Elliptical to In-Plane, $7000\,km$
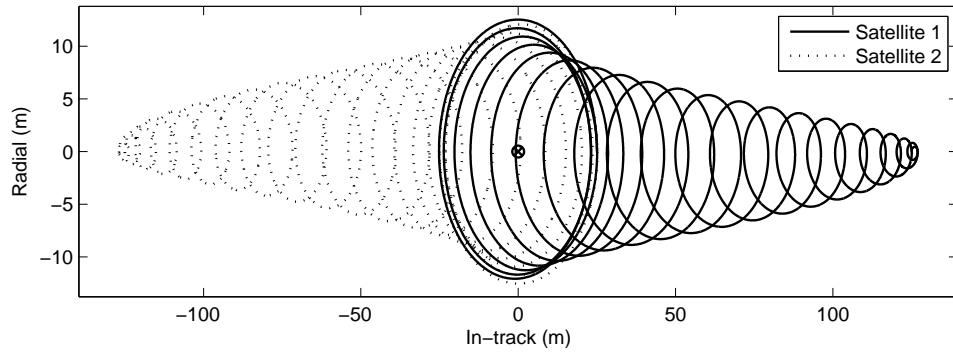
Figure B.9   Falling Frame Plot: Elliptical to In-Plane, $7000\,km$
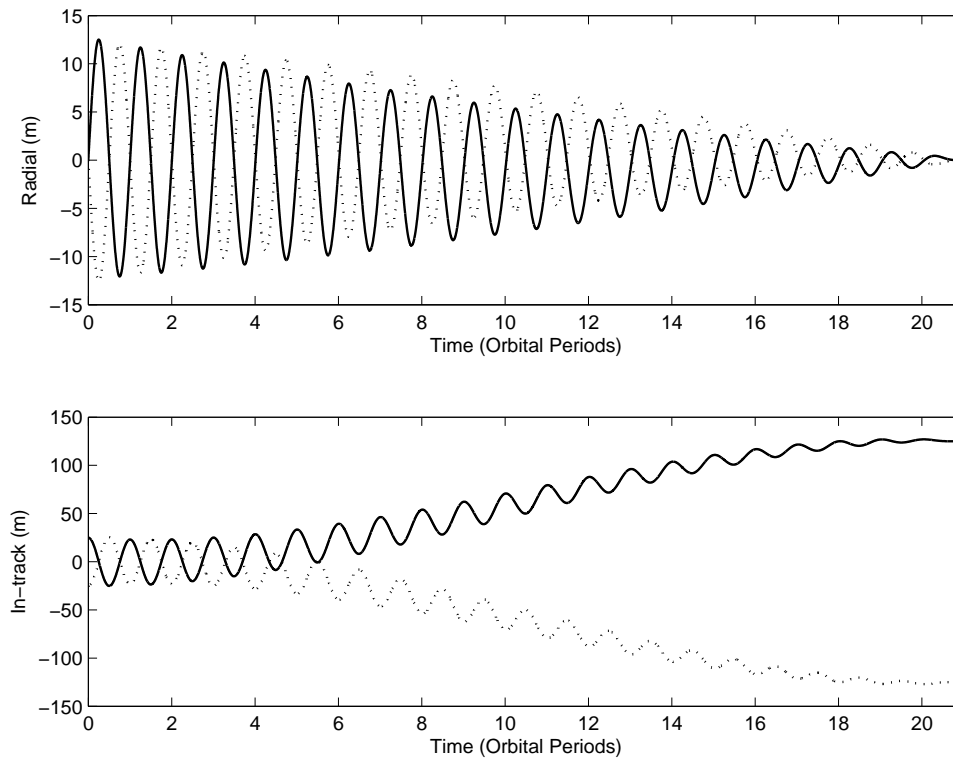
Figure B.10   Reconfiguration Time History Plot: Elliptical to In-Plane, $7000\,km$
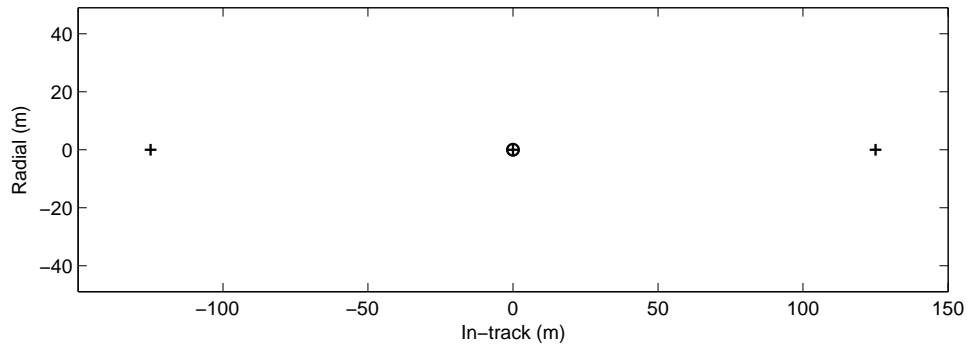
Figure B.11   Post Transfer Plot: Elliptical to In-Plane, $7000\,km$
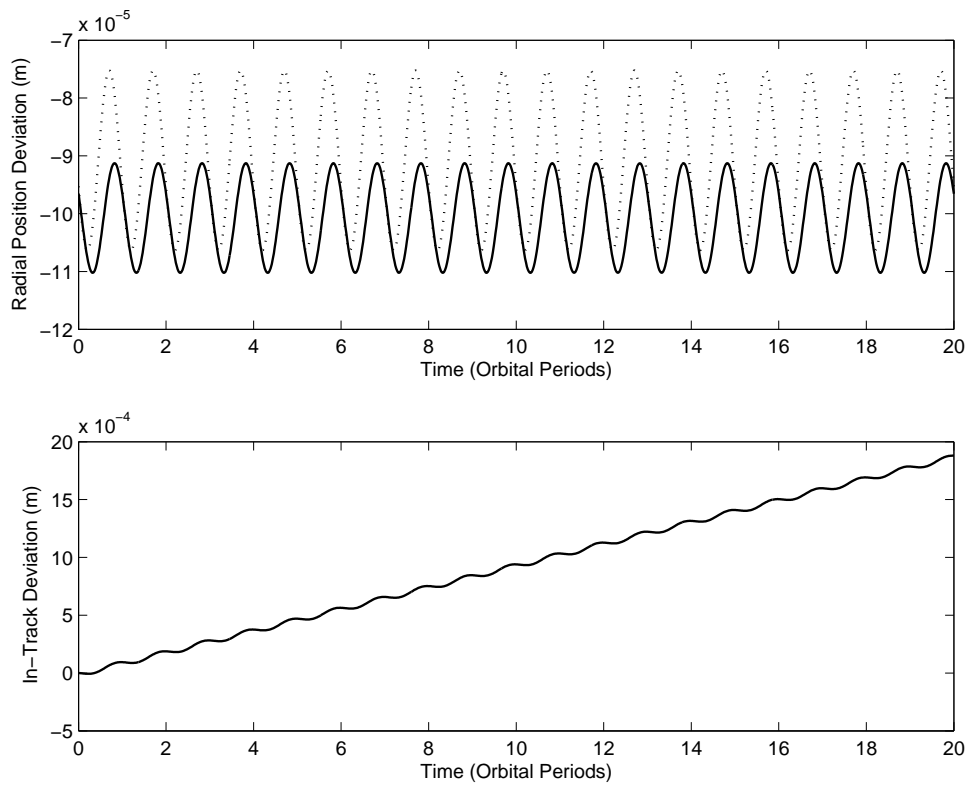
Figure B.12   Post Transfer Time History: Elliptical to In-Plane, $7000\,km$

B.2   Reconfiguration to an Elliptical Formation

This section contains the results for reconfigurations into a final elliptical formation with a semimajor axis of $75\,m$, such that the satellites are $150\,m$ apart when aligned in the in-track direction, from two separate initial formations: an in-plane formation with a separation distance of $50\,m$ and an elliptical formation with a semimajor axis of $25\,m$. The satellite positions and motion are with respect to a $7000\,km$ reference orbit.

B.2.1   In-Plane to Elliptical.   The following figures show the results of a reconfiguration from an in-plane formation with a separation distance of $50\,m$ to an elliptical formation with a $75\,m$ semimajor axis at a reference orbital radius of $7000\,km$:

Table B.3   In-Plane to Elliptical Reconfiguration Details, $7000\,km$

Reference Orbital Radius	$7000\,km$
Initial Formation	In-Plane: $50\,m$ separation
Final Formation	Elliptical: $75\,m$ semimajor axis
Total Time for Reconfiguration	54 Orbital Periods ($87\,hr$, $25\,min$, $40\,sec$)
Maneuver Cost	$\Delta v_1 = 0.02574\,m/sec$
	$\Delta v_2 = 0.02574\,m/sec$
Altitude Loss	$44.52\,m$
Control Cost	0.26
Constraint Cost	$1e{-}8$
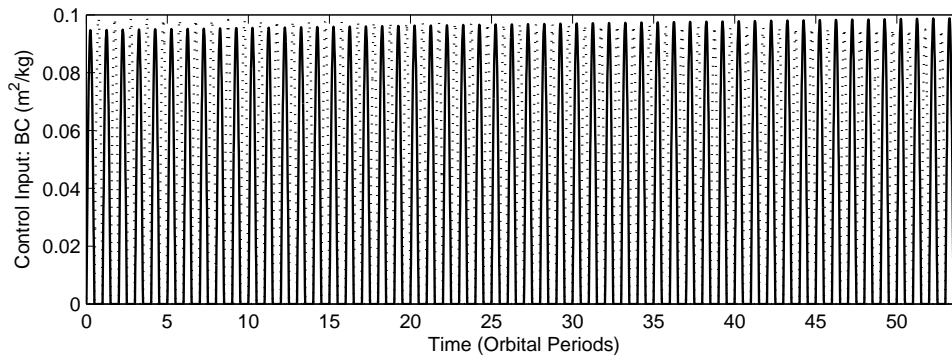
Figure B.13   Control Input: In-Plane to Elliptical, $7000\,km$
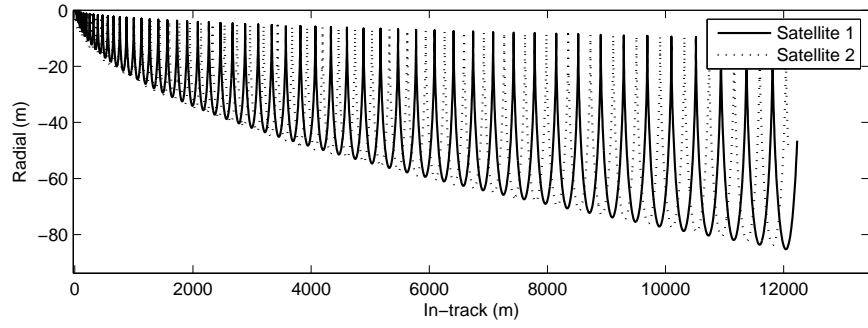
Figure B.14   Fixed Frame Plot: In-Plane to Elliptical, $7000\,km$
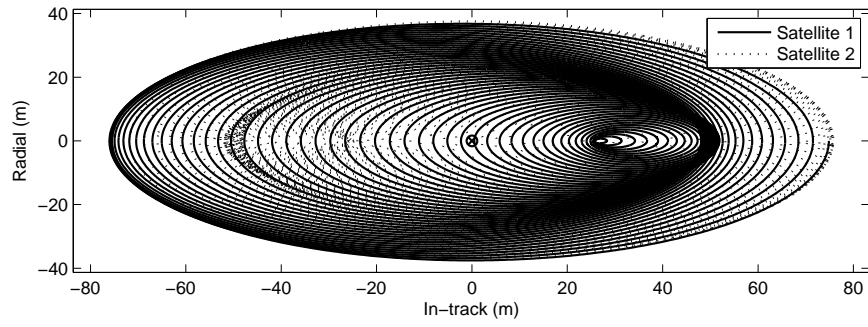
Figure B.15   Falling Frame Plot: In-Plane to Elliptical, $7000\,km$
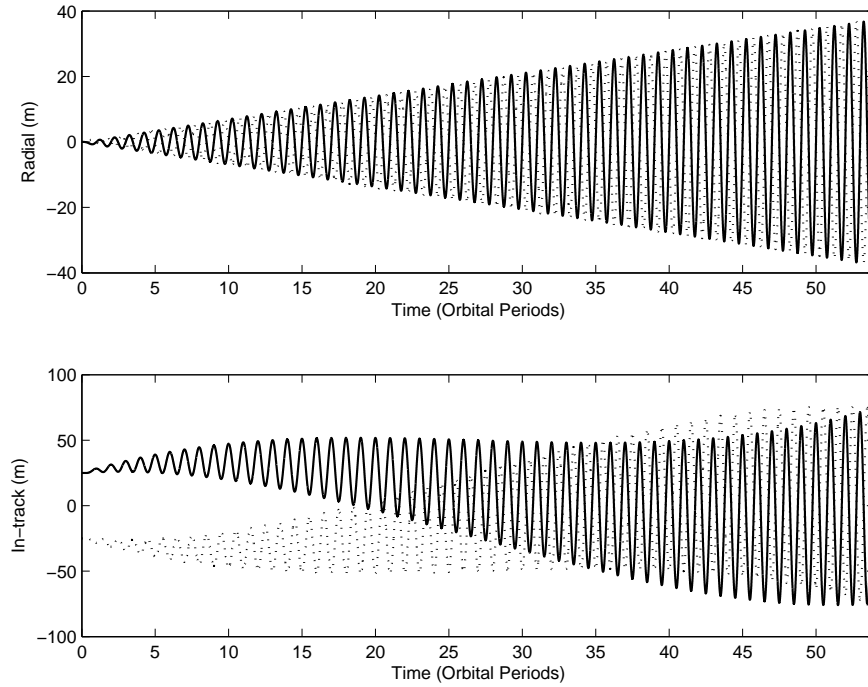
Figure B.16   Reconfiguration Time History Plot: In-Plane to Elliptical, $7000\,km$
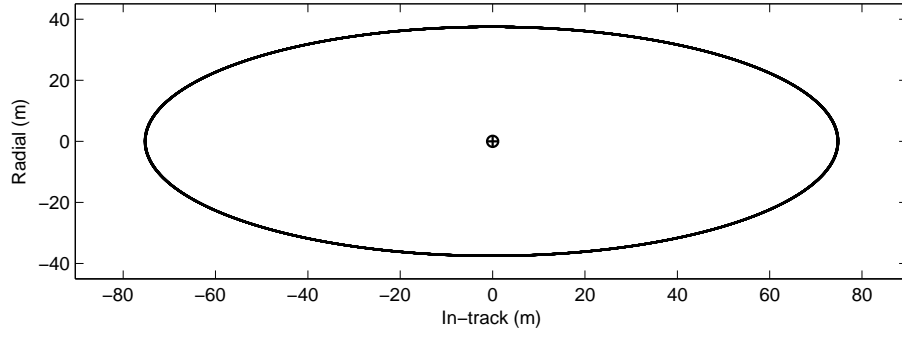
Figure B.17   Post Transfer Plot: In-Plane to Elliptical, $7000\,km$
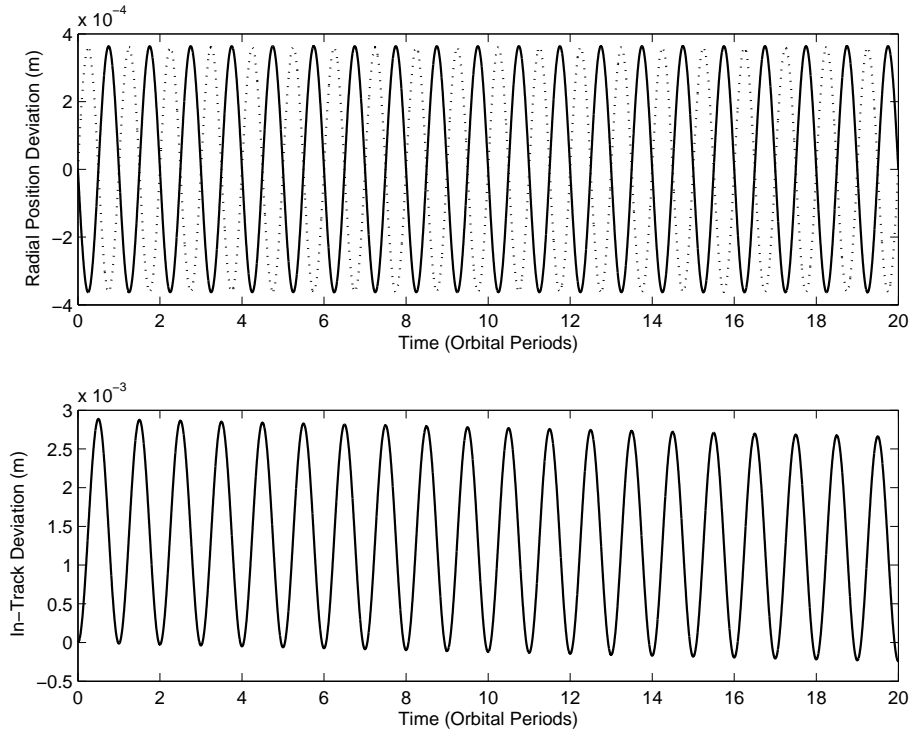
Figure B.18   Post Transfer Time History: In-Plane to Elliptical, $7000\,km$

B.2.2   Elliptical to Elliptical.   The following figures show the results of a recon-figuration from an elliptical formation with a $25\,m$ semimajor axis to another elliptical formation with a $75\,m$ semimajor axis at a reference orbital radius of $7000\,km$:

Table B.4   Elliptical to Elliptical Reconfiguration Details

Reference Orbital Radius	$7000\,km$
Initial Formation	Elliptical: $25\,m$ semimajor axis
Final Formation	Elliptical: $75\,m$ semimajor axis
Total Time for Reconfiguration	36 Orbital Periods ($58\,hr$, $17\,min$, $7\,sec$)
Maneuver Cost	$\Delta v_1 = 0.01716\,m/sec$
	$\Delta v_2 = 0.01716\,m/sec$
Altitude Loss	$29.68\,m$
Control Cost	0.17
Constraint Cost	$1e{-}8$
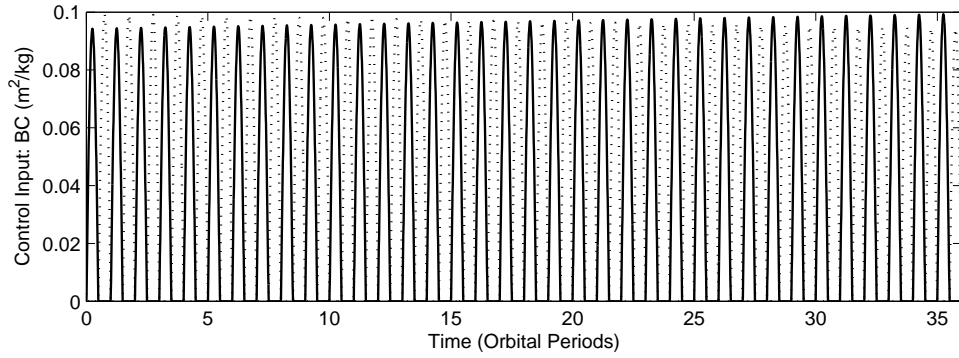
Figure B.19   Control Input: Elliptical to Elliptical, $7000\,km$
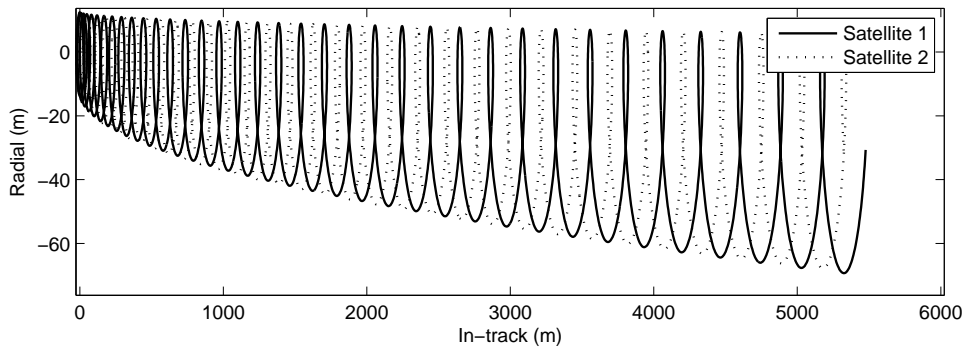
Figure B.20   Fixed Frame Plot: Elliptical to Elliptical, $7000\,km$
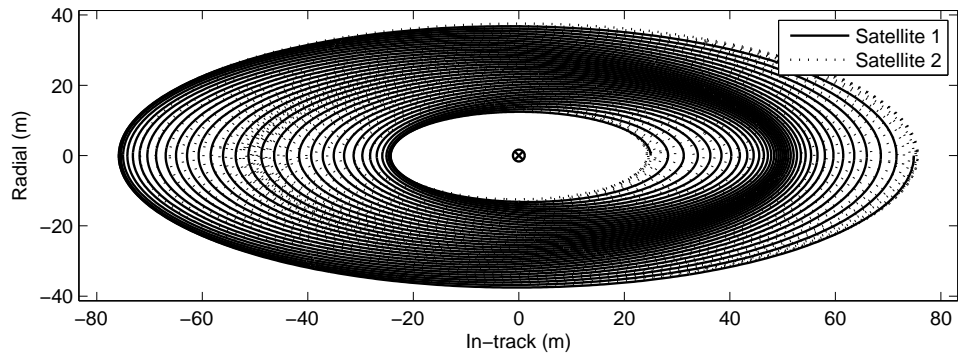
Figure B.21   Falling Frame Plot: Elliptical to Elliptical, $7000\,km$
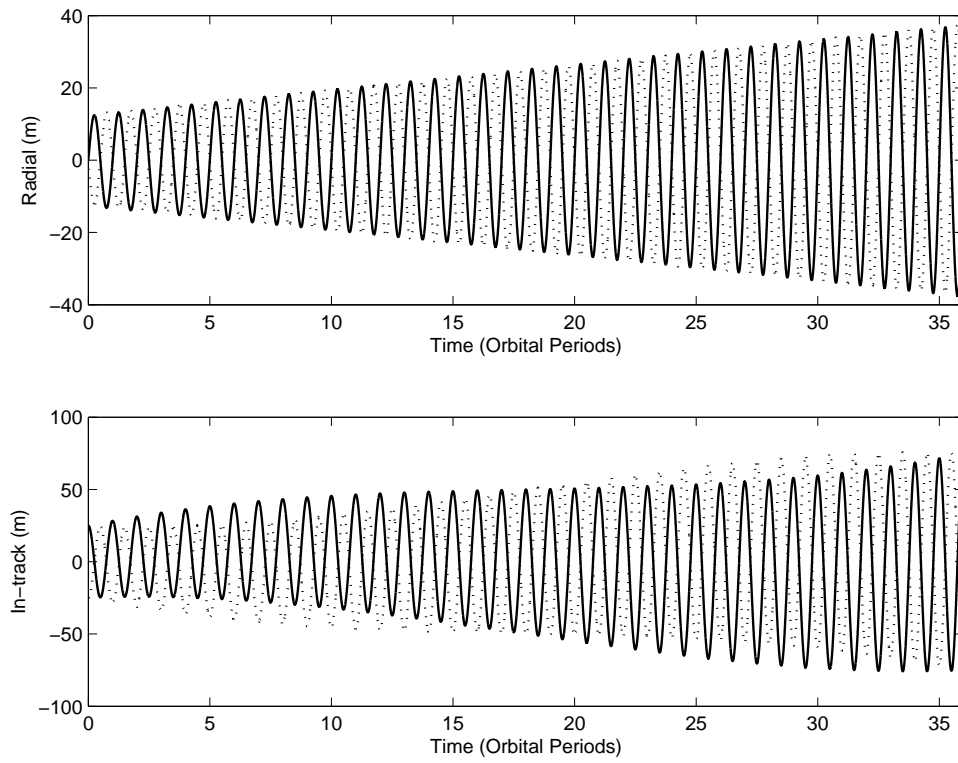
Figure B.22   Reconfiguration Time History Plot: Elliptical to Elliptical, $7000\,km$
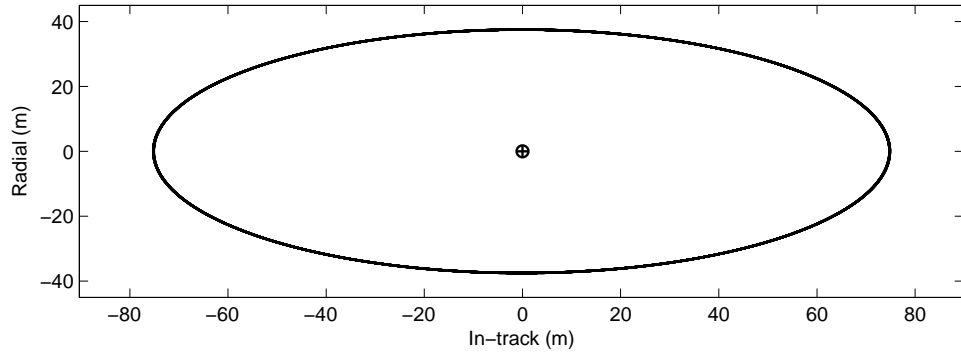
Figure B.23   Post Transfer Plot: Elliptical to Elliptical, 7000 km
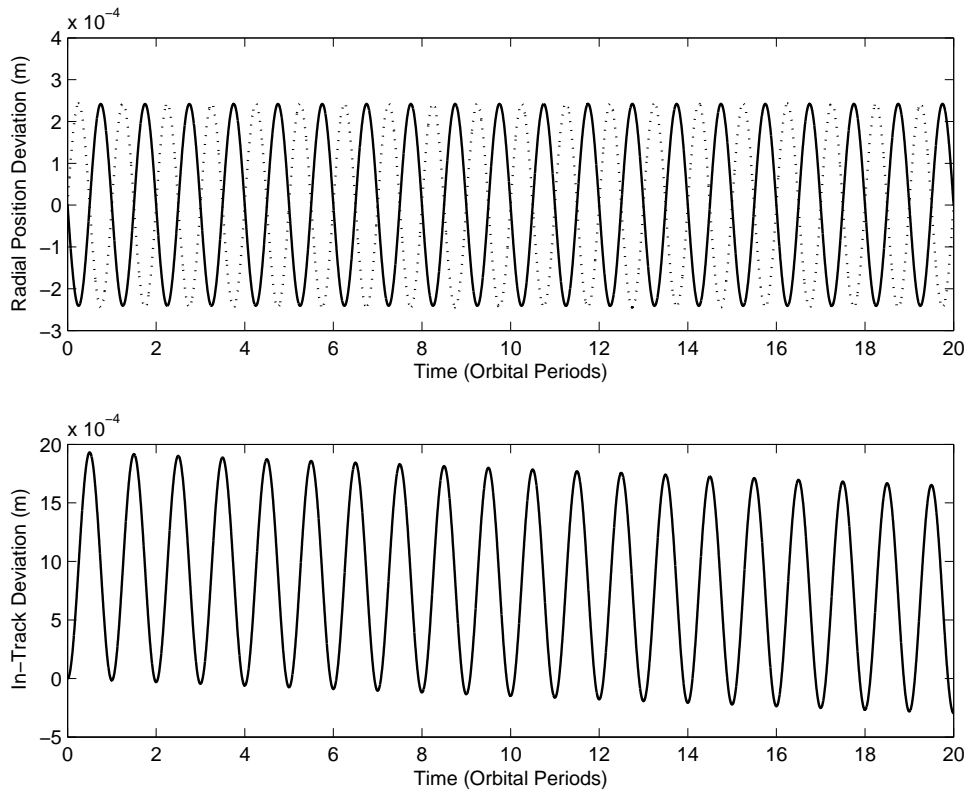
Figure B.24   Post Transfer Time History: Elliptical to Elliptical, 7000 km

Appendix C. Source Code

Shown below is the MATLAB® source code used to generate the results presented within
this study.

```
%*************************************************************************
%----------------------    TERMINAL_CONTROLLER    ------------------------
%*************************************************************************
% Terminal Controller:  Main piece of code used to determine the optimal
% reconfiguration of the user-specified, two-satellite formations.
% The user specifies whether to drive formation to an in-plane, elliptical
% (2x1), or a formation with zero in-track drift but no constraints on the
% radial oscillations, from some given initial formation or some initial
% position for each satellite. Takes the final state from the optimization
% routine and propagates it forward in time using the mean motion for the
% new altitude to show that the assumption of a time-invariant system
% holds.
% Code calls the following subfunctions:
%    - atmos_exp.m:  exponential atmospheric density model
%    - cw2_eom.m:    differential equations for the two-satellite formation
%    - ham_eom.m:    Hamiltonian system of equations for the two-satellite
%                    formation
% Written by: Blake Hajovsky
%    -- Original version: 10 Oct 06
%    --> Last update: 15 Feb 07

function terminal_controller
clear all

% Define the global variables:
global n0 rho u v0
tic % Start the clock
%*************************************************************************
%----------------------    USER INPUTS    --------------------------------
%*************************************************************************
% Define the initial formation:
%    init_form = 1 => in-plane formation (no in-track drift/radial osc.)
```

```matlab
%   init_form = 2 => elliptical (2x1 ellipse; no in-track drift)
%   init_form = 3 => post payload separation or any other user defined
%                    initial conditions
init_form = 2;
% If the in-plane or elliptical formation was chosen, define the in-track
% separation distance for the initial formation:
d_sep0 = 50;
% If the post-payload separation formation or any other formation was
% selected for the initial orbit, define the initial relative position of
% the satellites (meters):
%   x0 = [x y z | dx dy dz]'
x01 = [-10; 20; 0; -0.04; 0.005; 0]; x02 = [10; -20; 0; 0.04;
-0.005; 0];


% Define the final formation:
%   flg = 1 => in-plane (no in-track drift; no radial oscillation)
%   flg = 2 => elliptical (2x1 ellipse; no in-track drift)
%   flg = 3 => formation without radial constraint (w/ no in-track drift)
flg = 2;
% Define the final in-track separation distance:
d_sepf = 500;


% Define the optimization parameters and other values:
% Define the circular reference orbit radius (km):
r0 = 6800;   % km
% Define the length of time over which to optimize the system (orbital
% periods):
t_final = 8;
% Set the number of steps for the linear propagation of the controlled
% system:
Ns = 5000;
% Define the length of time to propagate the EOM after the optimization
% (orbital periods):
t_prop = 20;
% Set the weight on the final constraints (wcd = weight on drift,
% wcs = weight on separation distance):
wcd = 8e8; wcs = 8e8;
```

```matlab
% Specify whether or not to plot the 'fixed' plane, holding the relative
% reference frame constant (positive control inputs only):
% NOTE: Keep OFF if not being used to speed up the simulation.
%    fixed_frame = 0 => OFF
%    fixed_frame = 1 => ON
fixed_frame = 0;
% Specify where to create the folder that the *.eps files will be sent:
foldername = ['el2el_1']; mkdir(foldername)


%*************************************************************************
%----------------------  END USER INPUTS   ---------------------------
%*************************************************************************
% We should print to the screen what we have selected with the input from
% above as a check on what we are actually doing.  Do this here:
% First, print the initial formation:
if init_form == 1       % an in-plane formation has been selected
    disp(sprintf('Initial Formation: In-plane w/ separation of %4.2f m.',d_sep0));
elseif init_form == 2   % an elliptical formation has been selected
    disp(sprintf('Initial Formation: Elliptical w/ ''a'' = %4.2f m.',0.5*d_sep0));
    if start1 == 0, disp('Transfer begins from the RADIAL position.')
    elseif start1 == 1, disp('Transfer begins from the IN-TRACK position.')
    else
        % An incorrect selection has been made, so break the code here so
        % the problem can be corrected:
        error('An incorrect selection has been made for ''start1,'' where to
        begin the transfer.')
    end
elseif init_form == 3   % the user chose the initial conditions
    disp(sprintf('Initial Formation: User defined.'));
else
    % An incorrect selection has been made, so break the code here so the
    % problem can be corrected:
    error('An incorrect selection has been made for ''init_form,'' the initial
    formation.')
end


% Now, print the final formation:
```

```
if flg == 1           % an in-plane formation
    disp(sprintf('Final Formation: In-plane w/ separation of %4.2f m.',d_sepf));
elseif flg == 2       % an elliptical formation
    disp(sprintf('Final Formation: Elliptical w/ ''a'' = %4.2f m.',0.5*d_sepf));
elseif flg == 3       % formation w/out a radial constraint
    disp(sprintf('Final Formation: In-track separation distance only constrained
    w/ d = %4.2f m',d_sepf));
else
    % An incorrect selection has been made, so break the code here so the
    % problem can be corrected:
    error('An incorrect selection has been made for ''flg,'' the final formation.')
end
% Output the reference orbit radius and controlled time:
disp(sprintf('Reference Orbital Radius: %4.0f km.',r0));
disp(sprintf('Controlled over %2.0f orbital periods.',t_final));


%***************************************************************************
%------------------------ BEGIN MAIN SCRIPT ----------------------------
%***************************************************************************
% Define the Earth's mean equatorial radius and the gravitational
% parameter:
Re = 6378.137;      % km
mu = 398600.4418;   % km^3/sec^2

% Determine the mean motion of the reference orbit:
n0 = sqrt(mu/r0^3);

% Determine the reference velocity (km/sec) and convert to m/s:
v = sqrt(mu/r0); v_ref = v*1000;

% Assuming the atmosphere rotates with the Earth, calculate the atmospheric
% velocity in m/sec (angular velocity calculated based on sidereal day,
% 23h 56m 4.0905s = 86164.0905 sec):
w_earth = 2*pi/(86164.0905); v_atm = w_earth*r0*1000;

% Now, determine the reference velocity with respect to the atmosphere:
v0 = v_ref - v_atm;
```

```
% Determine the orbital period of the reference orbit:
t_period = 2*pi*sqrt(r0^3/mu);


% Call 'atmos_exp.m' to determine the atmospheric density at the reference
% altitude (kg/m^3):
rho = atmos_exp(r0);


%*************************************************************************
%-------------------  INITIAL FORMATION SET-UP   -----------------------
%*************************************************************************
% Determine the initial position of the satellites based on the initial
% formation selected and the desired transfer starting position:
if init_form == 1
    % An in-plane starting formation has been selected.  This particular
    % formation has only an in-track separation distance (all velocities
    % are zero and the radial/cross-track components are zero).
    x01 = [0; 0.5*d_sep0; 0; 0; 0; 0];
    x02 = [0; -0.5*d_sep0; 0; 0; 0; 0];
elseif init_form == 2
    % An elliptical formation has been selected.  The initial conditions
    % are dependent upon the point to the start the transfer.
    % This selection begins the transfer from the in-track separation
    % point (zero radial).  So, the initial conditions will have an
    % in-track separation and a radial velocity.  Determine these
    % values:
    in_sep1 = 0.5*d_sep0;
    in_sep2 = -0.5*d_sep0;
    % Now specify the radial velocities:
    v1 = 0.25*d_sep0*n0;
    v2 = -0.25*d_sep0*n0;
    % Define the satellites' states:
    x01 = [0; in_sep1; 0; v1; 0; 0];
    x02 = [0; in_sep2; 0; v2; 0; 0];
elseif init_form == 3, % Do nothing; initial conditions already specified.
else, % Do nothing;
end
```

```matlab
% Build the overall initial state vector:
x0 = [x01; x02];


%**************************************************************************
%--------------------- OPTIMIZATION ROUTINE ---------------------------
%**************************************************************************
% Determine the desired separation rate to meet the 2x1 ellipse constraint:
dr = 0.5*d_sepf*n0;


% Define some of the constants that will be used ahead:
n02 = n0^2; v02 = v0^2; v03 = v0^3; v06 = v0^6; rho2 = rho^2;


% Define the A1 matrix (6x6) for the state of 1 satellite:
A1 = [0, 0, 0, 1, 0, 0; 0, 0, 0, 0, 1, 0; 0, 0, 0, 0, 0, 1;...
    3*n02, 0, 0, 0, 2*n0, 0; 0, 0, 0, -2*n0, 0, 0; 0, 0, -n02, 0, 0, 0];


% Now form the overall A matrix.  Since the mean motion corresponds to the
% reference orbit, A1 = A2.  So form 12x12 A matrix using same entries:
A = [A1, zeros(6,6); zeros(6,6), A1];


% Define the control matrix for each satellite (6x1):
B1 = [0; 0; 0; 0; -0.5*rho*v02; 0];


% Now form the overall control matrix (12x2):
B = [B1, zeros(6,1); zeros(6,1), B1];


% Define the control penalty matrix R:
R = [0.25*rho2*v06, 0; 0, 0.25*rho2*v06];


% Define the final time:
tf = t_final*t_period;


% Define Qf, the final error weighting matrix:
Qf = eye(12)*wcd; Qf(2,2) = wcs; Qf(8,8) = wcs;


% Define the terminal constraint matrix (Mf) and the final constraint
% vector (psi) based on the formation-type selected:
```

```matlab
%    flg = 1 => in-plane (no in-track drift; no radial oscillation)
%    flg = 2 => elliptical (2x1 ellipse; no in-track drift)
%    flg = 3 => formation without radial constraint (no in-track drift)
d = d_sepf; if flg == 1
    % Define Mf, the terminal constraint matrix:
    Mf = zeros(12,12); Mf(1,1) = 2*n0; Mf(7,7) = -2*n0; Mf(2,2) = 1;
    Mf(8,8) = -1; Mf(4,4) = 1; Mf(10,10) = -1; Mf(5,5) = 1; Mf(11,11) = -1;
    % Define psi, the final constraint vector:
    psi = zeros(12,1); psi(2) = 0.5*d; psi(8) = 0.5*d;
elseif flg == 2
    % Define Mf, the terminal constraint matrix:
    Mf = zeros(12,12); Mf(1,1) = 2*n0; Mf(7,7) = -2*n0; Mf(2,2) = 1;
    Mf(8,8) = -1; Mf(4,4) = 1; Mf(10,10) = -1; Mf(5,5) = 1; Mf(11,11) = -1;
    % Define psi, the final constraint vector:
    psi = zeros(12,1); psi(2) = 0.5*d; psi(8) = 0.5*d; psi(4) = 0.5*dr;
    psi(10) = 0.5*dr;
elseif flg == 3
    % Define Mf, the terminal constraint matrix:
    Mf = zeros(12,12); Mf(1,1) = 2*n0; Mf(7,7) = -2*n0; Mf(2,2) = -1;
    Mf(8,8) = 1; Mf(5,5) = 1; Mf(11,11) = -1;
    % Define psi, the final constraint vector:
    psi = zeros(12,1); psi(2) = -0.5*d; psi(8) = -0.5*d;
else, error('Incorrect ''flg'' designator for formation-type!')
end


% Define the Hamiltonian Matrix:
H = [A, -B*inv(R)*B'; zeros(12,12), -A'];


% Find the forward transition matrix of Euler-Lagrange eqns, t=tf to t=t0:
Ph = expm(H*tf);


% Partition the transition matrix to separate the states and costates
% components:
state_length = length(x0); n1 = [1:state_length]; n2 =
[state_length+1:2*state_length]; tran11 = Ph(n1,n1); tran12 =
Ph(n1,n2); tran21 = Ph(n2,n1); tran22 = Ph(n2,n2);
```

```matlab
% Solve for the initial costates:
Sf = Mf'*Qf*Mf; a = Mf'*Qf*psi; lambda0 = ...
inv((tran22-Sf*tran12))*((Sf*tran11-tran21)*x0-a);


%*************************************************************************
%---------------------- Linear Propagation -------------------------
%*************************************************************************
% Now, use the state transition matrix to linearly propagate the initial
% states (defined) and costates (just found) to the final time:
y0 = [x0; lambda0]; t = tf*[0:1/Ns:1];


% We're going to multiply by R inverse, B transpose, and the time step
% quite a few times within the next loop.  So, calculate these things in
% advance to speed things along.
R_inv = inv(R); B_tran = B'; t_step = 1/Ns*tf;


% Initialize the summers:
cost1 = 0; eneg_cost = 0; control_tot1a = 0; control_tot2a = 0;


% Begin the forward propagation:
for i=1:Ns+1
    y(:,i) = expm(H*t(i))*y0;
    x_lin(:,i) = y(n1,i);
    u_lin(:,i) = -R_inv*B_tran*y(n2,i);
    cost1 = cost1 + u_lin(:,i)'*R*u_lin(:,i)*t_step;
    eneg_cost = eneg_cost + (0.5*rho*v03*(abs(u_lin(1,i))+...
        abs(u_lin(2,i)))*t_step);
    control_tot1a = control_tot1a + abs(0.5*rho*v02*u_lin(1,i)*t_step);
    control_tot2a = control_tot2a + abs(0.5*rho*v02*u_lin(2,i)*t_step);
end


%*************************************************************************
%----------------- Numerically Integrated Solution --------------------
%*************************************************************************
% Ideally, the analytical results for the controlled portion above should
% match what we get if the Hamiltonian system is integrated forward in time
% with the same inputs (same initial states and costates).  So let's
```

```matlab
% numerically integrate the EOM to verify the results:


% Set-up the parameters for ode45:
x0_ham = [x0; lambda0]; t_fin = t_final*t_period; tspan = [0
t_fin]; options = odeset('RelTol',1e-9,'AbsTol',1e-9);


% Call ode45 to propagate the Hamiltonian system forward in time:
[t_num,out] = ode45(@ham_eom,tspan,x0_ham,options);


% Separate the states and costates from the numerical integration:
x_num = out(:,n1); lam_num = out(:,n2);


% Grab and store the final state and costate from the numerical
% integration:
[n,m] = size(out); xf_all = out(n,:); xf_num =
xf_all(1:state_length); lamf_num =
xf_all(state_length+1:2*state_length);


% In the upcoming loop, we'll determine the control input at each time
% step.  To do this, we need the R and B matrices.  So form these outside
% the loop and then call from within:
%   Recall: rho2 = rho^2
%           v06  = v0^6
R1 = [0.25*rho2*v06]; R2 = R1;
inv_R1 = inv(R1);    % inverse of R1
inv_R2 = inv(R2);    % inverse of R2


% Define the control matrix for each satellite (6x1):
%   Recall: v02 = v0^2
B1 = [0; 0; 0; 0; -0.5*rho*(v02); 0]; B2 = B1;
B1_tran = B1';       % transpose of B1
B2_tran = B2';       % transpose of B2


% Determine the control input at each time step:
for jj = 1:n
    % Grab the costates:
    row1 = out(jj,:);
```

```
    con1 = row1(13:18);
    con2 = row1(19:24);
    lam3(jj,:) = con1;
    lam4(jj,:) = con2;

    % Using R, B, and the costate, determine the control input to each sat:
    u_num1(jj) = -inv_R1*B1_tran*con1';
    u_num2(jj) = -inv_R2*B2_tran*con2';
end

% Determine how close we are to meeting the terminal constraints for both
% the linear propagation and the numerical integration (output results
% later):
termc_drift_lin = xf_lin(5)-xf_lin(11)+2*n0*(xf_lin(1)-xf_lin(7));
termc_distance_lin = xf_lin(8)-xf_lin(2); termc_drift_num =
xf_num(5)-xf_num(11)+2*n0*(xf_num(1)-xf_num(7));
termc_distance_num = xf_num(8)-xf_num(2);


%*************************************************************************
%------------------- POST OPTIMIZATION ANALYSIS    ---------------------
%*************************************************************************
% We now have an optimal solution propagated from t0 to tf.  Let's see how
% well it actually performed.

% Given this optimal input, we now want to plot the controlled orbit in the
% fixed reference frame.  Set-up the parameters here:
x0_new = x0; tspan = [0 t_step]; t_count = 0; eneg_cost2 = 0;
control_tot1 = 0; control_tot2 = 0; for jj = 1:length(u_lin)
    for i = 1:2
        if u_lin(i,jj) <= 0, u_lin(i,jj) = 0;
        else, u_lin(i,jj) = 2*u_lin(i,jj);
        end
    end
    % This calculates the altitude loss based on the new control input:
    eneg_cost2 = eneg_cost2 + 0.5*rho*v03*u_lin(1,jj)*t_step;


    % Now calculate the control cost on each sat based on the new control
```

```matlab
    % input:
    control_tot1 = control_tot1 + abs(0.5*rho*v02*u_lin(1,jj)*t_step);

    control_tot2 = control_tot2 + abs(0.5*rho*v02*u_lin(2,jj)*t_step);


    % If we decided to check ourselves with the new input, we should run
    % this next part (specify in the 'User Inputs' at the beginning of the
    % script).  The note below the 'if' statement has a good explanation of
    % this loop's purpose:
    if fixed_frame == 1
        % With this 'new' control input, we want to propagate the EOM
        % forward again to ensure we get the same result:
        u = [u_lin(1,jj); u_lin(2,jj)];
        [t_n,x_n] = ode45(@cw2_eom,tspan,x0_new,options);


        % Now, grab the final values from the above integration:
        nm = length(x_n);
        x0_new = x_n(nm,:);
        x_new(jj,:) = x0_new;


        % Increment the time count and set the new tspan:
        t_count = t_count+t_step;
        t_span = [t_count-t_step, t_count];
    else, % Do nothing
    end
end


% Calculate the cost of the terminal constraints:
err_diff = Mf*x_lin(:,length(x_lin))-psi; cost2 =
err_diff'*Qf*err_diff;


% Calculate the change in semi-major axis as a result of the maneuver:
Energy0 = -(mu*1000^3)/(2*r0*1000); % meters^2 / sec^2
Energyf2 = Energy0 - 0.5*eneg_cost;     % meters^2 / sec^2
rf2 = -(mu*1000^3)/(2*Energyf2);    % meters
altitude_loss2 = r0*1000 - rf2;


% Now propagate the final state from the optimization forward over a user
```

```matlab
% defined time period to see the orbit post-optimization with zero control.
% Set up the parameters for ode45.m:
x0_new = xf_num(1:12); t_fin2 = t_prop*t_period; tspan = [0
t_fin2]; options = odeset('RelTol',1e-9,'AbsTol',1e-9);


% Calculate a new mean motion from the new altitude to use for the
% post-optimization propagation:
rf_km = rf2*10^-3; nf = sqrt(mu/rf_km^3); delta_n = nf-n0;
percent_change_n = delta_n/n0*100; n0 = nf;


% Calculate a new satellite vel wrt the rotating atmosphere from the new
% altitude:
vf = sqrt(mu/rf_km);            % km/sec
vf_ref = vf*1000;              % m/sec
vf_atm = w_earth*rf_km*1000;   % m/sec
vf_new = vf_ref - vf_atm;      % m/sec
change_v = (vf_new - v0)/v0*100;   % percent change v


% Turn-off the control:
u = [0 0]';


% Call ode45 to propagate the satellite EOM forward in time over the number
% of periods specified for the post-optimization analysis:
[t_num2,out2] = ode45(@cw2_eom,tspan,x0_new,options);


%*************************************************************************
%----------------------- PRINT TO SCREEN -------------------------------
%*************************************************************************
% Output the total control used:
disp(sprintf('Integral cost, Total: %5.2f',cost1));
disp(sprintf('Terminal cost, Total: %2.7f',cost2));
disp(sprintf('Control usage, Sat 1: %2.5f m/sec',control_tot1));
disp(sprintf('Control usage, Sat 2: %2.5f m/sec',control_tot2));
control_tot_init = control_tot1a + control_tot2a;
disp(sprintf('Control Check (Total from orig control): %2.5f m/sec',...
    control_tot_init));
disp(sprintf('Altitude loss (avg): %6.2f m',altitude_loss2))
```

```
disp(sprintf('Percent Change in Mean Motion: %1.6f',percent_change_n));

disp(sprintf('Percent Change in Relative Velocity: %1.6f',change_v));

disp(sprintf('Percent Change in Atmospheric Density: %1.6f',change_rho));


% Output the length of time the satellites were controlled (specified in

% terms of orbital periods, but convert to hours:min:sec):

tp_hr = floor(t_fin/(3600)); diff1 = t_fin-tp_hr*3600; tp_min =

floor(diff1/60); tp_sec = diff1-tp_min*60; disp(' ');

disp(sprintf('System controlled over %2.0f hr, %2.0f min, %2.1f sec',...

    tp_hr,tp_min,tp_sec));


% Output the terminal constraints:

disp(' '); disp('Terminal Constraints from NUMERICAL

INTEGRATION:')

disp(sprintf('Drift Constraint:    %0.5g',termc_drift_num))

disp(sprintf('Distance Constraint: %4.1f (m)',termc_distance_num))


%***************************************************************************

%------------------------ BEGIN PLOTTING   ---------------------------

%***************************************************************************

% Plot the results of the optimization (plot of controlled portion):

% Plot the control history:

figure(1) subplot(2,1,1)

plot(t/t_period,u_lin(1,:),'k',t/t_period,u_lin(2,:),'k:','LineWidth',1.2)

set(gca,'XLim',[0,t_final]) xlabel('Time (Orbital Periods)')

ylabel('Control Input: BC (m^2/kg)')


% Convert Figure 1 to .eps:

file1 = [foldername '\control_input']; print('-f1','-depsc',file1)


% Plot the radial/in-track plane for the numerical integration:

figure(2) subplot(2,1,1)

plot(x_num(:,2),x_num(:,1),'k',x_num(:,8),x_num(:,7),'k:',0,0,'ko',...

    0,0,'kx','LineWidth',1.2)

x_min = min(min(x_num(:,2)),min(x_num(:,8))); y_min =

min(min(x_num(:,1)),min(x_num(:,7))); x_max =

max(max(x_num(:,2)),max(x_num(:,8))); y_max =
```

```
max(max(x_num(:,1)),max(x_num(:,7)));
set(gca,'XLim',[1.1*x_min,1.1*x_max],'YLim',[1.1*y_min,1.1*y_max]);
xlabel('In-track (m)') ylabel('Radial (m)') legend('Satellite
1','Satellite 2')

% Convert Figure 2 to .eps:
file1 = [foldername '\falling_frame']; print('-f2','-depsc',file1)

% Plot the radial and in-track time histories of the numerical integration:
figure(3) subplot(2,1,1) plot(t_num/t_period,x_num(:,1),'k',...
    t_num/t_period,x_num(:,7),'k:','LineWidth',1.2)
set(gca,'XLim',[0,t_final]) xlabel('Time (Orbital Periods)')
ylabel('Radial (m)')

subplot(2,1,2) plot(t_num/t_period,x_num(:,2),'k',...
    t_num/t_period,x_num(:,8),'k:','LineWidth',1.2)
set(gca,'XLim',[0,t_final]) xlabel('Time (Orbital Periods)')
ylabel('In-track (m)')

% Convert Figure 3 to .eps:
file1 = [foldername '\reconfig_time_history'];
print('-f3','-depsc',file1)

figure(4) subplot(2,1,1) if flg == 1,
plot(out2(:,2),out2(:,1),'k+',out2(:,8),out2(:,7),'k+',...
        0,0,'k+',0,0,'ko','LineWidth',1.2)
else, plot(out2(:,2),out2(:,1),'k',out2(:,8),out2(:,7),'k:',...
        0,0,'k+',0,0,'ko','LineWidth',1.2)
end x_min = min(min(out2(:,2)),min(out2(:,8))); x_max =
max(max(out2(:,2)),max(out2(:,8))); y_min =
min(min(out2(:,1)),min(out2(:,7))); y_max =
max(max(out2(:,1)),max(out2(:,7)));
set(gca,'XLim',[1.2*x_min,1.2*x_max],'YLim',[1.2*y_min,1.2*y_max]);
xlabel('In-track (m)') ylabel('Radial (m)') if flg == 1
    axis equal
end
```

```
% Convert Figure 4 to .eps:
file1 = [foldername '\post_inplane2']; print('-f4','-depsc',file1)


% Post-Optimization time history plots:
figure(5) subplot(2,1,1) if flg == 1,
plot(t_num2/t_period,out2(:,1),'k',...
        t_num2/t_period,out2(:,7),'k:','LineWidth',1.2)
else, plot(t_num2/t_period,out2(:,1),'k',...
        t_num2/t_period,out2(:,7),'k:','LineWidth',1.2)
end y_min = min(min(out2(:,1)),min(out2(:,7))); y_max =
max(max(out2(:,1)),max(out2(:,7))); if flg == 1,
set(gca,'YLim',[-0.01,0.01]); else,
set(gca,'YLim',[1.4*y_min,1.4*y_max]); end xlabel('Time (Orbital
Periods)') ylabel('Radial (m)')


subplot(2,1,2) plot(t_num2/t_period,out2(:,2),'k',...
    t_num2/t_period,out2(:,8),'k:','LineWidth',1.2)
y_min = min(min(out2(:,2)),min(out2(:,8))); y_max =
max(max(out2(:,2)),max(out2(:,8)));
set(gca,'YLim',[1.4*y_min,1.4*y_max]); xlabel('Time (Orbital
Periods)') ylabel('In-track (m)')


% Convert Figure 5 to .eps:
file1 = [foldername '\post_time_hist'];
print('-f5','-depsc',file1)


figure(6) subplot(2,1,1) if flg == 1
    y1_norm = norm(out2(:,1));
    y2_norm = norm(out2(:,7));
    plot(t_num2/t_period,out2(:,1),'k',...
        t_num2/t_period,out2(:,7),'k:','LineWidth',1.2)
else
    plot(t_num2/t_period,out2(:,1)-d_sepf/4*sin(n0*t_num2)-out2(1,1),...
        'k', t_num2/t_period,...
        out2(:,7)+d_sepf/4*sin(n0*t_num2)-out2(1,7),'k:','LineWidth',1.2)
end set(gca,'YLim',[-0.008,0.008]); xlabel('Time (Orbital
Periods)') ylabel('Radial Position Deviation (m)')
```

```matlab
subplot(2,1,2) if flg == 1

    plot(t_num2/t_period,(out2(:,2)-d_sepf/2)-...
        (out2(:,8)+d_sepf/2),'k','LineWidth',1.2)

    xlabel('Time (Orbital Periods)')

    ylabel('In-Track Deviation (m)')

elseif flg == 2

    plot(t_num2/t_period,(out2(:,2)-d_sepf/2*cos(n0*t_num2))-...
        (out2(:,8)+d_sepf/2*cos(n0*t_num2)),'k','LineWidth',1.2)

    xlabel('Time (Orbital Periods)')

    ylabel('In-Track Deviation (m)')

end


% Convert Figure 6 to .eps:

file1 = [foldername '\post_hist_deviation'];

print('-f6','-depsc',file1)


% If we decided to run the simulation holding the relative frame fixed,

% let's plot the results:

if fixed_frame == 1

    % Plot these results:

    figure(7)

    subplot(2,1,1)

    plot(x_new(:,2),x_new(:,1),'k',...
        x_new(:,8),x_new(:,7),'k:','LineWidth',1.2)

    x_min = min(min(x_new(:,2)),min(x_new(:,8)));

    y_min = min(min(x_new(:,1)),min(x_new(:,7)));

    x_max = max(max(x_new(:,2)),max(x_new(:,8)));

    y_max = max(max(x_new(:,1)),max(x_new(:,7)));

    set(gca,'XLim',[1.1*x_min,1.1*x_max],'YLim',[1.1*y_min,1.1*y_max]);

    xlabel('In-track (m)')

    ylabel('Radial (m)')

    legend('Satellite 1','Satellite 2')


    % Convert Figure 7 to .eps:

    file1 = [foldername '\fixed_frame'];

    print('-f7','-depsc',file1)
```

```matlab
    % Now, we should propagate this final state forward without control to
    % show that it's equivalent to the other.
    nm = length(x_new);
    xf_new = x_new(nm,:);
    u = [0; 0];
    t_fin2 = t_prop*t_period;
    tspan = [0 t_fin2];
    [tf_n,xf_n] = ode45(@cw2_eom,tspan,x0_new,options);
else, % Do nothing
end


% Print to screen:
disp(' '); disp('Run completed.  Congratulations.')
toc % stop clock
return
%*************************************************************************
%-------------------   NEW FUNCTION: CW2_EOM.M   ------------------------
%*************************************************************************
% Function cw2_eom.m
% Clohessy-Wiltshire EOM for two satellites with a control input.
% The current state is passed as input to the function, but the mean motion
% (n), atmospheric density (rho), and control input (u) also need to be
% passed to the function.
function [dX] = cw2_eom(t,x) global n0 rho u v0


% Initialize commonly used values:
n = n0; n2 = n^2;


% Define the Earth radius, Gravitational parameter, and J2:
Re = 6378.137;      % km
mu = 398600.4418;   % km^3/sec^2


% Define the A1 matrix (6x6):
A1 = [0, 0, 0, 1, 0, 0; 0, 0, 0, 0, 1, 0; 0, 0, 0, 0, 0, 1;...
    3*n2, 0, 0, 0, 2*n, 0; 0, 0, 0, -2*n, 0, 0; 0, 0, -n2, 0, 0, 0];
```

C-17

```
% Now form the overall A matrix.  Since the mean motion corresponds to the
% reference orbit, A1 = A2.  So form 12x12 A matrix using same entries:
A = [A1, zeros(6,6); zeros(6,6), A1];


% Define the control matrix for each satellite (6x1):
B1 = [0; 0; 0; 0; -0.5*rho*(v0)^2; 0]; B2 = [0; 0; 0; 0;
-0.5*rho*(v0)^2; 0];


% Now form the overall control matrix (12x2):
B = [B1, zeros(6,1); zeros(6,1), B2];


% Define the EOM:
dX = A*x + B*u; return
%*************************************************************************
%------------------   NEW FUNCTION: HAM_EOM   --------------------------
%*************************************************************************
% Function ham_eom.m
% Subfunction called by 'ode45.m' to propagate the Hamiltonian EOM forward
% in time.
function [dX] = ham_eom(t,x) global n0 rho u v0


% Initialize commonly used values:
n = n0; n2 = n^2; v06 = v0^6; rho2 = rho^2;


% The input currently contains both the states and costates.  Split the
% input based on the number of states so the EOM can be easily defined.
state_length = 12; x0 = x(1:state_length); lam0 =
x(state_length+1:length(x));


% Define the A1 matrix (6x6) for the state of 1 satellite:
A1 = [0, 0, 0, 1, 0, 0; 0, 0, 0, 0, 1, 0; 0, 0, 0, 0, 0, 1;...
    3*n2, 0, 0, 0, 2*n, 0; 0, 0, 0, -2*n, 0, 0; 0, 0, -n2, 0, 0, 0];


% Now form the overall A matrix.  Since the mean motion corresponds to the
% reference orbit, A1 = A2.  So form 12x12 A matrix using same entries:
A = [A1, zeros(6,6); zeros(6,6), A1];
```

```
% Define the control matrix for each satellite (6x1):
B1 = [0; 0; 0; 0; -0.5*rho*(v0)^2; 0]; B2 = [0; 0; 0; 0;
-0.5*rho*(v0)^2; 0];


% Now form the overall control matrix (12x2):
B = [B1, zeros(6,1); zeros(6,1), B2];


% Define the control penalty matrix R:
R = [0.25*rho2*v06, 0; 0, 0.25*rho2*v06];


% Define the Hamiltonian dynamics:
dx = A*x0 - B*inv(R)*B'*lam0; dlambda = -A'*lam0;


% Form the output vector:
dX = [dx; dlambda]; return
%****************************************************************************
%-------------------------- ATMOS_EXP.M  ----------------------------
%****************************************************************************
% B. Hajovsky, 30 Aug 06
% Exponential Atmospheric Model
% Accepts as INPUT the orbital radius of the satellite in km; OUTPUTS the
% atmospheric density for that altitude based on the mean equatorial radius
% of Earth (density units: kg/m^3).
% NOTE: really only valid for altitudes less than 1000 km
% Taken from Vallado, pg 537
% Distances in km


function [rho_exp]=atmos_exp(R)
% Term Definitions:
% h0 = Base Altitude (km)
% rho0 = Nominal Density (kg/m^3)
% H = Scale Height (km)


% Define the Earth radius to calculate the altitude:
Earth_rad = 6378.137; % km; mean equatorial radius
r = R - Earth_rad;
```

```
if r>=0 & r<25, h0 = 0; rho0 = 1.225; H = 7.249; elseif r>=25 &
r<30, h0 = 25; rho0 = 3.899e-2; H = 6.349; elseif r>=30 & r<40, h0
= 30; rho0 = 1.774e-2; H = 6.682; elseif r>=40 & r<50, h0 = 40;
rho0 = 3.972e-3; H = 7.554; elseif r>=50 & r<60, h0 = 50; rho0 =
1.057e-3; H = 8.382; elseif r>=60 & r<70, h0 = 60; rho0 =
3.206e-4; H = 7.714; elseif r>=70 & r<80, h0 = 70; rho0 =
8.770e-5; H = 6.549; elseif r>=80 & r<90, h0 = 80; rho0 =
1.905e-5; H = 5.799; elseif r>=90 & r<100, h0 = 90; rho0 =
3.396e-6; H = 5.382; elseif r>=100 & r<110, h0 = 100; rho0 =
5.297e-7; H = 5.877; elseif r>=110 & r<120, h0 = 110; rho0 =
9.661e-8; H = 7.263; elseif r>=120 & r<130, h0 = 120; rho0 =
2.438e-8; H = 9.473; elseif r>=130 & r<140, h0 = 130; rho0 =
8.484e-9; H = 12.636; elseif r>=140 & r<150, h0 = 140; rho0 =
3.845e-9; H = 16.149; elseif r>=150 & r<180, h0 = 150; rho0 =
2.070e-9; H = 22.523; elseif r>=180 & r<200, h0 = 180; rho0 =
5.464e-10; H = 29.740; elseif r>=200 & r<250, h0 = 200; rho0 =
2.789e-10; H = 37.105; elseif r>=250 & r<300, h0 = 250; rho0 =
7.248e-11; H = 45.546; elseif r>=300 & r<350, h0 = 300; rho0 =
2.418e-11; H = 53.628; elseif r>=350 & r<400, h0 = 350; rho0 =
9.518e-12; H = 53.298; elseif r>=400 & r<450, h0 = 400; rho0 =
3.725e-12; H = 58.515; elseif r>=450 & r<500, h0 = 450; rho0 =
1.585e-12; H = 60.828; elseif r>=500 & r<600, h0 = 500; rho0 =
6.967e-13; H = 63.822; elseif r>=600 & r<700, h0 = 600; rho0 =
1.454e-13; H = 71.835; elseif r>=700 & r<800, h0 = 700; rho0 =
3.614e-14; H = 88.667; elseif r>=800 & r<900, h0 = 800; rho0 =
1.170e-14; H = 124.64; elseif r>=900 & r<1000, h0 = 900; rho0 =
5.245e-15; H = 181.05; elseif r>=1000, h0 = 1000; rho0 =
3.019e-15; H = 268.00; else, ERROR('Check Atmospheric Density
file!! Correct radius not found!') end
% Output the density measurement:
rho_exp = rho0*exp(-(r-h0)/H); return
%********************************************************************
%------------------------  END SCRIPT  ----------------------------
%********************************************************************
```

Bibliography

1. "The Air Force Research Laboratory Space Vehicles Directorate Page." AFRL/VS Homepage, http://www.vs.afrl.af.mil/, Accessed: 5 February 2007.

2. Bryson, Arthur E. *Dynamic Optimization*. Menlo Park CA: Addison-Wesley, 1999.

3. Bryson, Arthur E. and Yu-Chi Ho. *Applied Optimal Control*. Waltham MA: Ginn and Company, 1969.

4. Clohessy, W. H. and R. S. Wiltshire. "Terminal Guidance System for Satellite Rendezvous," *Journal of the Aerospace Sciences*, *Vol. 27*:pp. 653–658, 674 (September 1960).

5. Irvin, David J., Jr. *A Study of Linear vs. Nonlinear Control Techniques for the Reconfiguration of Satellite Formations*. MS thesis, AFIT/GA/ENY/01M-02. School of Engineering and Management, Air Force Institute of Technology (AU), Wright-Patterson AFB OH, March 2001 (ADA390156).

6. Jesse Leitner, Bauer, F. Folta D. Moreau M. Carpenter R. How J. "Distributed Spacecraft Systems Develop New GPS Capabilities," *GPS World* (February 2002).

7. Kaplan, Marshall H. *Modern Spacecraft Dynamics and Control*. New York: John Wiley and Sons, Inc., 1976.

8. Kirk, Donald E. *Optimal control Theory: An Introduction*. New York: Dover Publications, Inc., 1970.

9. Larson, Wiley J. and James R. Wertz. *Space Mission Analysis and Design* (Third Edition). Norwell MA and Torrance CA: Kluwer Academic Publishers and Microcosm Press, 1999.

10. Leonard, C. L., W. M. Hollister and E. V. Bergmann. "Orbital Formationkeeping with Differential Drag," *Journal of Guidance, Control, and Dynamics*, *Vol. 12*(No. 1):pp. 108–113 (1989).

11. Lewis, Frank L. and Vassilis L. Syrmos. *Optimal Control* (Second Edition). New York: John Wiley and Sons, Inc., 1995.

12. Martin, M., P. Klupar S. Kilberg and J. Winter. *TechSat 21 and Revolutionizing Space Missions Using Microsatellites*. Technical Report AIAA SSC01-1-3, Kirtland AFB, NM: Space Vehicles Directorate, 2001.

13. Meirovitch, Leonard. *Methods of Analytical Dynamics*. New York: Dover Publications, Inc., 1970.

14. "NASA Earth Observing One Mission Page." NASA EO-1 Homepage, http://eo1.gsfc.nasa.gov, Accessed: 5 February 2007.

15. "NASA Space Technology 5 Mission Page." NASA ST5 Homepage, http://nmp.nasa.gov/st5/index.html, Accessed: 5 February 2007.

16. Ogata, Katsuhiko. *Modern Control Engineering* (Fourth Edition). New Jersey: Prentice Hall, Inc., 2002.

17. Regan, Frank J. *Re-Entry Vehicle Dynamics*. New York: American Institute of Aeronautics and Astronautics, Inc., 1984.

18. Sabol, Chris, Rich Burns and Craig A. McLaughlin. "Satellite Formation Flying Design and Evolution," *Journal of Spacecraft and Rockets*, *Vol. 38* (No. 2):pp. 270–278 (March-April 2001).

19. Sparks, Andrew. "Linear Control of Spacecraft Formation Flying," *Proceedings of the AIAA Guidance, Navigation, and Control Conference*, (AIAA 2000-4438) (August 14-17 2000).

20. Stengel, Robert F. *Optimal Control and Estimation*. New York: Dover Publications, Inc., 1986.

21. Ulybyshev, Yuri. "Long-Term Formation Keeping of Satellite Constellation Using Linear-Quadratic Controller," *Journal of Guidance, Control, and Dynamics*, *Vol. 21* (No. 1):pp. 109–115 (January-February 1998).

22. Vallado, David A. *Fundamentals of Astrodynamics and Applications* (Second Edition). Microcosm Press and Kluwer Academic Publishers, 2004.

23. Wedekind, James T. *Characterizing and Controlling the Effects of Differential Drag on Satellite Formations*. MS thesis, AFIT/GSS/ENY/06-M14. School of Engineering and Management, Air Force Institute of Technology (AU), Wright-Patterson AFB OH, March 2006 (ADA446933).

24. Wie, Bong. *Space Vehicle Dynamics and Control*. Reston VA: American Institute of Aeronautics and Astronautics, Inc., 1998.

25. Wiesel, William E. *Spaceflight Dynamics* (Second Edition). McGraw-Hill, 1997.

26. Wiesel, William E. *Modern Astrodynamics* (First Edition). Aphelion Press, 2003.

Vita

Second Lieutenant Blake B. Hajovsky was raised in Cuero, Texas, and graduated from Cuero High School in 2001. He attended The University of Texas at Austin where he graduated with a Bachelor of Science degree in Aerospace Engineering and commissioned through Detachment 825 AFROTC in May 2005. Upon commissioning, he reported to the Air Force Institute of Technology at Wright-Patterson AFB in Dayton, Ohio, to attend the Graduate School of Engineering and Management. Upon graduation, he will be assigned to the 2nd Space Operations Squadron at Schriever AFB in Colorado Springs, Colorado.

REPORT DOCUMENTATION PAGE

Form Approved
OMB No. 0704–0188

1. REPORT DATE *(DD–MM–YYYY)*	2. REPORT TYPE	3. DATES COVERED *(From — To)*
22–03–2007	Master's Thesis	Sep 2005 – Mar 2007

4. TITLE AND SUBTITLE	5a. CONTRACT NUMBER
SATELLITE FORMATION CONTROL USING ATMOSPHERIC DRAG	5b. GRANT NUMBER
	5c. PROGRAM ELEMENT NUMBER

6. AUTHOR(S)	5d. PROJECT NUMBER
Hajovsky, Blake B., Second Lieutenant, USAF	5e. TASK NUMBER
	5f. WORK UNIT NUMBER

7. PERFORMING ORGANIZATION NAME(S) AND ADDRESS(ES)	8. PERFORMING ORGANIZATION REPORT NUMBER
Air Force Institute of Technology Graduate School of Engineering and Management 2950 Hobson Way, Building 640 WPAFB OH 45433-7765	AFIT/GA/ENY/07-M11

9. SPONSORING / MONITORING AGENCY NAME(S) AND ADDRESS(ES)	10. SPONSOR/MONITOR'S ACRONYM(S)
N/A	11. SPONSOR/MONITOR'S REPORT NUMBER(S)

12. DISTRIBUTION / AVAILABILITY STATEMENT

APPROVAL FOR PUBLIC RELEASE; DISTRIBUTION IS UNLIMITED.

13. SUPPLEMENTARY NOTES

14. ABSTRACT

This study investigates the use of a linear quadratic terminal controller to reconfigure satellite formations using atmospheric drag actuated control while minimizing the loss of energy of the formation. The linearized Clohessy-Wiltshire equations of motion are used to describe the motion of the two-satellite formation about an empty reference position maintained at the formation center. Reconfigurations to final in-plane and elliptical formations are simulated at orbital radii of $6800\ km$ and $7000\ km$, and the altitude loss and a Δv budget were recorded as performance measures for each reconfiguration. The final states of the spacecraft upon reconfiguration were propagated forward in time over 20 orbital periods to ensure the final conditions were achieved. Simulations proved that minimizing the loss of orbital energy effectively minimizes the loss in altitude, and drag actuated control is fully capable of controlling the radial and in-track motion of satellite formations, although the cross-track motion is uncontrollable.

15. SUBJECT TERMS

Satellite Formation Control, Satellite Drag, Atmospheric Drag, Relative Satellite Motion, Satellite Vehicles, Satellite Constellations, Control Theory, Optimization

16. SECURITY CLASSIFICATION OF:			17. LIMITATION OF ABSTRACT	18. NUMBER OF PAGES	19a. NAME OF RESPONSIBLE PERSON
a. REPORT	b. ABSTRACT	c. THIS PAGE			William E. Wiesel, Ph.D. (ENY)
U	U	U	UU	146	19b. TELEPHONE NUMBER *(include area code)* (937) 785–6565, ext 4312

Standard Form 298 (Rev. 8–98)
Prescribed by ANSI Std. Z39.18